THE UNIVERISTY OF READING

Ph.D. Dissertation

on the

Transmission of Wireless Power by Magnetic Resonance

Submitted by

Christopher A. Tucker

c.a.tucker@reading.ac.uk

Supervisors

Prof. Kevin Warwick & Dr. William Holderbaum

School of Systems Engineering

April 2013

Acknowledgements

The author would like to personally thank Professor Kevin Warwick for his guidance, forthrightness, and confidence that the work presented herein would satisfy what I was to expect from it. It was he who once told me that my unpublished ideas would overcome the threshold of a successful peer-review. Kevin inspired an application in this thesis, the coupling of the human nervous system to a machine using wireless power as a non-invasive medium, following his great work in *Project Cyborg*. When we had met at the E-Golem conference in Prague Summer 2005, I could have only barely imagined working with him would produce such spectacular results.

The author would also like to thank Dr. William Holderbaum for his camaraderie and devotion to taking whatever time was needed to get our first papers to the publisher. He was instrumental in the steerage in the flow of the story of the paper, especially in the relation of the mathematics and diagrams to the work. William displayed great tenacity in getting a point across in an otherwise undefined context, something I have taken away from our friendship.

I would like to convey my gratitude to James Anderson for talking plainly about how one goes about pursuing commercially those genuine ideas from academia. It is from those expressions and how they are leveraged to the interests of others that lies at the heart of the matter.

I would also like to thank Professor R. Price and Professor W. DeFord at the University of Utah, for their inspirational lectures and freedom in research philosophies that formed the foundation of the theory in this thesis. Dr. M. Arguelles for the courage to begin asking the questions while aware of their cost and Dr. S. Pierce for understanding the human condition is due to our insistence upon upholding our ideals.

I would like to convey my gratitude to my father for letting me spend countless hours in the basement of the family house as a pre-teen building coils and circuits trying to understand the “invisible” force that is magnetism. Without his support and openness to answering my relentless questions, I never would have begun this work.

Finally, I would like to thank S. McDevitt, C. Smith, R. Popko, N. Shebalin, and K. Kasey for their restless spirits and inspiration of what this work was to become.

The work is dedicated to those persons who stood by me as I obsessed over what was to become this thesis; without them, the rich diversity that is this world would have never been realized.

For Daniela

Table of Figures

Table of Tables

Abstract

The work involves investigation of a type of wireless power system wherein its analysis will yield the construction of a prototype modeled as a singular technological artifact. It is through exploration of the artifact that forms the intellectual basis for not only its prototypical forms, but suggestive of variant forms not yet discovered. Through the process it is greatly clarified the role of the artifact, its most suitable application given the constraints on the delivery problem, and optimization strategies to improve it.

In order to improve maturity and contribute to a body of knowledge, this document proposes research utilizing mid-field region, efficient inductive-transfer for the purposes of removing wired connections and electrical contacts. While the description seems enough to state the purpose of this work, it does not convey the compromises of having to redraw the lines of demarcation between near and far-field in the traditional method of broadcasting.

Two striking scenarios are addressed in this thesis: Firstly, the mathematical explanation of wireless power is due to J.C. Maxwell's *original* equations, secondly, the behavior of wireless power in the circuit is due to Joseph Larmor's fundamental works on the dynamics of the field concept. A model of propagation will be presented which matches observations in experiments. A modified model of the dipole will be presented to address the phenomena observed in the theory and experiments.

Two distinct sets of experiments will test the concept of single and two coupled-modes. In a more esoteric context of the zero and first-order magnetic field, the suggestion of a third coupled-mode is presented.

Through the remaking of wireless power in this context, it is the intention of the author to show the reader that those things lost to history, bound to a path of complete obscurity, are once again innovative and useful ideas.

Declaration of this thesis

I confirm that this is my own work and the use of all material from other sources has been properly and fully acknowledged.

Christopher Allen Tucker

Prague, Czech Republic
14 June 2013

Table of Contents

1 Introduction

Before the success of Marconi's 1902 radio transmissions to what later became the sole means of the wireless art, various alternative methods were investigated for the transport of energy and information over long distances without wires. The most well-known practical experiments five years earlier were performed by Tesla [103], who had discussed wireless transmission as early as his 1892 lectures delivered before the American Institute of Electrical Engineers in New York and the Institute of Electrical Engineers in London [13]. His methods focused on non-radiative means, in stark contrast to the work of Marconi [108]. Despite significant experimental successes, the work was not be taken up by the wider scientific community.

While Marconi, supported by the work of Heaviside, would go on to establish the practical "Hertzian" model of radio transmission, Tesla's work would lay dormant. At the heart of Tesla's work was the consideration his efforts relied heavily on theories espoused by Poynting and Larmor. A centerpiece of this understanding is the treatment of the space used as the carrier medium was extended from Maxwell's idea of non-radiative magnetic vortices [109], and of a disturbance contained in a structure [23].

Wireless energy transfer is most useful in near or mid-field regions, arguably in some radiative form. Near-field transfer is of the type exhibited in the transformer effect and usually obtained through mutually-inductive coils and capacitive effects. Mid-field regions exhibit behavior where the falloff is rapid, yet linear. It has been proposed that distances achievable by this scheme are generally very short, limited to a few times the diameter of the coils [31], losses occurring due to resistive and radiative effects.

Theoretical and practical methods of the wireless transfer of energy, distinguished by the broadcast frequency and circuit geometry, are limited in scope and application. Far-field power transmission involves higher frequencies where distances achieved are much greater than the radius of the coils. This requires either the use of microwave signals or optical beaming. In general, such techniques require both line-of-sight and complex tracking systems. The purpose of the research described in this thesis is to investigate efficient medium-range power delivery using small-scale antennas without tracking systems where the transmitter and receiver can lie at a distance regardless of position and orientation.

An important consideration to reflect is that Poynting, Larmor, and Tesla agreed on two fundamental principles: 1. The Earth acts as a conductor corridor, a charged shell capable as a transmission medium, and, 2. By designing a suitable circuit, pathways could be created allowing electrical

currents to pass between distant locations. A more subtle conclusion is that the coils could be designed in such a manner as their magnetic fields resonate, at least in part, with the Schumann resonance [110]. Haus [93] observed and mathematically incorporated some of these possibilities into his notion of evanescent waves which become more pronounced at higher frequencies in the near-gigahertz range.

This thesis presents the construction of high-efficiency resonance transformers which facilitate stable transmission of power and information at useful distances in two distinct forms—one with a single set of coils exhibiting a projection field, a second with two sets of tuned circuits exhibiting energy distribution regardless of coil orientation. In both cases, the velocity of electrons and their acceleration on the primary coil establish the relativistic paradigm of differential time in signal delivery. This would be in support of the remark by Tesla of velocity-inhibition and suggests these types of wireless transmission devices are both radiative, in terms of a projection, and non-radiative where the exchange of energy is along a series of standing planar waves existing as a power series along the distance between the coils. The series is supported by the power transformation in family time of magnetic fields in the distant circuits at resonance. Also, that in tandem with these planar waves, lie regions of radiative emissions where a coil is coupled to a load.

This thesis hypothesizes that the space between the transmitting and receiving coils is regarded as containing an electromagnetic field object suspended on a standing wave perpetuating signals less than 100 MHz yet yielding smooth power transmission over long-range distances, where the distance of transmission can be many times larger than the largest dimension of both coils involved in the transfer. In this way, the field object is composed literally of a series-progression of plane waves behaving as a virtual transmission line connected by the forces driven by the input oscillator or circuit the antenna are attached to. Irrespective of any larger implications or derivation away from magnetic resonance, the method still relies on the well-understood concept of inductive coupling and the transformer effect.

There are various referred methods of wireless energy transfer as contrasting examples to facilitate the analysis of the model illustrated in this thesis which differs from it in fundamental ways. While similarly pursuing inductive coupling of magnetic fields between resonant coils to allow the transmission of electrical currents at a distance, this thesis follows logic of the original Maxwell equations to Joseph Larmor to Nikola Tesla.

Apart from the singular model of the wireless transfer of power by projection, wireless transmission of energy through signaling [99] is accomplished by the creation of an inductive link which is maximized at a particular resonance frequency ω_0 given the physical characteristics of sets of tuned coils. It is commonly understood that energy transfer in the transformer model discovered by Michael

Faraday, permits the transfer of energy between circuits in close proximity. What is not so clear is what schemes are appropriate for longer distance transmission using the same or similar mechanisms. Some will argue that the near-field for these schemes do not exist, rather, the energy is expressed in the far-field exclusively, dependent on the type of antenna which typically are loops of a few turns, receiving energy from an externally driven sinusoidal source. Energy is stored in the field by the exchange between the inductive and capacitive components contained in the circuit, through damping of the frequency. This insists that there is a contiguous field over the distance that cannot be simply divided into near and far-field descriptions. Instead, it will be described as a mid-field region.

James Clerk Maxwell proposed mathematical solutions to the experimental observations of Michael Faraday and built a framework around what was to become field theory in his *A Dynamical Theory of the Electromagnetic Field* in 1865. Within thirty years, Poynting further developed the mathematical context of the free-space field concept to include energy and its distributions in 1884, Hertz first experimental confirmed the existence of electromagnetic waves in 1886, Larmor described the electron and its behavior under acceleration by a current in 1895, and Tesla, using more refined devices at higher potentials, demonstrated this work to the public at the IEE in London in 1892 and at the Chicago World's Fair in 1893.

In the electrical age of the Victorian Era, the utility of power was fluid and was formed in many imaginative scenarios. For the purposes of this thesis, expressions of the interfacing between humans and technology are the most interesting. In terms of wireless power, some consisted of a direct interfacing at the hands where energy was projected as a light so that the interface may be observed. This imagery is similar to that appearing in wizardry mythos and not unlike the stories of individuals purported to command the environment, casting thunderbolts as a sign of their power as early as the Middle Ages. The imagery serves to illustrate a consistent need in human society: 1. the human form is more than the sum of its parts, and, 2. by clever manipulation, machines could be constructed to control the environment.

Following the First World War, from the 1920s to the 1960s, the concept of signaling was isolated into its own category, due primarily to the development of the field of radio engineering following Marconi. It again became more embedded in human activities in the form of wireless-powered implants and cellular phones, spawning a plethora of devices in many more forms the author calls archetypes. The term is used purposefully in the Jungian sense of the word.

The investigation conducted in this thesis will inquire what constitutes free-space as a transmission medium, given the set of conditions imposed upon it. The goal is to yield a model of the

transportation of energy across free-space by magnetic resonance. The concept of signaling is relevant to the thesis as a more descriptive body of theory regarding radio-wave propagation and computational strategies, as opposed to purely electromechanical forces such as voltage and current. The dynamics of the field is of greater interest than simple expressions of power ratios.

The model constructed in response to the investigation is structured as:

1. modular components of the model architecture, each of the components forming a part of the whole argument,
2. in the attempt to demarcate a cross-compatibility between the circuit and field model,
3. propose methods to demonstrate the soundness of the model in a linear granularity,
4. propose an experiment to test the methods,
5. discover a measurement criterion of performance of a physical model, and,
6. discuss the results and extended components learned during the process.

The presentation will be an engineering-centric, scientific investigation where the material is organized appropriate for the subject matter. The thesis is divided into three categories: circuits, fields, and waves; each chapter serves to disseminate the contribution into distinct, yet interconnected, parts. As the author is aware of the divergence between circuit and field analytics, the circuit model will be tested in an experiment of a working prototype and the antenna at the interface will be where the author will attempt to converge the concept. This will not only provide a concrete expression for the theoretical musings, but to also make the concept more tangible. For such an abstract concept, a cast of the meaning of the expression should exhibit both a form and a function. This process will enumerate

- a circuit with antenna emitting radiation in a geometrically-defined pattern,
- as an ambient free-space field of a uniform structure, and,
- a behavior depiction in terms of Maxwell, Larmor, Poynting, and Tesla.

In an attempt to be concise and descriptive as possible, the remainder of the introduction will be to trace the specific parts of Maxwell's *original* equations that are directly relevant to the arguments pursued in the following sections. The focus in the short-term is then on past works to explain modern problems; therefore, the old masters will then be given direct attention [1].

1.1 Maxwell and Larmor

Maxwell's equations have been widely discussed in the literature. In their common and most derived form, these equations describe five electromagnetic quantities:

- The electric field $\mathbf{E}$, (in V/m),
- The magnetic field $\mathbf{B}$, (in T),
- The magnetic field intensity $\mathbf{H}$, (in A/m),
- The density of electric charge ρ, (in C/m^3),
- The density of electric current $\mathbf{J}$, (in A/m^2),

which have the vector forms, in the microscopic case,

$$\begin{aligned} \nabla \times \mathbf{E} + \frac{\partial \mathbf{B}}{\partial t} &= 0, \\ \nabla \cdot \mathbf{E} &= \frac{\rho}{\varepsilon_0}, \\ \nabla \times \mathbf{B} - \frac{1}{c^2}\frac{\partial \mathbf{E}}{\partial t} &= \mu_0 \mathbf{J}, \\ \nabla \cdot \mathbf{B} &= 0, \end{aligned} \tag{1}$$

and with Ampère's circuital law, in the macroscopic case,

$$\nabla \times \mathbf{H} = \mathbf{J} + \frac{\partial \mathbf{D}}{\partial t}, \tag{2}$$

where the constants are tied by the relationship, in free-space,

$$\varepsilon_0 \mu_0 c^2 = 1, \tag{3}$$

where,

- ε_0 is the electric permittivity of the vacuum, (in F/m),
- μ_0 is the magnetic permeability of the vacuum, (in H/m), and,
- c is the speed of light in a vacuum, (in m/s).

Not widely discussed is the fact that there exists two distinct versions of what is currently represented as "Maxwell's equations". Those by Maxwell himself and those by the Maxwellians [2]: Heaviside, Fitzgerald, Lorentz, and Hertz.

The modern and ubiquitous form of the Maxwell equations are the result of a vectorization of sets of equations by the Maxwellians to facilitate a reasonable description of moving charges yet ignoring rotations of energy in the field. Accounting for electromagnetic interactions outside the context of the "local" field was also discarded. While the reasons for the truncation allowed a simpler representation which suited the newborn field of radio engineering in the 19th Century, such a notion does not need to be held in the present era. Critically, the Maxwellians banished the vector and scalar potential functions from their version. As a result, the concept of the displacement current $\mathbf{D}$, central to understanding coupling by magnetic resonance, was neglected [3, 4]. The reason was that since neither it nor the resulting magnetic field were associated with moving charges, contrary to the position later argued by J.J. Thomson in his theory of corpuscles, or what Larmor called electrons, they simply were not necessary. To this day, the displacement current is still controversial and rather unclear [104, 105], yet a central part of electromagnetic theory.

For the purposes of this thesis and in terms of the experiment introduced later, both the Maxwellian and Maxwell equations were not sufficient to describe the antenna at its interface. Rather, because of the central role of accelerated electrons in its operation, the arrangement of the dynamics needed to be understood from a different point of view, namely that offered by Joseph Larmor in a series of publications from 1893 – 1897 [5, 6, 43]. In examining both theories—the Maxwellians on one side, Larmor on the other—one sees the places where they share commonality and differences. The points of view, however, are distinct and not directly compatible, therefore by their nature, divergent.

The divergence essentially revolves around Thompson's interpretation of the description of the electron, which Larmor had described in [5]: one side dissecting the problem from the point of view of radiation on the basis of electric actions, the other, electric actions on the basis of a mechanical theory of radiation—of radiant structures or field objects emitted by the exchange of energy at a distance between two conductors. Maxwell, et. al was to take the former while Larmor took the latter.

Maxwell's original expression of electromagnetic quantities, following *A Dynamical Theory of the Electromagnetic Field*, consists of expression of two systems A and B where one has influence on the other and the effects are compounded by coefficients of force. In terms of induction, Maxwell states that L, M, and N depend on the distribution of the magnetic effects due to two circuits, their relative position and subject to variation given its velocity.

Of the original 20 Maxwell equations, only six will be treated.

(A) The relation between electric displacement, true conduction, and the total current, compounded of both as a means of reduced momentum,

$$\begin{aligned} \mathrm{C}\frac{dw}{dt}\delta z &= \mathrm{X}\delta x + \mathrm{Y}\delta y, \\ \mathrm{X} &= \frac{d}{dt}\left(\mathrm{C}p^2 qu + \mathrm{C}pqv\right), \\ \mathrm{Y} &= \frac{d}{dt}\left(\mathrm{C}pqu + \mathrm{C}q^2 v\right), \end{aligned} \tag{4}$$

where the momentum of the system referred to as A is $\mathrm{L}u + \mathrm{M}v$ and B is $\mathrm{M}u + \mathrm{N}v$.

(B) The relation between the lines of magnetic force and the inductive coefficients of a circuit, as already deduced from the laws of induction and the resistive forces R and S, the equation of the current in x in A will be,

$$\xi = \mathrm{R}x + \frac{d}{dt}\left(\mathrm{L}x + \mathrm{M}y\right), \tag{5}$$

and that the current in y in B is,

$$\eta = \mathrm{S}y + \frac{d}{dt}\left(\mathrm{M}x + \mathrm{N}y\right). \tag{6}$$

(C) The relation between the strength of a current and its magnetic effects, according to the electromagnetic system of measurement.

(D) The value of the electromotive force in a body, as arising from the motion of the body in the field, the alteration of the field itself, and the variation of electric potential from one part of the field to another.

(E) The relation between electric displacement, and the electromotive force which produces it, as the work done in a unit of time arising from the variations of L, M and N of the conducting circuits A and B,

$$\frac{1}{2}\frac{d\mathrm{L}}{dt}x^2 + \frac{d\mathrm{M}}{dt}xy + \frac{1}{2}\frac{d\mathrm{N}}{dt}y^2. \tag{7}$$

(F) The relation between and electric current, and the electromotive force which produces it.

(G) The relation between the amount of free electricity at any point, and the electric displacements in the neighborhood.

(H) The relation between the increase or diminution of free electricity and the electric currents in the neighborhood.

Only those indicated above with equations, e.g., (A), (B), and (E), will be discussed in greater detail in their contributions. The others will be absorbed into the discussion only where necessary. It is relevant now to examine the expression of the terms as quantities of intrinsic energy of the field and show the applicability of this method, as opposed to strictly the Maxwellian equations (1) and (2), tied to unity in (3) for a more thorough mathematical description of the field more agreeing in geometry and by inspection, which has resulted in this particular wireless power scheme.

In order to do this, it will take the assumption where Larmor and Maxwell agree on the electric displacement (A and E). Larmor states regarding this term from the point of view of the medium:

> The problem of the æther has been first determinedly attacked from the side of electrical phenomena by Clerk Maxwell in quite recent times; his great memoir on a 'Dynamical Theory of the Electromagnetic Field' is of date 1865. It is in fact only comparatively recently that the observation of Ørsted, and the discoveries and deductions of Ampère, Faraday, and Thomson had accumulated sufficient material to allow the question to be profitably attacked from this side. Even as it is, our notions of what constitute electric and magnetic phenomena are of the vaguest as compared with our ideas of what constitutes radiation, so that Maxwell's views involve difficulties, not to say contradictions, and in places present obstacles which are to be surmounted, not by logical argument or any clear representation, but by the physical intuition of a mind saturated with this aspect of the phenomena. Many of these obstacles may, I think, be removed by beginning at the other end, by explaining electric actions on the basis of a mechanical theory of radiation, instead of radiation on the basis of electric actions. The strong point of Maxwell's theory is the electromotive part, which gives an account of electric radiation and of the phenomena of electromagnetic induction in fixed conductors; and this is in keeping with the remark just made. The nature of electric displacement, of electric and magnetic forces on matter, of what Maxwell calls the electrostatic and the magnetic stress in the medium, of electrochemical phenomena, are all left obscure [4, pp.445-6].

Which assumes a potential energy structure of imperfect consistency we call free-space. The term will be restricted to charged dielectric: A theoretical representation of a specific type of phenomenon extant between free-space conductors on a planetary surface. It is this structure the author argues is an accurate representation given the experimental evidence.

A line of agreement between Larmor and Maxwell begins both the foundation and the angle of approach to the problem-space for the formulations in this thesis, namely the displacement current. Form this beginning point, the thesis will explore those tools from both sets of the arguments to explain the physical model a wireless power scheme which exhibits magnetic resonance in the mid-field region, that is, at the end of the projection field $\bar{\mathbf{H}}$. At present, this seems the best tool to yield

an accurate mathematical representation. This thesis will restrict the discussion of this when it approaches quantum field theory, deferring the model to an example of sufficiently large dielectric medium given a transmission frequency. Simply, moving charges in the experiment are described by the Larmor formula and Bloch waves for an irregular medium.

Rather than using the Lorentz/Larmor theory of retarded time, family time [26] is used to describe length contraction given forces, velocities, and wave propagation, guised in Poincare's [42] non-Euclidean approach. This is possible because the case is restricted to that of two resonant conductors having a conduction-current between them.

Some questions to answer are the following:

- What forces allow the propagation of the free-space wave of electric and magnetic components resulting from action in parallel conductors, or resonant objects?
- What forces counteract the propagation of the free-space wave of electric and magnetic components resulting from action in parallel conductors, or resonant objects?
- While it is clear such objects exchange energy across free-space, how does the nature of the disturbance and the displacement taking place mirror what is being observed in the experiment?

The significance of the displacement current lies in the inclusion of a strain on the medium, which could be filled with charged matter of either a light or dark predisposition, depending on how it is defined. Particularly, this thesis will describe the medium which can experience electric strain where a magnetic field is impressed.

Maxwell's derivation of strain is unrelated to the modern day derivation for displacement current in the vacuum, which is based on consistency between Ampère's law for the magnetic field and the continuity equation for electric charge. Maxwell imagined the displacement as a sea of molecular vortices existing in free-space and the displacement a strain on the medium.

However, when considering polarized circuits, the ambiguity in Maxwell's derivation clears.

The consequences of clarity are costs in the form of an exchange of forces at the boundary whose periodicity suggests the ability to create artificial electrical structures with a polarization.

Once Maxwell's sea of molecular vortices had been abandoned, along with it the æther, an interpretation of displacement current evolved that treated free-space explicitly as a separation of free-

space from material media, unlike Maxwell's original concept.[1] This is a feature associated with the potentials, relative to free-space [7, 8] and yield the curl will describe the actual linear displacement.

If the vector (f, g, h) denotes the curl of the medium, or twice the absolute rotation of the portion of the medium at the point considered, and the medium is supposed of crystalline-like quality, in that the geometry is distributed and well-ordered along its principal axes, so that the field object Ω_0 would be of the form,

$$\Omega_0 = \frac{1}{2}\int\left(a^2 f^2 + b^2 g^2 + c^2 h^2\right) d\upsilon, \tag{8}$$

where $d\upsilon$ is an element of volume inclusive at the boundary. It follows that for an internal equilibrium of the structure, it must have,

$$a^2 f\, dx + b^2 g\, dy + c^2 h\, dz = -d\varphi, \tag{9}$$

a complete differential and that over any boundary enclosing a region devoid of elasticity the value of φ must be constant. Such a boundary is the surface of a conductor; φ is the electric potential in the field due to charges on the conductors; (f, g, h) is the electric displacement in the field, circuital by its very nature as a rotation, and $\left(a^2 f, b^2 g, c^2 h\right)$ is the electric force derived from φ. The charge on a conductor is the integral of $\int(f, g, h)\, dS$ over a surface S enclosing it, and cannot be altered except by opening up a channel devoid of elasticity, in the medium, between this conductor and another containing like properties so that electric discharge occurs only by the impression of force on the elastic quality of the medium [6].

At the interface between two dielectric media, taken to be crystalline as above, the condition comes out to be that the tangential electric force is continuous. When the circumstances are those of equilibrium, and therefore an electric potential may be introduced, this condition allows discontinuity in the value of the potential in crossing the interface, but demands that the amount of this discontinuity shall be the same all along the interface; these are precisely the circumstances of the observed phenomena of voltaic potential differences. The component, normal to the interface, of the

---

[1] The final disengagement of "vacuum" from real media occurred with the international agreement to use the material-unrelated terms *electric constant* and *magnetic constant* to replace the seemingly material-related terms *permittivity* of vacuum and *permeability* of vacuum. These constants have *defined* (not measured) values that refer to free space, which is viewed as an unattainable idealization; not as a real, observable medium, not equivalent even to a quantum vacuum.

electric displacement is of course always continuous, from the nature of that vector as a flux. This will be used to imply that calculation of the **B** field at the interface along with its projection $\bar{\mathbf{H}}$, given **D** will describe the type of emitted field and its relative geometry.

The magnetic field, calculated as a function of its intensity, is subject to a property called relativistic-time, or velocity-inhibition. In free-space, it is,

$$\begin{aligned} \mathbf{B} &= \nabla \times \mathbf{A} = \frac{\mu_0}{4\pi} \int_0^{120\pi} \frac{\mathbf{J}\alpha \times r}{r^3} d\upsilon, \\ \bar{\mathbf{H}} &= \varepsilon_0 \frac{\partial \mathbf{D}}{\partial t} \cdot \frac{4}{3}\pi r^3, \end{aligned} \tag{10}$$

where the energy revealed at the boundary of the antenna and the free-space boundary is given by $\bar{\mathbf{H}}$, $\alpha = \left(t - \frac{v}{c} \right)$ a relativistic-time factor, also called family time [26], $d\upsilon$ an element of volume. In area enclosed by $\bar{\mathbf{H}}$, ε_ϕ is free-electricity where the field is considered ambient; its motion is given by the direction of **A**. The application of this hypothesis is illustrated by characteristics of stored and distributed energy properties shown in ordinary geometries of a simple loop antenna, the restriction of such properties to this arrangement exclusively.

Larmor states the energy given off by the acceleration of an electron can transform its energy at the interface of an antenna to sustain a magnetic field. When accelerating or decelerating the electron releases the force applied by acceleration, the energy radiated is given by,

$$P = \frac{e^2 a^2}{6\pi\varepsilon_0 c^3}. \tag{11}$$

Given in terms of the scalar and vector potential, addressed in §2.1.4,

$$\mathbf{E} = -\nabla\varphi - \frac{\partial \mathbf{A}}{\partial t}. \tag{12}$$

Equation (12) illustrates the expectation that the energy in the field in due primarily to both potentials at the interface of the antenna to free-space. Also, that the transmission path which yields the energy *must* contain some inherent structure for transfer to occur. This will be known as the “virtual transmission line” later in the thesis.

1.2 Poynting and Tesla

Following the work of Maxwell, J.H. Poynting would describe the energy in the field; following the work of Maxwell, Poynting, and Larmor, N. Tesla would experimentally-verify these mathematical works [9, 13, 14, 15, 52]. By the end of the 19th Century, the stage was set for later experimenters and inventors to create what became known as "the wireless art" or radio.

Poynting commented [9] on Maxwell's theory which alludes to later commentaries by Larmor [6]:

> I am not sure that there has hitherto been any distinct theory of the way in which the energy developed in various parts of the circuit has found its way thither, but there is, I believe, a prevailing and somewhat vague opinion that is some way it has been carried along with the conductor by current. Probably Maxwell's use of the term 'displacement' to describe one of the factors of the electric energy of the medium has tended to support this notion. It is very difficult to keep clearly in mind that this 'displacement' is, as far as we are yet warranted in describing it, merely something with direction, which has some of the properties of an actual displacement in incompressible fluids or solids. When we learn that the 'displacement' in a conductor having a current in it increases continually with time, it is almost impossible to avoid picturing something moving along the conductor, and it then seems only natural to endow this something with energy-carrying power. Of course, it may turn out that there is an actual displacement along the lines of electromotive intensity. But it is quite as likely that the electric 'displacement' is only a function of the true displacement, and it is conceivable that many theories may be formed which this is the case, while they may all account for the observed facts. … It seems to me then that our use of the term is somewhat unfortunate, as suggesting to our minds so much that is unverified or false, while it is so difficult to bear in mind how little it really means.
>
> I have therefore given several cases in considerable detail of the application of the mode of transfer of energy in current-bearing circuits according to the law given above, as I think it is necessary that we should realize thoroughly that if we accept Maxwell's theory of energy residing in the medium, we must no longer consider a current as something conveying energy along the conductor. A current in a conductor is rather to be regarded as consisting essentially of a convergence of electric and magnetic energy from the medium upon the conductor and its transformation there into other forms. The current through a seat of so-called electromotive force consists essentially of a divergence of energy from the conductor into the medium. The magnetic lines of force are related to the circuit in the same way throughout, while the lines of electric force are in opposite directions in the two parts of the circuit—with the so-called current in the conductor, against it in the seat of electromotive force. It follows that the total E.M.I. round the circuit with a steady current is zero, or the work done in carrying a unit of positive electricity round the circuit with the current is zero. For work is required to move it against the E.M.I. in the

> seat of energy, this work sending energy out into the medium, while an equal amount of energy comes in the rest of the circuit where it is moving with the E.M.I. This mode of regarding the relations of the various parts of the circuit is, I am aware, very different from that usually given, but it seems to me to give us a better account of the known facts.
>
> It may seem at first sight that we ought to have new experimental indications of this sort of movement of energy, if it really takes place. We should look for proofs at points where the energy is transformed into other modifications, that is, in conductors. Now in a conductor, when the field is in a steady state, there is no electromotive intensity, and therefore no motion and no transformation of energy. The energy merely streams round the outside of the conductor, if in motion at all in its neighborhood. If the field is changing, energy can pass into the conductor, as there may be temporary E.M.I. set up within it, and there will be a transformation. But we already know the nature of this transformation, for it constitutes the induced current. Indeed, the fundamental equation describing the motion of energy is only a deduction from Maxwell's equations, which are formed so as to express the experimental facts as far as yet known. Among these are the laws of induction in secondary circuits, and they must therefore agree with the law of transfer. We can hardly hope, then, for any further proof of the law beyond its agreement with the experiments already known until some method is discovered of testing what goes on in the dielectric independently of the secondary circuit.

The above, in the opinion of the author, is trying to compartmentalize that the size, shape, and space taken by an electromotive force appearing in free-space as a field, is wholly dependent upon the apparatus, or antenna, projecting it. Poynting's comments infer that plane waves propagate on a transmission line driven by the currents and its field is distributed along a surface, even is the line and surface are virtual. The length of transmission is dependent upon the intensity at the field and the permittivity of the waveguide. In free-space at 20C and one atmosphere, attenuation of the field past the mid-field region, described in detail in Section 2, occurs at a ratio of the coil radius to the distance, typically sixteen times [10]. The number is a conservative estimate. A simple experiment showing a measurably-powered state of a loop and receiver illustrates the propagation of photons in an emission pattern constituting a free-space field containing a periodic structure created by the presence of the coils [11] and that the emitted field is quantized [12].

Tesla undertook experimental verification of these theories as early as 1892 [13], and presented his results in 1900 [103]. Tesla was to focus his efforts on wireless power transmission, first through stationary waves then by signaling, sending power to remotely light bulbs and turn motors. In a body of research over a period of years from 1894 to 1908 at his laboratories in New York and Colorado Springs. Tesla's method was to project waves by magnetically coupling coils acting as an interface between the oscillator circuit and free-space. It is Tesla's method that is the founding principle of this

work. However, in this thesis, it is also interesting to understand what is going on in the dielectric of free-space by using “indirect” methods. The reason for this is that it is the author’s opinion that with the available resources, a direct test can only be useful when there is a framework describing a definite medium, i.e., the æther or dark matter.

Tesla’s macroscopic vision was to use stationary waves to broadcast between antipodes on the surface of the planet as a means to send power, which differed from the radiative model constructed by Hertz. In brief, the difference is subtle; Tesla espoused the transfer of energy at a distance without wires by standing waves, Hertz espoused the transfer of energy in the same manner via radiation.

Tesla’s notion of wireless power transfer was to use the planet as both source and conductor with towers at positions of an antipode to excite kinetic energy dispersed in the ionosphere while the wave transmitted along the surface of the planet. Receivers were constructed with simple aerials which would absorb these currents. In terms of propagation, Tesla’s main emphasis was the use of standing waves, similar to those observed in waveguides to accomplish power transmission. He noted the advantage of these waves is their omnipresence on the planet surface and long wavelength; coupled with the use of the grounding plane, it is possible in this method to use single-wire receivers. The planet can be considered as a resonant cavity due to the high conductivity between altitudes. In practical terms, this means an anything with an antenna can absorb currents where the wire length is directly proportional to the magnitude. Tesla introduced a profound concept that to this day has been largely unexplored. If history had unfolded as Tesla had envisioned, the modern electrical grid would look like that represented in Fig.1.1.

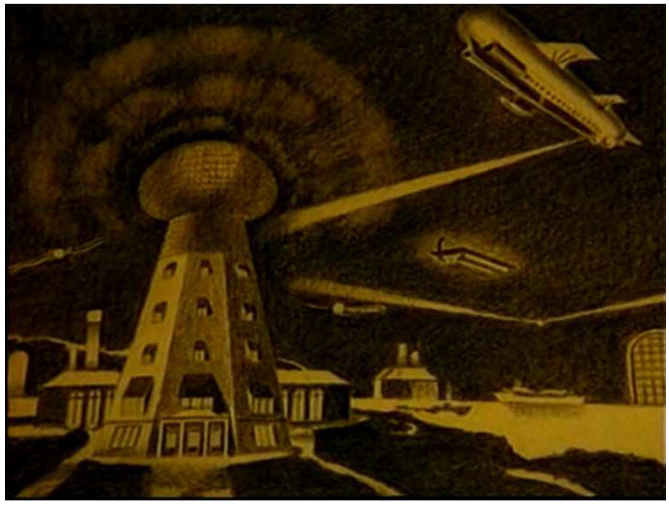

Fig.1.1. Tesla’s vision of wireless power.

After experimental trials at Wardenclyffe from a period of 1899 – 1903, some sporadic work as late as 1911, Tesla’s work went unfinished. The tower was demolished during the First World War.

Afterwards, Tesla abandoned his standing-wave hypothesis and exclusively experimented with radiative, or radiation-based emission, models [14]. At the time, prevailing attention was toward Marconi's broadcasting system and not the transmission of power. After the publication of the work on the Yagi antenna [15] in 1926 and the development of shortwave [16], wireless power would fade from view.

Forty years passed before interest in wireless power resurfaced. In the 1960s, short-wavelength transmission experiments [17] and the modeling of prototypical forms showed positive results [18]. A rethinking of inductive transfer began to surface in solving problems associated with subcutaneous implants [19]. While many divergent types of wireless power transmission have resulted, especially since 2004, this thesis will focus on a radiation-based emission of power in the form of plane waves from loop antenna over distances of one meter operating at frequencies up to 5 MHz.

This thesis will explore two distinct expressions of wireless power: That of a single primary loop transmitter/receiver system, and that of a primary/secondary loop pair transmitter/receiver system. The former will exhibit the author's notion of the mid-field region of the radiation model of a single coupled-mode, while latter will exhibit Tesla's stationary or standing waves and tunable wave cavity of two coupled-modes.

A brief outline of what is to be presented in this thesis is the following.

Chapter 2 will describe the theoretical and mathematical model of a circular loop antenna consisting of two primary coils. It will be shown that the circuit has a specific behavior given the nature of its arrangement. Section 2.1 will discuss a coupled-mode with a projection and the forces that are contiguous. Section 2.2 will discuss the behavior as also embedded in the unique circuit which drives the coupled-mode. Section 2.3 will discuss the propagation model and the equations which are capable of describing it. Section 2.4 will discuss several sets of experiments, relevant to a single coupled-mode, in various forms. In light of what is described in the introduction regarding humans and wireless power [20], biomedical implants will be one such experiment. This section will also discuss optimization of the model.

Chapter 3 will discuss two coupled-modes in terms of an existing circuit, namely, that of Nikola Tesla in his U.S. Patent #645,546 of 1900.

Chapter 4 will discuss a novel model of the dipole, given the theory and experimental evidence presented in the previous chapters.

Chapter 5 will present conclusions and suggestions for future research.

An important contribution of this thesis is, contrastingly to the use of the Maxwell-Heaviside version of Maxwell's equations in the literature survey, using the 1865 versions to begin the formation of the theoretical framework from where the arguments and analytics are derived from it. Tracing through three, selected because of their appropriateness to the subject: The relation between electric displacement, conduction and current, between the lines of magnetic force and inductive forces, and between electric displacement and electromotive force. It will be shown in the thesis the novel contribution is framed in the expression of these Maxwell equations.

Contrastingly to other literature, this thesis will discuss the geometry and ambience of the magnetic field in terms of Joseph Larmor conception of objects. Outside of some works in the early 20th Century, it seems most have ignored what is otherwise a very powerful set of tools to quantify the forces responsible for magnetic resonant coupling. This thesis will choose a set of equations and force-representations that will be used to explain *why* the phenomenon is at it appears given experimental evidence.

2 Power transmission and magnetic-resonant modes in an inductively-coupled circuit

The theory and those specific original Maxwell equations from Chapter 1 will now be applied to a physical model. A circuit consists of two distinguishable parts: a transmitter and a receiver. The transmitter is comprised of a regulated amplification and timing components connected to a loop antenna and a capacitor. The amplifier is connected to a source of direct current (dc) power. The receiver is comprised of a loop antenna, a capacitor, and a load such as a lamp or motor. The receiver is placed at a distance away from the transmitter. The circuit will transmit radio-frequency electrical energy into free-space the form of photons exchanged between two or more coupled resonators, depending how they are chained together [106]. At certain distances and antenna orientations, work performed by the energy transfer can be observed at a receiver by an illuminated lamp or turning motor. A pair of circular loops of a sufficiently similar geometry set at a distance form a closed induction circuit illustrated in Fig.2.1. These loops form a resonant circuit, a waveguide, and a virtual transmission-line simultaneously.

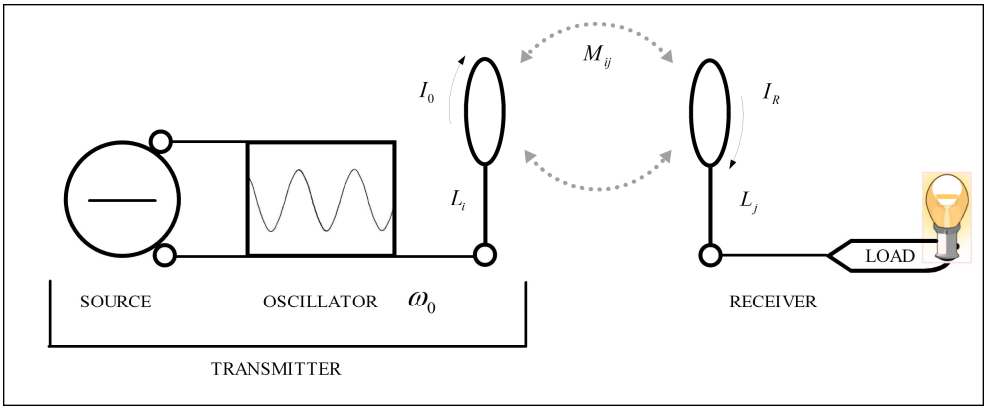

Fig.2.1: The prototype model for the transmission of power by magnetic resonance.

On examination of Fig.2.1, current flows from source to oscillator to coil loop L_i, accelerating electrons at a rate given loop curvature and ratio of loop circumference to wavelength; torque is given as a function of the current I_0. In this model, current at sufficient levels, that is, as a property of the components used to construct the oscillator, there is enough torque so that photons are projected into free-space in the form of radiation at a characteristic angular frequency ω_0.

The description of the number of photons emitted by a given arrangement is shown by the energy, γ_0, of the photons emitted by the antenna is given by,

$$\gamma_0 = \hbar\omega_0, \tag{13}$$

and the number of photons per second, γ_t, is given by the presence of circuital power J_0 ,

$$\gamma_t = \frac{J_0}{\gamma_0}. \tag{14}$$

At a distance, coil loop L_j absorbs the photons converting them back into electron currents via a voltage gap. The current is then coupled to perform work powering a load. The process involves:

1. The transfer of energy between input current contained in the oscillator, accelerated given a amplitude impressed as a magnitude on the coil wire of the transmission antenna,
2. the transit of photons, γ_0 , across free-space, and,
3. the transfer of energy between free-space and the constitution of electrical currents in the coil wire of the receiving antenna.

The flow pattern in time occurs at locations where the energy is not contained in the field, (E_θ, H_θ), where the magnetic flux $\Phi_M \to 0$. At these points, the field manifests as a projection encompassing an area $\bar{\mathbf{H}}$ which extends at a length from the antenna, L_i, to a surface in free-space, S_θ, at its boundary. The boundary is where there is equilibrium in the force exerted by the displacement, **D**, and that exerted by the medium. $\bar{\mathbf{H}}$ denotes the mid-field region. At S_θ, the far field begins. The parameters ε_0, μ_0, and σ_0 are invariant with position except at S_θ [21].

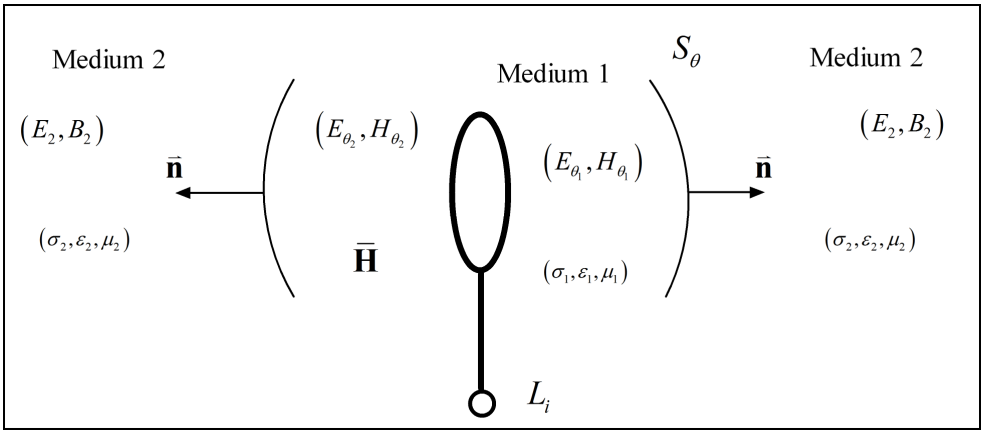

Fig.2.2. Areas where the field pushes in the medium and fall-off radiation from a loop antenna.

For the conservation of electric charge, a difference in the flux at the surface normal, $\vec{\mathbf{n}}$, to the antenna must imply a change in the total electric charge *q* contained within the volume denoted by S_θ as $\frac{\partial q}{\partial t}$. Power in the form of photons projected toward the boundary yields the displacement of energy from the loop in combination with its circuit. Concurring with Larmor, the boundary has elasticity and is susceptible to strain. In addition, concurring with the original Maxwell, the boundary is the point of dispersion. For linearization, the field is considered homogenous across the space with charges considered evenly distributed experiencing a uniform motion. The antenna therefore creates a disturbance as a deformation of the medium. At the boundary of the displacement, the rotational property of S_θ or instantaneous torque, τ_0, is given by,

$$\tau_0 = \nabla \times \mathbf{D}, \tag{15}$$

because of Fitzgerald's proposition of the identity of electromagnetic radiation as an exchange of force [22],

$$\nabla \times \mathrm{F} = \nabla\,(\nabla \cdot \mathrm{F} - \delta \mathrm{F}), \tag{16}$$

when,

$$\rho = 0, \text{ and } \mathbf{J} = 0. \tag{17}$$

Equation (11) will yield a wave equation in the form of,

$$\frac{1}{c^2}\frac{\partial^2 \psi}{\partial t^2} = \Delta \psi. \tag{18}$$

The field is therefore subject to uniform external forces dependent upon conditions of temperature and pressure and has a susceptibility, which is expected. Therefore, energies and frequencies limited by a given geometry share a common state of equilibrium. The effect of the equilibrium is analogous to inflating a balloon. The tension at the surface holding the energy inside is given by the shearing forces between the field at its border and the medium. Gauss's theorem transforms the surface into a changing flux of the electric field through the closed surface formed by the volume of open surfaces. More precisely, any "missing" flux of the current density $\mathbf{J}$ is absorbed from the flux of the vector $\varepsilon_0 \frac{\partial \mathbf{E}}{\partial t}$ or at the potential vector $\mathbf{A}$.

In terms of magnetic flux, an energized circular loop emits a magnetic field $\mathbf{B}$ of a given intensity and geometry according to the Biot-Savart and Neumann principles. Both propose that the contribution of each piece of the wire contained in the loop varies inversely as the square of the distance. Over the entire length of the wire, each contribution adds up to a total field that varies inversely as the distance from the loop. The contribution to the magnetostatic field at the origin of a current element, δI, at position $\mathbf{r}$ is,

$$\delta \mathbf{B} = \frac{\mu_0 \mathbf{r} \times \delta I}{4\pi r^3}, \tag{19}$$

given by the relationship of its radial length and the infinitesimal of the magnetic field, shown in Fig.2.3.

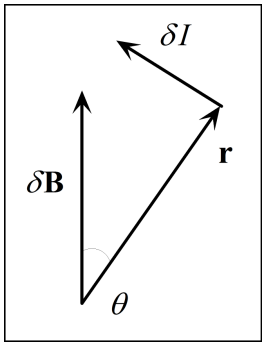

Fig.2.3. Ray relationships between the magnetic field, radial vector, and infinitesimal current.

The quantity, δI, is the current multiplied by the length of travel resulting from integrating the current density, $\mathbf{J}$, along the surface over a small element of volume (8). In particular, for a thin wire whose length element δs has a total current I_0 traversing it in the direction of δs, $\delta I = I\delta$s, and negatively otherwise. The proposition holds for mono-directional currents only. In the bi-directional case, an oscillator creates a rotational force through π phases, the direction of the current changes twice in a cycle throughout all of δs. The displacement at the molecular level of the conductor is given by Maxwell in (4).

The model of wireless power transfer, illustrated in Fig.2.1, consists of two distinct views of operation, that of a system of coupled modes and that of projection. The first view is expressed by the utilization of a pair of coils, one acting as a transmitter or primary coil, the other as a receiver or secondary coil. The combination of these two, or more [106], antenna is a coupled-mode [24]. The second view as a transmission antenna projecting a force.

Some of the pertinent questions in this case will involve realizing the geometry of the scheme, the manner of energy storage, and its boundary conditions. To address the latter question requires a key assumption: that the medium is not devoid of neither particles nor energy.

In the model, the magnetic field is assumed to have a simple symmetry as in the case of free-space fields. Ampère's law yields the value of the magnetic field throughout the space without complex integrations, such as those used when solving for mutual inductance. Gauss' theorem will describe the shape of the magnetostatic field in cases with spherical symmetries, generally applied here. For the special case of magnetic induction on the axis of a circular current loop, several assumptions are discussed in the remainder of this section of L_i and L_j.

The arrangement illustrated in Fig.2.1 is analogous to a pair of Helmholtz coils. However, each half of the circuit is not connected to the other by wire, rather, utilize the dielectric of free-space as a means of connection.

The first view, of a coupled-mode, is manifest as a flux-linkage between symmetrical antennas. It is by design dependent upon the **B** field. Geometry of the coupling mode is shown in Fig.2.4.

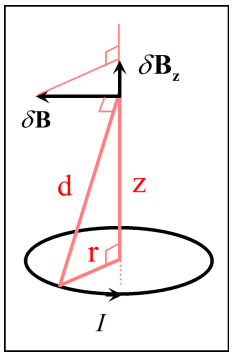

Fig.2.4. Geometry of the coupling-mode magnetic field.

For a circular current loop, all radial contributions will cancel out; the resulting magnetic induction **B** is oriented along the axis where $\mathbf{B} = \mathbf{B}_z$. Because of the symmetry of the triangles consisting the interior of the loop, shown in Fig.2.4, the contribution $\delta\mathbf{B}_z$ is r/d times (19), as,

$$\delta\mathbf{B}_z = \frac{r}{d}\frac{\mu_0 I}{4\pi d^2}\delta s. \tag{20}$$

All the elements, δs, add up to the circumference,

$$\mathbf{B}_z = 2\pi r\frac{r}{d}\frac{\mu_0 I}{4\pi d^2} = \frac{1}{2}\frac{\mu_0 I r^2}{d^3}, \tag{21}$$

while the field at the center of the loop is,

$$\mathbf{B} = \frac{\mu_0 I}{2r}, \tag{22}$$

at peak value where $z = \frac{r^2}{d^2}$.

What is essential to understand next is how the medium will be treated lying between a set of loops in a coupled-mode. To accomplish the treatment, Maxwell's original equation (5) will be converted into a differential equation describing a mode of propagation in a waveguide.

A waveguide, for the purposes here, is considered as an infinite system of transmission lines and the waves traveling along these lines move away along the vector normal from the source at a constant frequency, as illustrated in Fig.2.2. The wavefront resembles an infinite series of parallel planes of constant peak-to-peak amplitude normal to the phase velocity vector.

Analogous to a pair of Helmholtz coils, consider two loops shown in Fig.2.1 sharing the same horizontal axis, or in axial alignment. Let their respective latitudes be $+a$ and $-a$, magnetic induction is along the axis of axial alignment at distance z.

$$\mathbf{B} = \frac{1}{2}\mu_0 I r^2 \left\{ \left[r^2 + (a-z)^2 \right]^{-3/2} + \left[r^2 + (a+z)^2 \right]^{-3/2} \right\}. \tag{23}$$

The second derivative of (23) with respect to z at $z = 0$, is

$$\mathbf{B}''(0) = 3\mu_0 I r^2 \left(4a^2 - r^2\right)\left(r^2 + a^2\right)^{-7/2}. \tag{24}$$

The value $a = \frac{1}{2}r$ is the largest value where the magnetic induction has a single maximum value along the axis. When values of a are large, $\mathbf{B}''$ is positive at the center where $z = 0$ indicating a minimum value present. The configuration where the separation between the two loops is equal to their radius, $2a = r$, yields a magnetic field, which is almost uniform, near the center of the loop, as,

$$\mathbf{B} = \left(\frac{4}{5}\right)^{3/2} \frac{\mu_0 I}{r} \approx .071554 \frac{\mu_0 I}{r}. \tag{25}$$

The scalar potential of the magnetic field at the center of the loop, and where it is equidistant between two loops are examples of a current-free region. It takes the form of a multivalued function whose gradient is the magnetostatic induction. For a simply-connected region under coupled-modes, such a potential is well-defined up to a uniform additive constant. Otherwise, an ambiguity arises whenever the region contains loops which are interlocked with loops of outside current. In that case a continuous potential can only be defined with a modulo operation for a certain number of discrete quantities, each of which corresponds to one piece of the outside current.

The method described above fits to (19) that in static distributions, all currents must circulate in closed loops where $\nabla \times \mathbf{J} = 0$. Equation (19) cannot express with dynamic distributions where local electric charges may vary according to the inbound flux of current. A more sophisticated method is required.

By the Kelvin-Stokes formula, the circulation of a vector around an oriented loop is equal to the flux of its rotational element, or curl, through any smooth oriented surface bordered by that loop yields Ampère's law in integral form,

$$\mu_0 I \equiv \mu_0 \iint_S \mathbf{J} \cdot dS, \tag{26}$$

which is the same as the geometry on the plane,

$$\int_{\partial S} \mathbf{B} \cdot d\mathbf{r}. \tag{27}$$

The simplest and most fundamental direct application of Ampère's law is to first formulate under the Biot-Savart and Neumann principles, then extend the flow of magnetic induction **B** analogous to a straight wire or a waveguide keeping in mind the intensity is inversely proportional to the distance.

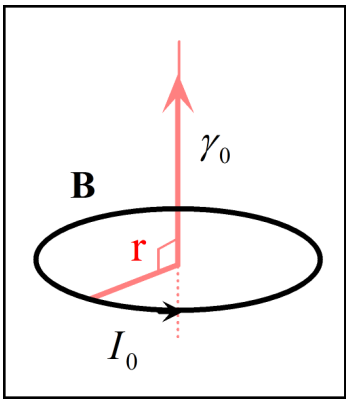

Fig.2.5. Projection of energy by a current impressed on the loop.

Consider a circular loop of radius r whose axis is a straight wire carrying an instantaneous current I_0. The magnetic induction **B** at the loop is tangential; the projection of the motion is constant as long as $I(t)$ is. The magnetic circulation and Ampère's law then gives,

$$2\pi r\mathbf{B} = \mu_0 I, \tag{28}$$

or equivalently,

$$\mathbf{B} = \frac{\mu_0 I}{2\pi r}. \tag{29}$$

Maxwell amended the static law of Ampère into the following generalization that holds in all cases including changing charge distributions [23],

$$\nabla \times \mathbf{B} - \frac{1}{c^2}\frac{\partial \mathbf{E}}{\partial t} = \mu_0 \mathbf{J}, \tag{30}$$

which agrees with the vectorized version of Faraday's law,

$$\nabla \times \mathbf{E} + \frac{\partial \mathbf{B}}{\partial t} = 0. \tag{31}$$

The curl of $\mathbf{B}$, given (30), is the characteristic of a rotating component of $\mathbf{B}$. The curl is illustrated in Fig.2.6.

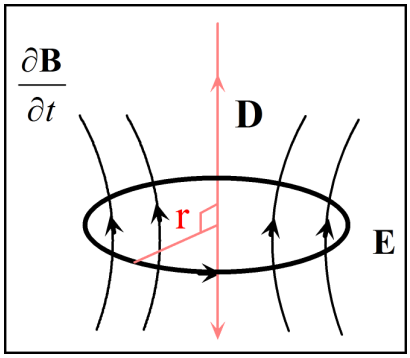

Fig.2.6. Field lines following an axis of displacement.

By the action of the curl, the propagation takes the form of the displacement $\mathbf{D}$. The displacement has a component, called directional current, or group velocity in terms of waves, along the magnetic flux lines. The intensity of $\mathbf{D}$ linearly decreases with distance. $\mathbf{B}$ couples to perform work where $\frac{\partial \mathbf{B}}{\partial t}$ can flow in a second coil. The measurement of the intensity $\mathbf{D}$ will be determined by the velocity of field flow. For example, let $\boldsymbol{\upsilon}$ be the vector field of a fluid flow. At a given point in the flow, a small wheel with blades whose axis is oriented in the direction of $\nabla \times \boldsymbol{\upsilon}$ at any point is placed in the flow in order to measure radial intensity. Then the angular velocity ω_1 of the wheel's rotation from the action of the current will maximize, where its value will be equal to $\frac{|\nabla \times \boldsymbol{\upsilon}|}{2}$. Assuming $\boldsymbol{\upsilon}$ has arbitrary coordinates $P(x,y,z)$, $Q(x,y,z)$, and $R(x,y,z)$, then $\nabla \times \boldsymbol{\upsilon}$ has the coordinates,

$$\frac{\partial R}{\partial y} - \frac{\partial Q}{\partial z}, \frac{\partial P}{\partial z} - \frac{\partial R}{\partial x}, \frac{\partial Q}{\partial x} - \frac{\partial P}{\partial y}. \tag{32}$$

The arcs cast by (25) form boundaries in three-dimensions of $\nabla \times \boldsymbol{\upsilon}$ at the interface with the antenna and feedback from the receiving object, illustrated in Fig.2.7.

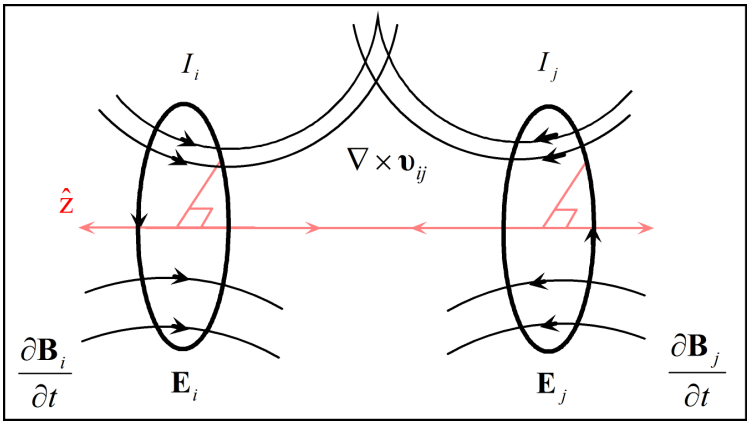

Fig.2.7. Flux linkage between two inductively-coupled coils.

The magnetic scalar potential, φ_0, for $\mathbf{B}$ created by the loops illustrated in Fig.2.7 is proportional to the currents, $I_{i,j}$, in the loop and to the solid angle-space, Ω_0, subtended by the side of the loop facing the observer, as,

$$\begin{aligned} \mathbf{H} &= -\nabla\, \varphi_0, \\ \varphi &= -\frac{\mu_0 I}{4\pi}\Omega_0. \end{aligned} \tag{33}$$

An ambiguity arises in the solid angle because there is a modulo operation of 4π; the angle is an approximation that becomes loses precision each time the value is taken. The sign convention is such that the side of a small loop is seen at a solid angle, which exceeds a multiple of 4π by a small positive quantity.

The second view, of projection, is manifest as a wavefront from a single transmission antenna. The length and intensity of the projection, $\bar{\mathbf{H}}$, is due to both the properties of the antenna and the power applied by the circuit. Modification of Fig.2.4 to include projection is shown in Fig.2.8.

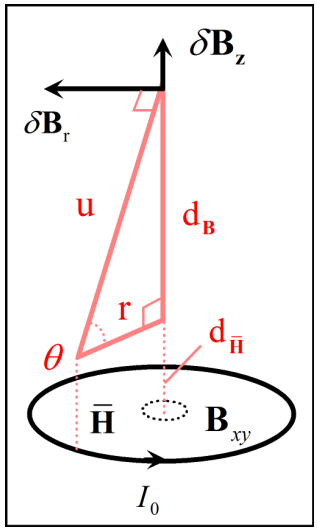

Fig.2.8. Field geometry extending away from the projection.

The projection is the formation of the waveguide, carrying energy across free-space displacing it as it exhibits motion away from the antenna in both the positive and negative directions of $\hat{z}$. For convenience, it is divided up into amplitude zones, A_λ, where measurements are taken to obtain the geometry of the emission by mapping its intensity. The projection of the loop is illustrated in Fig.2.9.

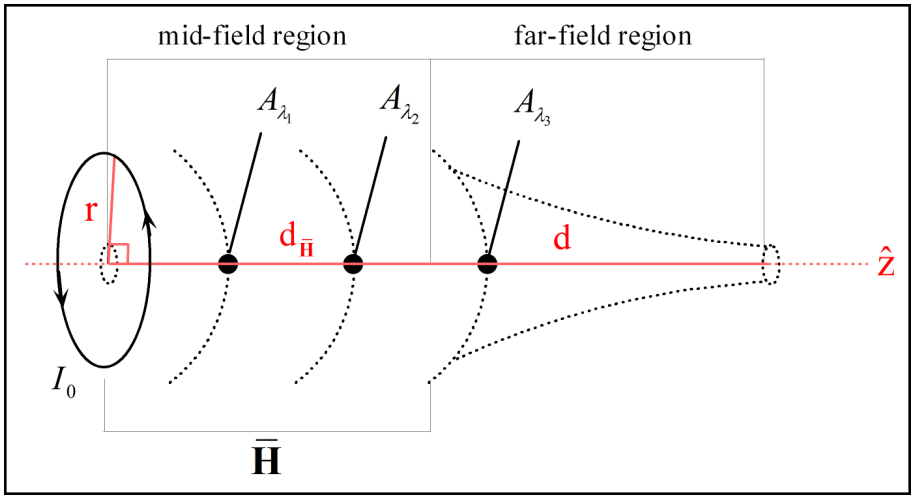

Fig.2.9. Projection field forming the mid-field region by intensity.

A composite of both the coupled-mode and projection is shown in Fig.2.10.

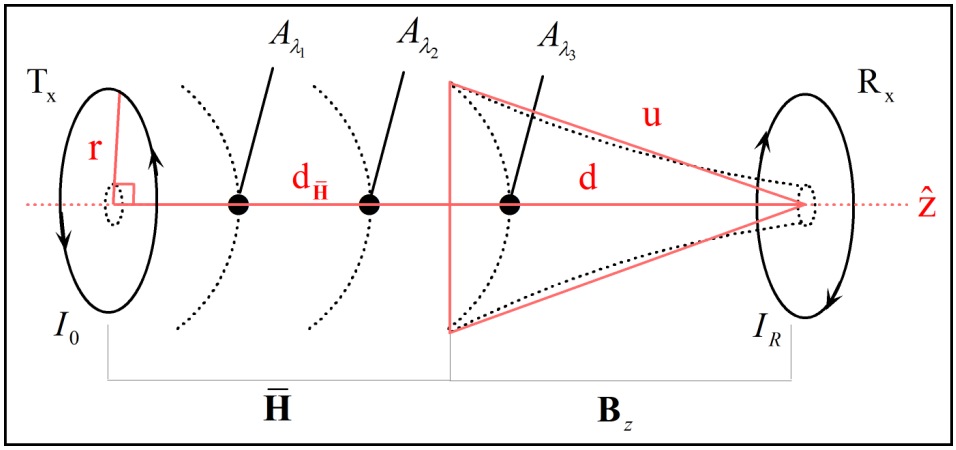

Fig.2.10. Projection of field and its geometry between two inductively-coupled coils.

The PDE description of the system will be elliptic, where its spatial solutions take a hyperbolic form consisting of *sinh* and *cosh* functions. Quantization of the field components and manifesting them in an experiment will be the aims of the following sections in this document.

2.1 A single coupled-mode with projection

The relationship between the loops and the amount of energy transported between them is described by how they are coupled. Coupling will only refer to the relationship *between loops* and not to free-space. Energy across free-space and its impedance is not by the phenomenon of coupling, rather, it is the consequence of coupling between the object which allows the transit of energy. Magnetic loops of a relatively small size and number of turns exhibit a magnetic field density sufficient to be an excellent model for experimentation.

A mode describes the energy in patterns of electric, magnetic, and force generated by the loops. The magnetic field intensity $\mathbf{H}$, is related to the magnetization, M, of the surrounding space on the antenna by susceptibility, χ_v. For the dipole moment in the conductor,

$$\mathrm{M}=\chi_v\mathbf{H}. \tag{34}$$

The boundary condition will be the surface S_θ. Analogous to the case of the thin current sheet the assumption is taken that the thickness of the loop structure is negligible. Therefore, Ampère's law will yield the instantaneous power density on an "approximately-closed" contour,

$$J_{\bar{\mathbf{H}}} = H_{A_\lambda} r_i^3 + H_i \ell_i^2, \tag{35}$$

If the medium is assumed homogenous and isotropic and the surface impedance of the boundary linearly approaches zero, it is considered a primitive waveguide. Any discontinuity in a waveguide facilitates a coupling between some or all desirable modes [24] in varying magnitudes.

Two electrical objects, consisting of inductive and capacitive components of relative value to each other, form a closed induction circuit. The linking is due to attractive resonators in a waveguide of characteristic impedance is imbued, purely by intuition, as sharing properties with transmission-line resonator with small losses [24, 25, 26]. A single coupled-mode can be identified by placing a receiving loop at an amplitude zone A_{λ}.

L_i is a circular loop with a voltage gap no greater than the size of its radius. Because of its low radiation resistance and high reactance, impendence matching is difficult to a sinusoidal oscillator. Therefore, L_i is connected in parallel to a capacitor powered by a switching amplifier. Comparably, the loop antenna L_j can also be connected in parallel to a capacitor whose value is no greater than that of L_i.

Wave impedance is the ratio of the transverse components of the electric E_0 and magnetic H_0 fields. For a transverse-electric-magnetic (TEM) plane wave traveling through a nearly-homogeneous medium at a given temperature and pressure, wave impedance is everywhere equal to the intrinsic impedance of the medium. The wave impedance, in terms of fields is

$$\mathbf{Z} = \frac{|\mathbf{E}|}{|\mathbf{H}|},\ Z_0 = \frac{E_0^-(x)}{H_0^-(x)}. \tag{36}$$

Disassembling the components of (36) into finer parameters, the free-space impedance is

$$Z_0 = \sqrt{\frac{j\omega_0\mu_0}{\sigma_0 + j\omega_0\varepsilon_0}}, \tag{37}$$

In (37), j is an imaginary unit, and ω_0 is the angular frequency. In the case of a dielectric where the conductivity is zero, the equation reduces to,

$$Z_0 = \sqrt{\frac{\varepsilon_0}{\mu_0}}. \tag{38}$$

Calculated at 20C and one atmosphere,

$$\begin{aligned} Z_0 &= 376.73\Omega \\ &= 119.92\pi\Omega, \end{aligned} \tag{39}$$

isolated from the conductivity of free-space for the value considered in the present definition of the unit of the Ampère. For any waveguide in the form of a hollow metal tube of conductivity σ_0, such as circular guide, the wave impedance of a traveling wave is dependent on the resonance frequency f_0, but is assumed uniform throughout the guide. For transverse electric (TE) modes of propagation the wave impedance is

$$Z_e = \frac{Z_0}{\sqrt{1-\left(\frac{f_c}{f_0}\right)^2}}, \tag{40}$$

where f_c is the cut-off frequency of the mode. For transverse magnetic (TM) modes of propagation this value is

$$Z_m = Z_0\sqrt{1-\left(\frac{f_c}{f_0}\right)^2}\,. \tag{41}$$

Above the cut-off $\left(f_0 > f_c\right)$, the impedance is real (resistive) and the wave carries energy. Below cut-off the impedance is imaginary (reactive) and the wave is evanescent, the latter shown to be an effective scheme [31]. These expressions neglect the effect of resistive loss in the walls of the waveguide, or at the surface boundary S_θ. The presence of a dielectric resulting from atmospheric phenomena chaotically shifts in impedance through π modifying f_c.

To keep selectivity as narrow as possible only the emission of a single frequency is discussed. The choice comes at a cost: impedance is not a function of the properties the circuit, rather, combined with that of free-space. The radiation pattern exhibits a topological surface from an energized oscillator. The field is quantifiable at certain lengths from the antenna but has fractal dispersion geometry, similar to task of calculating the length of a shoreline, so what constitutes the observable boundary is relative to the technical sophistication of the laboratory of the experimenter. Generally, the observable free-space electromagnetic field has its boundary at an edge where the energy stored at the horizon vanishes, as $\Phi_{\mathrm{M}} \to 0.$ Depending on the geometry of the coils and the intensity of energy stored, the boundary shifts.

Some applications where the waveguide or transmission-line containing more than one type of dielectric medium occurs, such as complex microstrip [27], in terms of the boundary conditions, the wave impedance will in general vary over the cross-section of the line, as a waveguide transient [28].

A similar notion, investigated by Aharonov-Bohm [29], suggests such a scheme at lower temperatures reveals interesting conclusions about the nature of S_θ. The dipole, as the supporting phenomenon of a coupled-mode in both its real and imaginary valued term, interacts with the space surrounding the loop causing the displacement **D**.

Referring to Fig.2.1, consider a system of resonators consisting of a pair of magnetic dipole loop antenna L_i, L_j separated by a distance, which contain a single coupled-mode [24]. L_i, L_j are set on a work-plane as to contain a periodic structure. To perform an analysis, a software package called *Comsol Multiphysics* is used to simulate the electromagnetic characteristics of the scheme. The work-plane consists of two circular loops of a material with conductivity σ_m and radius r_i. These loops are aligned in such a way so that the center of their radii shares a common axis or an axial alignment. The FEM layout is illustrated in Fig.2.11.

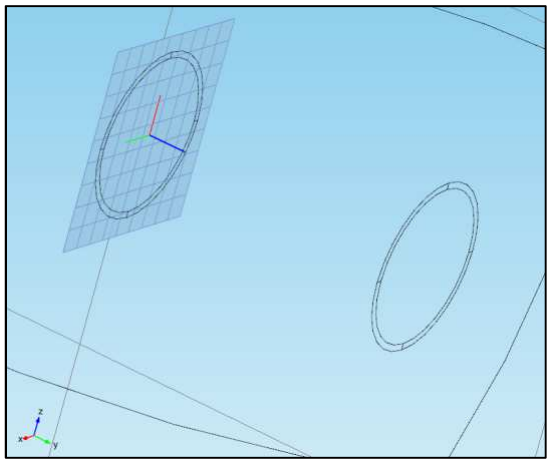

Fig.2.11. FEM model workspace layout.

The investigation is interested in considering small antenna sizes with a high efficiency. In the model, the loop size is the most critical property. If coil loop is wound at a specific ratio of circumference to wavelength, it is equivalent to an antenna connected to an electrically-short transmission line. To maximize the emission of radiation, the magnetic loop should be at a ratio of its circumference to its quarter wavelength. Such a magnetic loop will be shown to have the ideal ratio, $\Re_0$, in terms of maximum transmission efficiency, is when this ratio falls on an exponential scale,

$$\begin{aligned} \Re &= \frac{2\pi r_i}{0.25\lambda}, \\ \Re_0 &= 10^x, \\ x &= -1,-2,-3...n. \end{aligned} \tag{42}$$

This allows the model to allow loops with a radius of 3 centimeters that are set apart at a distance of 6 centimeters. The loop surface lies on the *x, y* plane while *z* between the loops forms the axial line.

In consideration of the efficiency of energy transfer, the receiving antenna collects electromagnetic photons, the amount given the area its surface occupies and the influence, in the form of feedback, it imposes on the space surrounding it [30]. With the introduction of a voltage gap, electrical energy is extracted in the form of power and work is performed by this method.

In consideration of the surrounding medium of free-space, the arrangement of the antenna in space is a periodic locally-approximated waveguide with implicit time-dependence $\mathrm{e}^{j\omega t}$; uncoupled spatial dependences are $e^{-j\beta_1 z}$ and $e^{-j\beta_2 z}$. In a coupled-mode, the spatial equations [24] are,

$$\begin{aligned} \frac{d}{dz}a_i &= -j\beta_i a_i - j2\kappa_{ij}\cos\left(\frac{2\pi z}{l}\right)a_j, \\ \frac{d}{dz}a_j &= -j\beta_j a_j - j2\kappa_{ji}\cos\left(\frac{2\pi z}{l}\right)a_i, \end{aligned} \tag{43}$$

given their coupling with a weak time dependence,

$$\begin{aligned} \frac{da_i}{dt} &= j\omega_i a_i + j\kappa_{ij}a_j, \\ \frac{da_j}{dt} &= j\omega_j a_j + j\kappa_{ji}a_i, \end{aligned} \tag{44}$$

relative to the coupled state of the resonators,

$$\kappa_{ij} = \kappa_{ji} = \frac{M_{ij}}{\sqrt{L_i L_j}}, \tag{45}$$

as a weakly-coupled system, where $\kappa_{ij} < 0.01$. This is in contrast to a “strongly-coupled” scheme [31]. The attention on weak-coupling is referring to the weak time dependence (44) for a system taking an assumption low coupling coefficient κ_{ij} affects efficiency η_{ij} weakly and properties of the circuit affect η_{ij} strongly.

2.1.1 The coupling coefficient

In consideration of the geometry of the scheme presented in the previous sections, the variables to be solved are: the coupling coefficient κ_{ij}, the mutual inductance M_{ij}, the quality factors Q_i and Q_j expressed by coils L_i and L_j, by the contributions of their fields E_0 and H_0.

To understand the effectiveness of the scheme and the work done at a distance, the energy-storage ability of the system is determined by the coupling coefficient in transfer mode. The intensity of flow of the energy across the distance is determined by κ_{ij} between coils L_i and L_j at a distance d. When a current I_0 is applied to coil L_i, the power transfer flows from coils L_i to L_j, and L_j to L_i.

The coupling coefficient in (45) is solved for a series of coils of characteristic size and geometry. The linkage between the series of magnetic resonant coils is defined at each coupling where M_{ij} is the mutual inductance, L_i and L_j are the self-inductances of the coils. The inductance can be calculated since its size and geometry are already specified, by the approximation of the inductance of a circular loop [32, 33]:

$$L_i \approx \mu_0 \mu_r n_i^2 r_i \left(\ln \frac{8r_i}{a_i} - 2 + Y \right), L_j \approx \mu_0 \mu_r n_j^2 r_j \left(\ln \frac{8r_j}{a_j} - 2 + Y \right), \tag{46}$$

Where r_i, r_j is the loop radius, a_i, a_j the wire radius, n_i, n_j the number of turns, and Y the flow constant of the skin-effect of the emitted radiation, given the resonance frequency, which is the approximated to be the same at the surface of both coils. The resonance frequency of the system,

$$f_0 = \frac{1}{2}\left(f_i + f_j \right), \tag{47}$$

is comprised of the resonance frequency $f_i, f_j, \ldots f_n$ of each of the coils,

$$f_{i,j} = \frac{1}{2\pi\sqrt{L_{i,j} C_{ij}}}, \tag{48}$$

and the frequency error between each half of the circuit,

$$f_e = \left| f_i - f_j \right|. \tag{49}$$

A consideration of the design is not only to keep the antenna small but also to keep the resonance frequency f_0 low enough as to not to be deleterious to human tissue. Studies have shown that a frequency spectrum between 100 kHz and 4 MHz is suitable [34]. The theoretical specification of the antenna is calculated where,

$$\begin{aligned} &n = 3, \\ &r = 30\,\text{mm}, \\ &a = 0.4\,\text{mm}, \\ &\varepsilon_0 = 8.85 \cdot 10^{-12}\,\text{F}\cdot\text{m}^{-1}, \\ &\mu_0 = 4\pi \cdot 10^{-7}\,\text{H}\cdot\text{m}^{-1}, \\ &\mu_r = 0.99994, \\ &Y = 0. \end{aligned} \tag{50}$$

The material properties of the coil is for an insulated copper wire wound in concentric loops so the total loop surface is comprised of a number of turns. Equal to a Litz winding, each turn insulated from the other reduces the contribution of the skin effect Y.

The winding has legs as to allow the loop to be mounted into a circuit board and projected along a plane linear to the earth. The additional inductance of the legs is taken into consideration. A C#.NET program called *Circuit calculator*, built specifically for performing and visualizing the relationships of the values of wireless power by magnetic resonance, calculates the theoretical specification of the model. Given (48), a capacitance of 100nF is chosen; the calculation sequence is shown in Fig.2.12. The table of values for the model loops $L_{i,j}$ and resonance frequencies $f_{i,j}$ is listed in Table 2.1.

Table 2.1. Loop coils theoretical specification.

TABLE 2.1
LOOP COILS THEORETICAL SPECIFICATION

Coil	L_i	L_j
Coil radius (mm)	30	30
Wire radius (mm)	0.4	0.4
Wire length (cm)	65	65
Number of turns	3.5	3
Leg length (cm)	3	3
Number of legs	3	2
Loop inductance (μH)	2.0306	1.4918
Total inductance (μH)	2.1207	1.5519
Resonance frequency (Hz)	345607.761	404004.671
Differential frequency (Hz)		58396.910
System frequency (Hz)		374806.212
Differential system frequency (Hz)		433203.126
Wavelength (m)		692.037

In terms of the prototype, a frequency of approximately 400 kHz is expected to be the resonance frequency for the physical loop antenna. Mutual inductance is next to be solved.

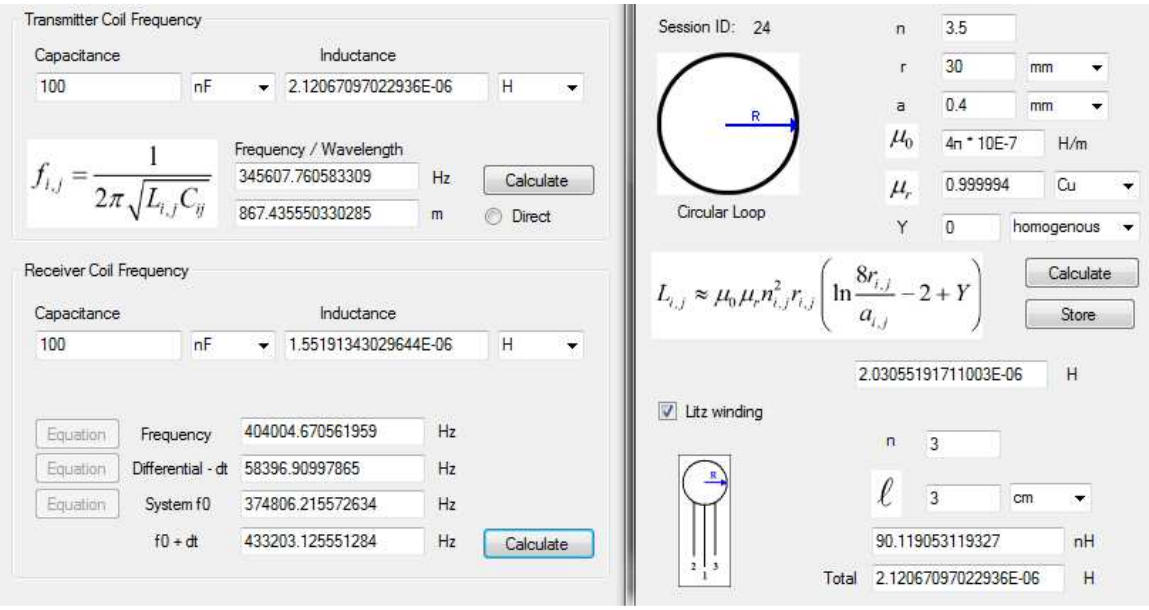

Fig.2.12. Calculator values for (a) system resonance frequency, and (b) inductance of the transmission loop.

Mutual inductance

The mutual inductance between two coils is dependent purely on the geometry of the scheme. An energized loop affects action at a distance. Its attraction, or mutual inductance, is given by the Neumann formula [35],

$$M_{ij} = \frac{\mu_0}{4\pi} \oint_{C_i} \oint_{C_j} \frac{s_i \cdot s_j}{|d|}. \tag{51}$$

The infinitesimal positions s_i and s_j in (51) are derived under the assumption that the magnetic field is evenly distributed, more concentrated toward the center of the loop than in other places, and in a mostly linear distribution. In this form, the loop wire is considered to be contained of coaxial circular filaments [32].

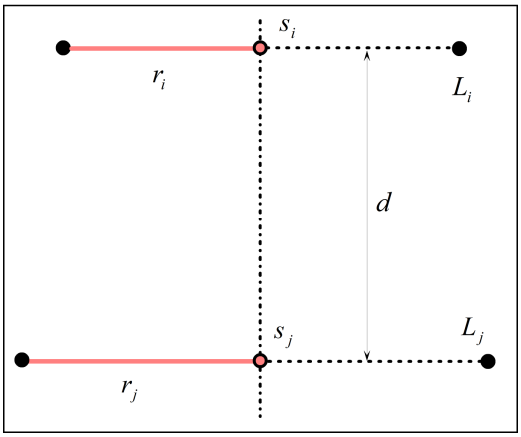

Fig.2.13. Coil properties describing (51).

Mutual inductance is exclusively the property of coupling between coils L_i and L_j. The magnetic flux intercepted by one coil is analogous to a unit of current flowing in the other [36], the mutual inductance of the i^{th} and j^{th} elements and the integration over the surface S_θ show the mutual inductance is also,

$$M_{ij} = \frac{\int\int_{S_j} \mathbf{B}\cdot\vec{\mathbf{n}}\,dS}{I_{L_i}}, \tag{52}$$

where $\mathbf{B}$ is the flux intercepted by the receiver coil, I_{L_i} is the current passing through the first coil, $\mathbf{n} = \left(n_x, n_y, n_z\right)$ is the unit surface normal vector, and dS is an infinitesimal area element of the local appearance of S_θ as S_j. It is possible to transform the surface integral in (52) into a simpler line integral by using the magnetic vector potential,

$$\mathbf{B} = \nabla\times\mathbf{A}, \tag{53}$$

together with Stokes theorem, which states that a surface integral of the curl of a field equals the closed line integral over the rim of the surface,

$$M_{ij} = \frac{\int\int_{L_j} (\nabla\times\mathbf{A})\cdot\mathbf{n}\,dS}{I_{L_i}} = \frac{\oint_{S_\theta} \mathbf{A}\cdot\mathbf{t}\,dl}{I_{L_i}}, \tag{54}$$

where $\mathbf{t}=\left(t_x,t_y,t_z\right)$ is the unit tangent vector of the curve S_θ and *dl* is an infinitesimal line element. The mutual inductance, then, depends upon the parameters $\frac{r_i}{r_j},\frac{d}{r_j},$ and its proportionality to the radii, as,

$$M_{ij}=\mu_0\sqrt{r_i r_j}\,\frac{2}{\alpha}\left[\left(1-\frac{\alpha^2}{2}\right)K(\alpha)-E(\alpha)\right], \tag{55}$$

where $K(\alpha)$ and $E(\alpha)$ are elliptic integrals and α is obtained by,

$$\alpha=\sqrt{\frac{4r_i r_j}{\left(r_i+r_j\right)^2+d^2}}. \tag{56}$$

Using [32] to find the value where,

$$M_{ij}=\alpha\sqrt{r_i r_j}=\alpha r_j\sqrt{\frac{r_i}{r_j}}\,(\mu\mathrm{H}), \tag{57}$$

Where α is determined as depending on the variable,

$$u^2=\frac{\left(1-\frac{r_i}{r_j}\right)^2+\frac{d^2}{r_j^{\,2}}}{\left(1+\frac{r_i}{r_j}\right)^2+\frac{d^2}{r_j^{\,2}}}, \tag{58}$$

from (53). A calculation was performed in *Circuit calculator* for the mutual inductance M_{ij} based on (57) and (58) from the specifications listed in Table 2.1,

$$\begin{aligned} u^2&=0.5,\\ M_{ij}&=0.0042558\,\mu\mathrm{H}, \end{aligned} \tag{59}$$

where the result is used to calculate the discrete value of

$$\kappa_{ij}=0.002346. \tag{60}$$

The coupling strength between resonators is described by the coupling coefficient. Besides what has already been described as methods for calculating the coupling strength, another method [37] is to consider the bandwidth of the transmission, as

$$\text{bandwidth} = \frac{2\left(f_i - f_j\right)}{f_i - f_j}, \tag{61}$$

Where f_i and f_j are the split resonance frequencies of the resonators, which are most effective using a narrow bandwidth. In the sense of the arrangement illustrated in Fig.2.35, there is shown a separation of the resonators into their electric and magnetic components. To maintain cohesion in the beam of energy exchanged between L_i and L_j, insights into the *why* the coupling is so significant to magnetic resonant power transmission are important to ascertain. A novel approach [38] called the perturbation method, strives to glean insights about those components which most affect the overall coupling. The following equation, modified,

$$\kappa_{ij} = \frac{\int_{L_i} \mu H_0^+ \cdot H_0^* dv - \int_{L_i} \varepsilon E_0 \cdot H_0^- dv}{\int_{L_j} \varepsilon \left|E_0\right|^2 dv}, \tag{62}$$

implies that the motivation to understanding the coupling coefficient is where E_0^- makes the strongest contribution toward the intensity of H_0^+ and what circuital components would support the transfer. It also suggests that increasing the amount of magnetic field at the loop would result in additional improvements. In its most basic sense, answering these subtle questions takes time and experience and they are addressed as motivations in this thesis; they will irrevocably remain a most important topic of future research. However, the author can identify that it is the *contribution of potential magnetic vector decomposition on the interface*, which is of greatest importance to grasp if understanding of the scheme is to advance.

The description of the interface is that of the loop is in situ with free-space. The transmission loop and the “amount of magnetic lines” crossing the receiving loop is a typical description of a radiated magnetic field and its effect on distant objects. An example is shown in Fig.2.14.

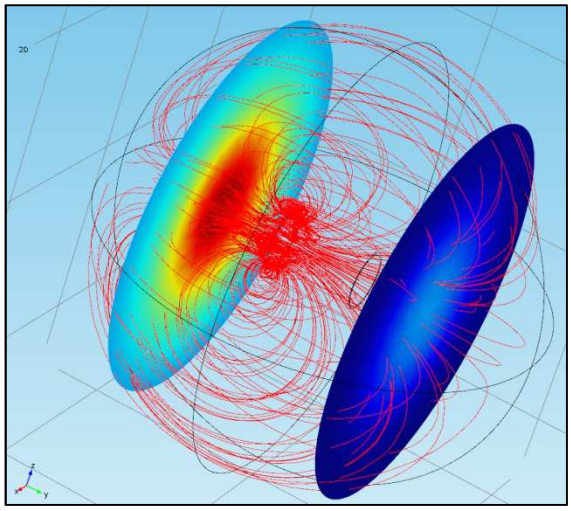

Fig.2.14. Magnetic coupling of low-κ modes of distant resonators in space and time.

As noted in [39], the distance does not affect modal coupling, rather, spatial extensions in the z direction relate more closely to the transport of electrical power due mutual inductance, expressed in the **E** and **H** fields. In such effects, broadcast power is subject to attenuation over the impedance of free-space if the potential is assumed to contribute minimally to the fields. Nevertheless, it is important to keep in mind that the boundary does not describe and is independent of the sinusoid as well as its wave function. Therefore, the presence of the antenna and the presence of physical free-space constitute the entirety of the signal. If one considers the argument that the waveform is unique from its conductor—in the manner of induction described by Faraday as well as the original equations of Maxwell—the disturbance and the displacement open the door to questions of what in free-space is allowing the equilibrium of the forces of the currents driving radiation and its influence between antenna at distances greater than those described for the skin-effect.

To model the relative position and motion of the energy in terms of the exchange of photons, the path and intensity is described by the density of magnetic lines, illustrated in Fig.2.14.

The antenna, by the nature of its size, geometry, and symmetry couples the magnetic component of the energy on the coil-wire surface to an interface [30]. Under closer examination and consistent with the circuit architecture, the presence of the impressed wave is wholly due to the properties of the inductor L_i, L_j with the potential of free-space $\mathbf{A}$ given its impedance Z_0. The magnetic loop, at a ratio to its quarter wavelength, contains the effects of a full ac cycle impressed on it by the incident wave in terms of transmission or reception.

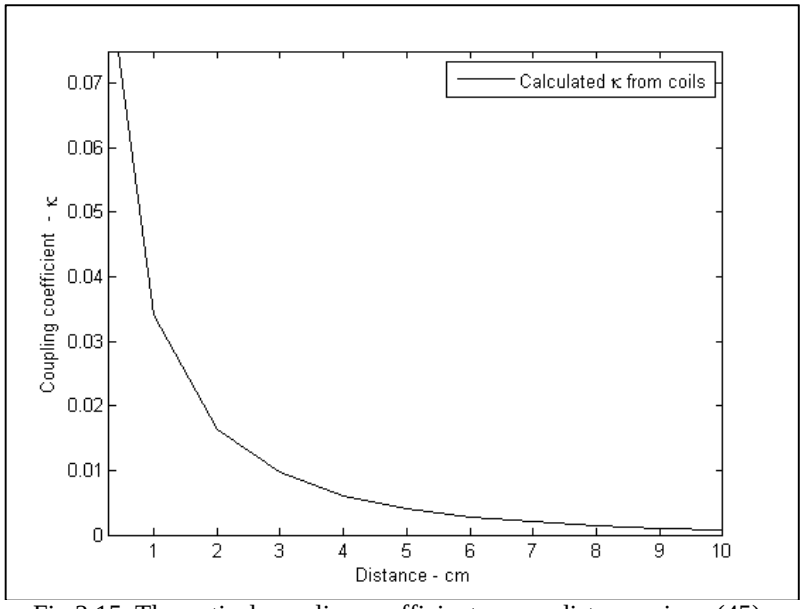

Fig.2.15. Theoretical coupling coefficient over a distance given (45).

The data in Fig.2.15 is derived from the calculation of coupling, shown in (45) in context of antenna as a function of transmitted power, in the manner of free-space interpretation of (48, 52, 54). The result is the value of κ_{ij} attenuated by free-space. As is shown, the solution of this type of description suggests that a different analytical tool is required to show the mechanisms responsible for energy transmission. As the purpose of the arrangement is to transport energy efficiently, the numerical solution of the circuit power is intended to measure the quantity of energy stored between the resonators and the dissipated power at the receiver available to a load. Therefore, coupled-modes in space describe the distribution of an energized field while coupled-modes in time yield the rate at which energy is transported.

2.1.2 Coupled-mode power

The energy stored and dissipated between two coupled objects describes a power distribution system. While the pursuit of a wired analog is desirable to some applications [10], for the purposes here, it is more effective to consider the coupling in terms of energy transport by the virtual waveguide. It is argued by the author that this particular methodology will yield greater insights not only about the model under investigation, but also about the environment where the model is operating.

Energy transfer is an observable result in the context of forces moving charges. In the driven case, one can quantify forces due to amplification. In more subtle cases, the distribution of forces on charges is described by the Lorentz-Fitzgerald transformation [40, 41] used in special relativity and the source of Minkowski light cones and other innovative spatial geometries with moving forces [42, 43].

The Larmor force transfers energy between the field and the charges. The power $F \cdot v$ of the force equation is $q\mathbf{E} \cdot v$, thus the power received by the electric charges per unit of volume is $\mathbf{E} \cdot \mathbf{J}$. Charge carriers convert power at the receiver from the local electromagnetic field into other forms of energy, including the kinetic energy of particles. Conversely, $\mathbf{E} \cdot \mathbf{J}$ can be negative, in which case there is a transfer of energy from the charge carriers to the field. One process is as a time reversal of the other. In this, it is preferred to retain the family-time solution of Maxwell's equations to the motion of the sources and changes in the field that are reticent.

The geometry of a circular loop is such that the radiation takes the pattern of a hyperbolic function, a transmitter of a primary loop in an exchange of energy with a primary loop of a receiver in a theoretical context is shown in Fig.2.7.

In terms of the total magnetic intensity, $\mathbf{H}$, comprised of the projection $\bar{\mathbf{H}}$, and the flux density as $B_0 = \mu_0 H_0$ emitted between antenna. Solving $\nabla \times \boldsymbol{\upsilon}_{ij}$ for all desired measurement points of H_0 will indicate the amount of energy the field stored at the given point. To calculate this value reliably, it will require a fitted solution to Poynting's Theorem.

It is desirable to express the energy as a property of the electric field and current density and compare this with the value of $\nabla \times \boldsymbol{\upsilon}_{ij}$ for an arbitrarily-given H_0. The quantity $\mathbf{E} \cdot \mathbf{J}$ is expressed in terms of the electromagnetic fields by taking the dot product of the current density into $-\mathbf{E}$ on both sides of the Ampère-Maxwell equation,

$$-\mathbf{E} \cdot (\nabla \times \mathbf{H}) + \mu_0 \mathbf{H} \frac{\partial \mathbf{H}}{\partial t} + \varepsilon_0 \mathbf{E} \cdot \frac{\partial \mathbf{E}}{\partial t} = -\mathbf{E} \cdot \mathbf{J}. \tag{63}$$

The identity,

$$\mathbf{E} \cdot (\nabla \times \mathbf{H}) = \mathbf{H} \cdot (\nabla \times \mathbf{E}) - (\nabla \cdot \mathbf{E}) \times \mathbf{H}, \tag{64}$$

and Faraday's law yield,

$$-\mathbf{E} \cdot (\nabla \times \mathbf{H}) = H_0 \cdot \frac{\partial H_0}{\partial t} + (\nabla \cdot \mathbf{E}) \times \mathbf{H}. \tag{65}$$

The point where this occurs is at a potential value for equilibrium of the energy exchange between H_0 and the current density at an arbitrary point,

$$(\nabla \cdot \mathbf{E}) \times \mathbf{H} + \frac{\partial}{\partial t} \frac{\varepsilon_0 \mathbf{E}^2 + \mathbf{H}^2}{2} = -\mathbf{E} \cdot \mathbf{J}, \tag{66}$$

yields Poynting's theorem around that point.

$$\mathbf{S} = \mathbf{E} \times \mathbf{H}, \tag{67}$$

showing the density of power is emitted is a relative property of the antenna at the interface [107]. At any point in the volume, given the possible locations shown in Fig.2.7, the time-averaged energy stored is,

$$\frac{1}{2} \varepsilon_0 \left(\mathbf{E}^2 + c^2 \mathbf{H}^2 \right). \tag{68}$$

Equation (68), a derivation of the Poynting theorem, will show that a variation of energy in a given volume comes from power that is either delivered directly by sources or radiated across the surface—as flux flowing along a cavity or in this particular model, a virtual waveguide. The implication is that a perfect electrically-short loop antenna at a favorable ratio would have efficiency of radiation at maximum, indicating a related amount of power transfer and energy storage in the volume.

The physical model is for the case of circular loops in §2.3.1. These cavities, while homogenous in free space, maintain a total internal reflection [84]. To sustain the state of equilibrium of the field, an opposing force is allowing the suspension. This implies a force-driving element, appearing in the circuit as the acceleration value of electrons flowing in the conductor of the antenna.

The observable behavior in the physical model will be discussed firstly from the point-of-view of the magnetic potential $\mathbf{A}$ as $\mathbf{B} = \nabla \times \mathbf{A}$, then to the transition to circuital mathematical properties.

2.1.3 Efficiency, quality, and loss

To understand the behavior of coupled-mode characteristics, described in §2.1.1, these are used in real-world problems. The worthiness of the model is in terms of its overall efficiency, that is, by a comparison between the energy stored at the input to the energy dissipated including those in losses. The efficiency of the model is measured by the equation [44],

$$\eta_{ij} = \frac{\kappa_{ij}^2 Q_i Q_j}{1 + \kappa_{ij}^2 Q_i Q_j}, \tag{69}$$

Where η_{ij} is dependent on the coupling coefficient κ_{ij}, but also by the qualities Q_i and Q_j of the coils L_i and L_j. The quality of a coil [45] is obtained,

$$Q_i = \frac{\omega_0 L_i}{R_i}, Q_j = \frac{\omega_0 L_j}{R_j}, \tag{70}$$

as a property of the energy stored in the angular frequency ω_0 the inductance L, and the free-space projection $\bar{H}_0$ with the dissipation by the resistance R of the i^{th} and j^{th} coils. The quality factor is then determined by,

$$\frac{1}{Q_i} = \frac{1}{R_i}\sqrt{\frac{L_i}{C_i}} + \frac{1}{R_{pi}}\sqrt{\frac{L_i}{C_i}} = \frac{1}{Q_{R_i}} + \frac{1}{Q_{L_i}} \tag{71}$$

comprised of the inductance L, resistance R, and capacitance C, and of the i^{th} and j^{th} coil in the oscillator and receiver circuits. The scheme is defined so that the system is performing work, the unloaded quality Q_{L_i} is neglected. The quality factors then become,

$$Q_i = \frac{1}{R_i}\sqrt{\frac{L_i}{C_i}}, Q_j = R_j\sqrt{\frac{C_j}{L_j}}, \tag{72}$$

for both cases of a series and parallel configuration in an ideal circuit arrangement. The coils are arranged within their respective circuits as to maximize the amount of energy stored between the inductances and the capacitances. The maximum energy stored in $L_{i,j}$ and $C_{i,j}$ is,

$$\begin{aligned} u_{L_i} &= L_i I_0^2,\ u_{C_i} = C_i V_0^2, \\ u_{L_j} &= L_j I_R^2,\ u_{C_j} = C_j V_R^2, \end{aligned} \tag{73}$$

which is discussed in greater detail in §2.3.1. The loop can be treated as a standard oscillator in coupled mode defining (43)(44) as

$$a_i(t) = \sqrt{\frac{L_i}{2}} I_0(t). \tag{74}$$

It is well-understood that quality factor has a direct consequence upon the efficiency of an electrical transmission circuit.

The remaining component relevant to the properties of coupled-modes is the losses in the system resulting from the materials used in the construction of the loops. Losses in the system are observed as dissipation of the energy stored. For the losses due to ohmic resistance [58],

$$R_{i,j} = \sqrt{\frac{\mu_0 \omega_0}{2\sigma_m}} \sum_{i=1}^{n_i} \sum_{j=1}^{n_j} \frac{\ell_{i,j}}{4\pi r_{i,j}}, \tag{75}$$

Where σ_m is the conductivity of the material, n the number of turns, ℓ the wire length of the coil, and $r_{i,j}$ the wire radius of the i^{th} and j^{th} coils. The calculation of the quality factor and the losses for the system are shown in Table 2.2.

Table 2.2. Energy, quality, and loss specification.

TABLE 2.2
ENERGY, QUALITY, AND LOSS SPECIFICATION

Coil	L_i	L_j	L_m
Resonance frequency (Hz)	345607.761	404004.671	433203.126
Oscillator current (A)	1.25		
Oscillator voltage (V)	6.20		
Ohmic resistance (Ω)	0.00593	0.00508	168820.035/cm
Energy storage (μJ)	7.158	6.269	
Quality factor	776.583	775.472	3.225
Magnetic field **B** (T)	2.618E-05		
Scheme efficiency	0.7682		

Column L_m in Table 2.2 is provided for the object impressed on free-space as a function of the inductance and resistivity of the medium. Averaged, the potential efficiency is very high for the coupled-mode, although it will be shown in experiments that it is transformed solely on the properties of the material consisting the antenna. In *local* space, the efficiency is observed to be very high but it refers to the ability of the loop to transform the acceleration of electrons into photons, not including any of those quantum considerations here. Efficiency of the transmission over distance is the linear decay of power over $1/r$. This is discussed in terms of radiated power of the antenna in §2.3.2. Energy storage in Table 2.2 is shown per cycle.

With these baseline criteria for the expected properties of the antenna as a function of the materials and geometry of the wire established, the next chapter will address the circuit model that can sustain the oscillations. The criteria is the means by which differentiating models will be judged to be used in commonplace application, such as that in §2.4. The system under consideration is designed with compactness in mind and each component chosen for an expected level of performance. The purposeful choice of using the type of oscillator described herein is not by accident; it is chosen for its simplicity and size.

2.1.4 The magnetic potential

The magnetic vector decomposition is useful to describe the nature of the field object between the resonators as a result of the forces that shapes the object. The field model is centered around the assumption that the geometry can be understood from topological arguments of the forces in the region.

The model uses the magnetic vector potential $\mathbf{A} = \left(A_x, A_y, A_z \right)$ to construct a finite solution by casting a projection A_t as the dot product of the tangent vector and the magnetic potential, as,

$$A_t = A_{t_x} \cdot t_x + A_{t_y} \cdot t_y + A_{t_z} \cdot t_z. \tag{76}$$

(76) is the response of the potential to the disturbance of the wave. Its magnitude is relative to the energy stored in the field object. While not appearing inside the field, it occurs at the limit of the field at its boundary and is symmetrical along the space between coupled-mode objects. The field has dispersion dependent on the geometry of the antenna; the transmitter and receiver placed at separations in all three Cartesian directions. The unity of the potential in context with the field object is observable under measurement of an unpowered antenna and is extant at the nulls to the left and right minor lobes. Modal magnetic resonance coupling is more effective at describing magnitudes of magnetic flux density in terms of the potential, one such is description is in terms of displacement currents.

The antenna loop carries a complex current,

$$I\left(t\right) = I \cos \omega t, \tag{77}$$

which is confined to the loop near its surface—the surface of the conductor consisting of Litz wire. The vector potential from the loop is expressed as,

$$\mathbf{A}\left(r\right) = \frac{\mu_0 \mathbf{I}}{4\pi} \oint_{\ell} \frac{e^{-jkr'}}{r'} dl', \tag{78}$$

where $\mathbf{I} = I \cos \omega t$. To simplify the appearance of the harmonic current in the following equations, it is expressed as

$$\mathbf{I} = \mathbf{u}_{\gamma}. \tag{79}$$

By inspection of (78), the evaluation of the potential depends of the location where dl' is being observed, as anticipated. Expansion of the exponential form,

$$e^{-jkr'} = e^{-jkr} e^{jk(r-r')} \approx e^{-jkr}\left[1 - jk\left(r' - r\right)\right], \tag{80}$$

similar to the approximation of the electric dipole [21]. Equation (78) is written as,

$$\mathbf{A}(r) = \frac{\mu_0 I}{4\pi} e^{-jkr}\left[\left(1 + jkr\right)\oint_\ell \frac{dl'}{\rho'} - jk\oint_\ell dl'\right]\mathbf{u}_\gamma. \tag{81}$$

For the purposes here, the second integral in (81) is zero since all it indicates is to continue moving the observation around the circle to the starting point of integration. Therefore, evaluation of the first integral in (81) yields, by vector identity [46],

$$\oint_\ell b dl' = \int_{\Delta s}\left(\mathbf{u}_\mathbf{n} \times \nabla b\right)\cdot ds, \tag{82}$$

to convert to a surface integral. The scalar b is equal to the inverse of the amplitude $1/r'$, the unit vector $\mathbf{u}_\mathbf{n} = \mathbf{u}_\mathbf{z}$, since the loop is wholly in the $x-y$ plane and projecting along z. This results the vector to be decomposed into,

$$\begin{aligned}\oint_\ell \frac{dl'}{r'} &= \int_{\Delta s}\left(\mathbf{u}_\mathbf{z} \times \nabla \frac{1}{r'}\right)\cdot \mathbf{u}_\gamma ds, \\ &= -\int_{\Delta s}\left(\mathbf{u}_\mathbf{z} \times \nabla \frac{\mathbf{u}_{r'}}{\left(r'\right)^2}\right)\cdot \mathbf{u}_\gamma ds,\end{aligned} \tag{83}$$

where the surface integral yields the factor πa^2. Because it is expected by geometric inspection the shape to be homogenous and elliptical, the result requiring representation in spherical coordinates. Taking the vector relation,

$$\mathbf{u}_\mathbf{z} \times \mathbf{u}_\mathbf{r} = \sin\theta \mathbf{u}_\gamma, \tag{84}$$

gives,

$$\oint_\ell \frac{dl'}{r'} = \frac{\pi a^2}{r^2}\sin\theta. \tag{85}$$

Using (84) in (81) and evaluating reveals the interaction of the vector potential with the field object. This is,

$$\mathbf{A}(\mathbf{r}) \approx j\frac{\mu_0\left(I\pi a^2\right)\kappa}{4\pi}\frac{e^{-jkr}}{r}\sin\theta\mathbf{u}_\gamma. \tag{86}$$

Equation (86) suggests there are observable effects at the boundary between the field object and the potential. The result was simulated and is shown in Fig.2.16.

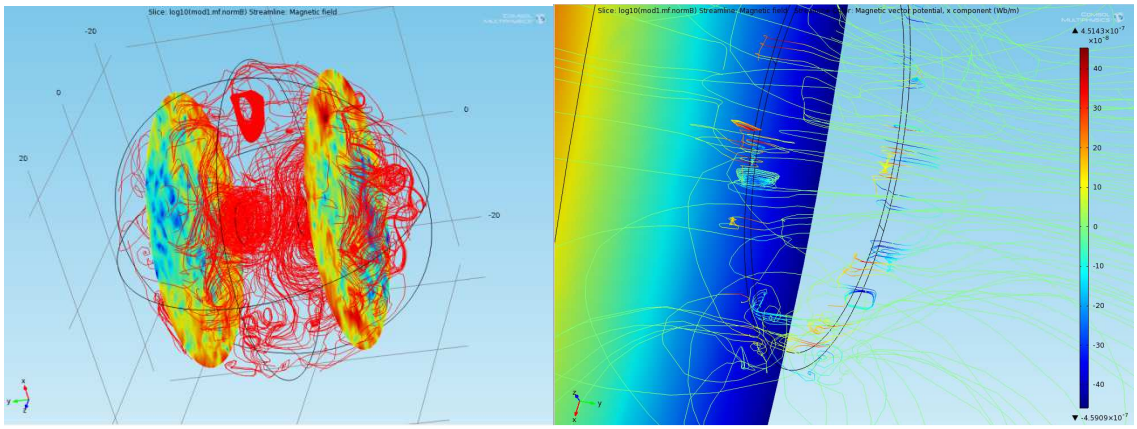

Fig.2.16. (a) The vector potential in the magnetic field, (b) the potential component on the loop interface.

The simulation shows that the electromagnetic potential in enmeshed in the field, as predicted, but also is in motion at the boundary between the field and free-space following the $x-y$ plane of the loops. What is interesting is that motion is closely connected to the interfacing of the loop and the medium and that it occurs in differential degrees of magnitude. What is *most* interesting is that if the potential can influence the line integral at the interface. If it can significantly move it away from zero, it would show a second coupled mode inside the scheme.

Two questions asked are: is the potential, $\mathbf{A}$, a component of the entirely contained within the magnetic intensity $\mathbf{H}$, else a coupling to $\mathbf{B}$? Is it a property of the medium inferring a transfer of force between $\mathbf{B}$ and $\mathbf{A}$? The use of the Maxwell displacement current $\mathbf{D}$ is the form of the displacement because of the forces between antenna and a field object [47], as,

$$\mathbf{B} = \nabla\times\mathbf{A} = \frac{\mu_0}{4\pi}\int\frac{j\times r}{r^3}d\upsilon + \frac{\mu_0}{4\pi}\int\frac{(\partial\mathbf{D}/\partial t)\times r}{r^3}d\upsilon. \tag{87}$$

The sequence of solutions to find the potential, in terms of a circuit, is difficult when trying to decompose the potential vector on the interface to quantify the dependence of the potential on coupling; this is especially difficult when there is no definition, outside of the impedance, of free-space. We have free-space in the sense of that on a planet, we have free-space in the sense of the "vacuum" of outer space, and we have the contention that there is dark matter filling the apparently empty space. Can there be a unification [25, 48] by using the Minkowski cones and time dilation of

Einstein's special theory? Are electromagnetic forces and the charges that populate them strictly dependent on the quantum effects, i.e., the duality of the electron [49] and its esoteric properties? Can wave-particle duality be expressed in such energized structures? The author contends this provides sufficient material to support the notion of free-space waveguides, constructed by the scheme, and energy can be transmitted across them. It could very well indicate evidence of properties only visible in the quantum universe, are also available to the macro world [50]. The model would then be described topologically as a waveguide field [51], $\mathrm{WG} \rightarrow \mathrm{F}$, and the primary contributor to the closure of currents in an open circuit across free-space.

The substantive claim presented in this thesis is of an independence of the magnetic field from its electric counterpart in terms of force and attraction—described in terms of the magnetic potential at the interface of the antenna. It is most observable under particular conditions in the antenna where the radius of the antenna is expressed as a ratio, $\Re$, of the loop circumference to its wavelength as an exponential function, shown in (42), whose $\mathbf{B}$ field takes the form of (21) and (22), upon application of a true conduction current the field lines extend from the center of the loop form a hyperbolic plane along the z and $-z$ directions, as shown in Fig.2.17.

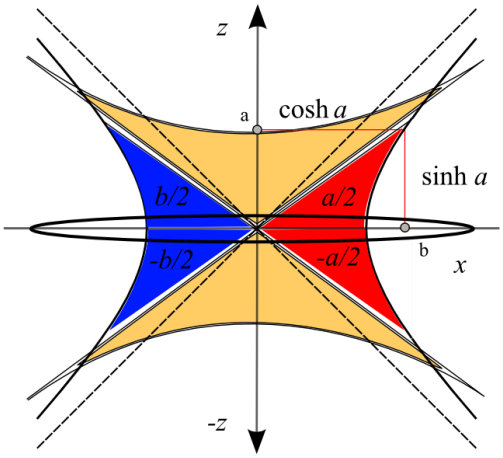

Fig.2.17. A single loop projecting a magnetic field.

The presence of the field in free-space emitted by a magnetic loop is obtainable by discrete trigonometric functions, given its projection [30]. The effective area, where forces deform the isotropy into a discernible shape, transforms into a composite of sufficient flux density providing the appearance of a closed surface. The equilibrium of the area is dependent upon the magnetic energy contained within and where the boundary is discerned. Although in fact the boundary is indeterminate at extreme positions along the curvature of field propagation, where the received power approaches zero is such a boundary. Description of this boundary is given by the infinitesimal of the magnetic field. The surrounding free-space is considered as a periodic locally-approximated waveguide [107]

with implicit time-dependence $e^{j\omega t}$ that, uncoupled, have the spatial dependences $e^{-j\beta_1 z}$ and $e^{-j\beta_2 z}$, respectively where $\beta_1 \approx \beta_2$ are propagation constants. For the geometry shown in Fig.2.8 with a period Λ, the coupling coefficient takes the form $2\kappa_{TR}\cos\left(2\pi z/\Lambda\right)$. The spatial equations (43) given their weak time dependence of amplitudes a_T and a_R (44), and coupled state (45), when equivalent to the relationship of the stored energy at resonance via conductance G and resistance R attenuating the transmission, contributing simultaneously to a complex impedance Z_0 and admittance Y_0, construes that the forces exchange energy in constructive and destructive interference patterns as a global oscillatory force representing the waveguide [26, 107, 111].

It is proposed that if a special circuit could accelerate electrons in an antenna, the emitted radiation could be controlled and directed by manipulating the presence of the magnetic component. An increase of **B** will yield a greater mutual inductance (54). With the addition of metallic accretion discs, that is, "accretion" meaning discs forming a uniform conductive surface, lying in the x-y plane and projecting along z so that a corona effect occurs in the gap between the disc and the inner loop surface. Such discs are aligned with their centers at the same point as the loop center, illustrated in Fig.2.18.

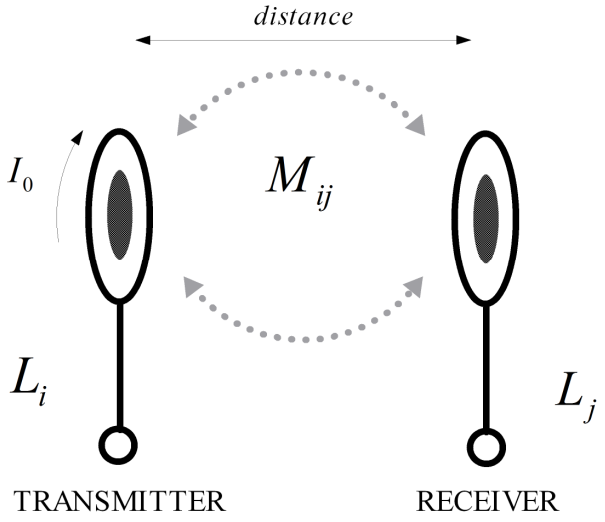

Fig.2.18. Schematic drawing of two circular loops with center discs.

Under normal atmospheric pressures and temperatures, a magnetic field has a potential flux density which is evenly distributed, is concentrated toward the center of a loop rather than in other places, and can be modified to induce currents at a distance [107]. An energized circular loop antenna emits a magnetic field of a given intensity which is a product of the current dependent upon a spherical

surface and the geometry expressed by the antenna. The radius r_i of the loop i is given as a ratio, $\Re_i$, of loop circumference to resonance wavelength, λ_i, expressed as an exponential power function v,

$$\begin{aligned} \Re_i &= \frac{2\pi r_i}{(0.1)0.25\lambda_i}, \\ \Re_i &= 10^v, \\ v &= -1,-2,-3...n. \end{aligned} \tag{88}$$

With respect to the loop described by (124), the magnetic field in the x-y plane takes the following form,

$$B_{xy} = \frac{\mu_0 I_0}{4\pi r_i^2} \cdot 2\pi r_i = \frac{\mu_0 I_0}{2r_i}. \tag{89}$$

where I_0, is the current applied to the loop. Contrastingly, the field at a distance d along the z-axis from the center of the loop i is,

$$B_{\mathbf{z}} = 2\pi r_i \frac{r_i}{d} \frac{\mu_0 I_0}{4\pi d^2} = \frac{1}{2} \frac{\mu_0 I_0 r_i^2}{\left(d_{\mathbf{B}}^2 + r_i^2\right)^{\frac{3}{2}}}, \tag{90}$$

in which $d_{\mathbf{B}_z}$, is the ordinal field distance. When a current, I_0, is applied to the loop, the magnetic field lines extend from the center of the loop and form a curvature as a hyperbolic plane along the z and $-z$ directions, as illustrated in Fig.2.17.

The presence of the field in free-space emitted by a magnetic loop is obtainable by discrete trigonometric functions, given its projection. The effective area, where forces deform the isotropy into a discernible shape, transforms into a composite of sufficient flux density providing the appearance of a closed surface.

The equilibrium of the area is dependent upon the magnetic energy contained within the area and where the boundary is discerned. Although the boundary is indeterminate at extreme positions along the curvature of field propagation, where the received power approaches zero is such a boundary. Description of the momentum of energy propagation is given by the infinitesimal of the magnetic field.

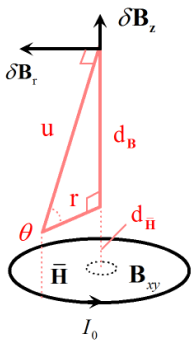

Fig.2.19. Geometry of a projection and infinitesimal field in the circular loop.

Fig.2.19 illustrates the geometry of the energy pattern emitted from a circular loop by its intensity in motion across free-space, displacing the space given its magnitude, $\bar{\mathbf{H}}\cdot\delta\mathbf{B}_z$, in both the positive and negative directions of z. The phenomenon of projection, $\bar{\mathbf{H}}$, is manifest as a wavefront from a transmission antenna where an acceleration force has been applied to electrons on its conductive interior. The length and intensity of the projection is due simultaneously to the geometry of the antenna and the power applied to it.

In Fig.2.19, the length of transmission along the z-axis is a component consisting of the projection field length $d_{\bar{\mathbf{H}}}$ and the ordinal field distance $d_{\mathbf{B}_z}$, given its radial size, $r_{\mathbf{B}_r}$, and the infinitesimal field $\delta\mathbf{B}$. The length of u is given by the persistence of amplitudes to the limit of their ambience, manifest as $\mathbf{B}$ given in both directions of propagation in z. By calculating the angle θ and integrating around the loop, one can determine the amount of energy present in $\mathbf{B}$.

The magnetic flux density is dependent upon the current applied to the loop antenna. An increase of $\mathbf{E}$ or $\mathbf{B}$ will quasi-linearly increase the flux density of the field, given thermodynamic laws. The assumption is that an increased $\mathbf{B}$ will yield an equal increased amount of $\mathbf{E}$ in the model.

The model under consideration is a weakly-coupled, low κ, system at resonance behaving analogously to a locally-approximated transmission-line resonator [31, 111]. Under such conditions, the complex current and voltage operating on the loops take the form,

$$\begin{aligned} I(z) &= I_0 \cos\left(\frac{\pi z}{l}\right), \\ V(z) &= -jZ_0 I_0 \sin\left(\frac{\pi z}{l}\right), \end{aligned} \tag{91}$$

where I_0 is the current in the short-circuit and l is the length of the attractive transmission path. The simple impedance, Z_0, is that of free-space, ~377Ω. The average stored magnetic energy $\langle W_m \rangle$ in the loop at resonance ω_0 is,

$$\begin{aligned} \langle W_m \rangle_{\omega_0} &= \frac{1}{4}\int_0^l L|I_z|^2\, dz = \frac{1}{4}L|I_0|^2 \int_0^l \cos^2\left(\frac{\pi z}{l}\right) dz \\ &= \frac{1}{8}Ll|I_0|^2. \end{aligned} \tag{92}$$

The average stored electrical energy does not need to be calculated separately since the system is at resonance. i.e., $\langle W_e \rangle_{\omega_0} = \langle W_m \rangle_{\omega_0}$ as,

$$\langle W_{total} \rangle_{\omega_0} = \langle W_e + W_m \rangle_{\omega_0} = \langle 2W_m \rangle_{\omega_0} = \frac{1}{4}Ll|I_0|^2. \tag{93}$$

The surrounding free-space is considered as a periodic locally-approximated waveguide [24, 107] with implicit time-dependence $e^{j\omega t}$ that, uncoupled, has the spatial dependences $e^{-j\beta_1 z}$ and $e^{-j\beta_2 z}$, respectively, where $\beta_1 \approx \beta_2$ are the propagation constants. For the geometry shown in Fig. 3 with a period Λ, the coupling coefficients κ_T (transmitter) and κ_R (receiver) take the form $2\kappa_{TR}\cos\left(2\pi z/\Lambda\right)$. Therefore, the spatial equations are,

$$\begin{aligned} \frac{d}{dz}a_T &= -j\beta_T a_T - j2\kappa_T \cos\left(\frac{2\pi z}{l}\right)a_R, \\ \frac{d}{dz}a_R &= -j\beta_R a_R - j2\kappa_R \cos\left(\frac{2\pi z}{l}\right)a_T, \end{aligned} \tag{94}$$

given a weak time dependence of the amplitudes a_T and a_R to resonance frequencies ω_T and ω_R,

$$\begin{aligned} \frac{d}{dt}a_T &= j\omega_T a_T + j\kappa_T a_R, \\ \frac{d}{dt}a_R &= j\omega_R a_R + j\kappa_R a_T, \end{aligned} \tag{95}$$

relative to the coupled state of the resonating elements L_i and L_j,

$$\kappa_T \approx \kappa_R = \frac{M_{ij}}{\sqrt{L_i L_j}}. \tag{96}$$

The mutual inductance of the i^{th} and j^{th} elements and the integration over the spherical surface S_j from Fig.2.19 is therefore,

$$M_{ij} = \frac{\int\int_{S_j} \mathbf{B} \cdot \vec{\mathbf{n}}\, dS}{I_{L_i}}, \tag{97}$$

proportional to the current I_0 of the opposing resonator L_i, yielding the property that energy can be applied to the system to a maximum point that the waveguide can sustain. The dissipated power, while a property of the load present, is also a property of the power sustained in the magnetic field, as,

$$\begin{aligned} \langle p_d \rangle &= \frac{1}{2} R \left| I(z) \right|^2 + \frac{1}{2} G \left| V(z) \right|^2 \\ &= \frac{1}{2} R \left| I_0 \right|^2 \int_0^l \cos^2\left(\frac{\pi z}{l} \right) dz + \frac{1}{2} G \left| V_0 \right|^2 \int_0^l \cos^2\left(\frac{\pi z}{l} \right) dz, \end{aligned} \tag{98}$$

shown in (134) to be equivalent to the relationship of the stored energy at resonance via conductance G and resistance R attenuating the transmission, contributing to both a complex impedance Z_0 and admittance Y_0. This is suggestive of an oscillatory force acting in a waveguide.

Once the electrons within the conductive material are accelerated, they subsequently radiate energy in a quantized form upon deceleration [5]. The energy emitted in the form of radiation from the charge q with acceleration a is given by,

$$\langle p_e \rangle = \frac{q^2 a^2}{6\pi\varepsilon_0 c^3}, \tag{99}$$

where c is the speed of light. The emission of energy, in a dipolar form is,

$$\langle p_\gamma \rangle = \mu_0 \sin^2\theta, \tag{100}$$

where θ is the angle between the direction of acceleration and the emission. The radiation is polarized such that the emission field is parallel to the acceleration force on the electron.

It is proposed here that if a circuit could accelerate electrons in an antenna, the emitted radiation could be controlled and directed by manipulating the presence of the magnetic component. An increase of

B would then yield a greater value of M_{ij} with the addition of metallic accretion discs, that is, "accretion" meaning discs forming a uniform conductive surface, lying in the x-y plane so that a thermodynamic event occurs in the gap between the disc and the inner loop surface connecting the two as a coupled potential. Such discs can be aligned with their centers at the same point as the loop center.

The magnitude of projection at a distance from the loop is given by the quantities of $\cosh a$ and $\sinh a$, as shown in Fig.2.17, between the limit at the transient zone, at point 'b', and the center. Point 'a' is where the influence of the magnetic field is at a maximum, such that a second loop absorbs a maximum quantity of transmitted power yielded by the first loop. The power densities in the darker grey zones, labeled $\pm a/2$ and $\pm b/2$, based on their orientation on the x and z-axis, are equal unless there is an azimuthal field present. The power density in these zones is dependent upon the current I_0 applied to the loop.

If a loop is set at a distance with a second loop of the same number of turns, loop radius, and wire diameter (to a reasonable degree of equal approximation) the field "lines" extend the hyperbolic plane from (x_0, y_0, z_0) to (x_1, y_1, z_1) with less curvature θ than that observed in the case of a singular loop. The limit between the distance, given by $(x_1 - x_0, y_1 - y_0, z_1 - z_0)$, and the fall-off of the field, given by $1/r^2$, is asserted here as being due to the curvature of the propagation and the substantive waveguide and is not necessarily dependent upon the size of the loop.

The addition of a conductive media lying along the x-y plane, perpendicular to z, will contort the zones. If a flat metallic sheet is placed in the plane of a length and height greater than the diameter of the loops, then energy is absorbed on its surface.

Contrastingly, the introduction of a metal disc at the center of the receiving loop will increase the magnitude of **B**. The propensity of the discs to enhance the magnetic field has a greater influence on the receiver as opposed to the transmitter.

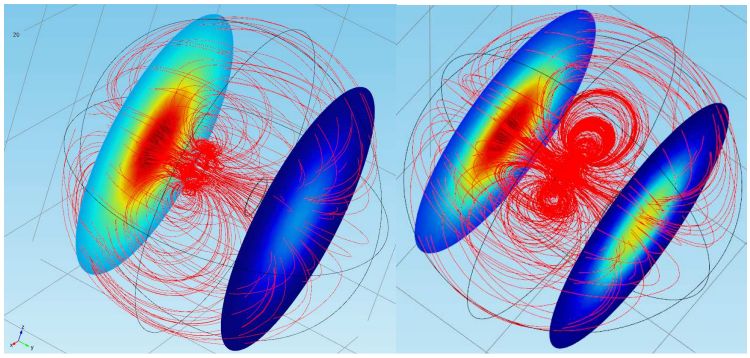

Fig.2.20. (a) Magnetic flux of loop antenna, (b) disc adds flux strength.

The magnetic loop, at a ratio to its quarter wavelength, contains the effects of a full alternating-current (AC) cycle impressed on it by an incident wave [30]. The rate of exchange of energized particles is then represented by the density of “magnetic lines”, illustrated on the left side of Fig.2.21. The right side of Fig.2.21 meanwhile shows the same loop system with an accretion disc added at the center of the transmission loop. The more attraction between the loops, so the more efficiently the energy is transferred.

The lines in Fig.2.21a and Fig. 2.21b show the magnetic flux density while the slices at the ends show magnetic field intensity at the loop at norm $\mathbf{B}$. For the purposes of the paper, the number or “density” of field lines precludes a higher magnetic flux in the region while a shade from dark to light denotes greater intensity.

The strength of the magnetic field generated by the loop may be increased by adding turns n of conducting wire, instead of a single turn and increasing the length of the legs m shown in Fig.2.18. In terms of the experiments which have been performed and are reported on in this paper , the loop was constructed where $n = 3$ and $m = 4$ cm. In terms of calculating the magnitude, it is perhaps more appropriate to consider the magnetic field in terms of $\mathbf{H}$ where $\mathbf{B} = \mu\mathbf{H}$.

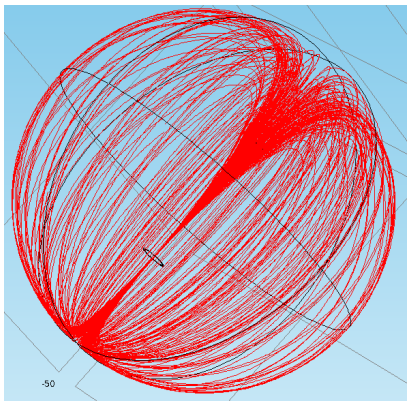

Fig.2.21. Propagating energy in $\mathbf{B}$.

A single disc is placed inside the receiving loop so that it lies on the x-y plane while its center lies along the *z*-axis, as shown in Fig.2.56, where the magnitude of $\mathbf{B}$ is directed through its center. With the addition of the disc, distortions are present by imbalances in the field, where additional transformed energy, J_ϕ, appears in the azimuthal field, shown in Fig.2.23 as,

$$J_\phi = f(r,\theta)\hat{\phi}. \tag{101}$$

A disc, approximated as a consecutive sequence of wire-turns in the form of a spiral where the width w between the winding arms approaches twice the wire radius, as, $w \to 2a$, has a surface radius of 12 mm. It is expected the disc will increase the magnitude of $\mathbf{H}$ relative to its size with the addition of the new vector u. The azimuthal magnetic field is expressed as a second order phenomenon. An increase in energy in the field is observed by an increased conversion of electric current into $\mathbf{H}$.

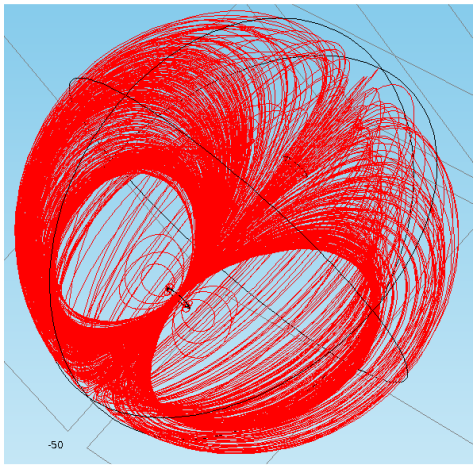

Fig.2.22. Density of azimuthal $\mathbf{B}$ field.

Distance does not directly affect modal coupling [6], rather, spatial extensions in the *z*-direction relate more closely to the transport of electrical power, expressed in terms of the $\mathbf{E}$ and $\mathbf{B}$ fields, attenuated along its length. Therefore, broadcast power is subject to an attenuation rate dependent upon a value of impedance. The appearance of an azimuthal component when the disc is placed inside the loop is likely due to shearing effects, or imbalances in the equilibrium state of the magnetic field consisting the waveguide as it transforms from isotropy toward anisotropy in the x-y plane.

Experimental work on this aspect of the theory is presented in §2.4.2.

2.2 The circuit model

As it is primarily intended that the system transmit waves, under such conditions the oscillator is considered to be the driving-force of the system. Without oscillations, waves would not propagate.

For comparative purposes, if the antenna was charged with a non-oscillating current such as that provided by a direct current (dc) power supply, the receiver would not see the signal and magnetic energy statically emitted into space, given the area, dA, of the conductor. There would be no explicitly defined coupled-mode and the signal would not couple to a distant load. As far as the field object is concerned, it is randomly generated with no cohesion in the ambience.

The task of this section is to describe the construction of a circuit, which illustrates the diagrammatic representation of the source, the oscillator, and the loops illustrated in Fig.2.1. The circuit model will also attempt to satisfy the mathematical descriptions of the previous sections while introduce a reconciliation of the circuit verses field model discontinuities [52] only in the confines of an agreement of the supposition of resonant circuit-as-antenna correlation.

To satisfy these aims, a circuit which consists of a transmitter and a receiver is required consisting of a compact oscillator driving a magnetic-resonant loop antenna. The coupling of the source and oscillator objects are wholly responsible for the character of the manifest field between the antennas, as described in §2.1.

The most immediate and obvious question is what kind of oscillator to use: compact, powerful, and the ability to impress the expected currents on the loop. Efficiency is important here as the transmission scheme has a criterion of “worthiness”; it is taken into consideration when choosing the oscillator type.

In the early days of radio, numerous types of oscillators for signaling were based upon the spark-gap transmitter first used by Hertz [53, 54]. As the transmission of radio waves evolved from telegraphy into voice, increasingly the oscillator needed to be free from noise for broadcasting. As the spark-gap started to fall out of favor, sinusoidal oscillators able to contain modulation were proposed in the form of the regenerative circuit by Armstrong [55]. The universality of the scheme showed that any radio-frequency oscillator was a topology containing feedback; this topology could be modified to provide a controllable reduction in feedback loop coupling on the antenna circuit. If the method of coupling was to split the characteristic impedance of the circuit through an amplification stage, it functions as a combination of an oscillator and mixer, which converts the modulation directly to the baseband.

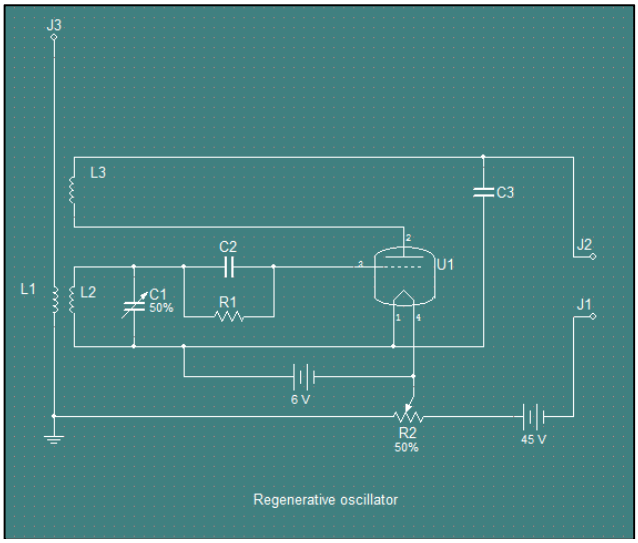

Fig.2.23. The regenerative oscillator.

On examination of Fig.2.23, the driving force of the vacuum tube U1 is carried across a pair of inductances, a coupling coil, L2, and tickler coil, L3, along with tuning capacitor, C1. The capacitors C2 serves to suppress leakage from the grid of U1, capacitor C3 for frequency bypass. The application of dc power to the triode amplifies the signal incoming to terminals J1 and J2 treating the beat frequency of the antenna scheme and power impressed on it as if the entire package was a combination of source and oscillator amplifying the resonant frequency of the antenna. If the circuit is modified to split the antenna into two equal phases and the driving amplitude powering each 180° phase-shift, a circuit with twice as much applied power could be constructed. Such a circuit is the push-pull oscillator.

The push-pull oscillator is a type of electronic circuit that can drive both a positive and a negative current phase-shift into a load. Appearing in the early 1920s, later described in detail by Hoag [56], the model is a highly-efficient oscillator which contains a complementary pair of power-drivers, one dissipating or sinking current from the load to the negative power supply, and the other supplying or sourcing current to the load from a positive power supply over a center-tapped coil during a complete duty cycle. Because of the high-efficiency and the simplicity of the model, it is ideal for wireless power transmission shown in Fig.2.1. Since the scheme is based on induction, the oscillator will have to be modified to also phase-shift the antenna inductance through the cycle.

An inductively-coupled push-pull oscillator is shown in Fig.2.24. When voltage is first applied by the dc source, V1, the fluctuation of the voltage makes the grid of U1 positive and the grid of U2 negative. Because the current is lagging behind the voltage, it is expressed as changes in the plate current. The lag of the current is an important feature, which is directly captured in this type of oscillator, the dipole is created on the plate. The resonance between the inductance and capacitance in

the plate circuit causes voltage changes on the plate, which fed through the plate to grid capacitance or by magnetic coupling between the two tank circuits, reverses the polarity of the grids, switching them exactly opposite. As this continues, the tank circuit impresses the voltage changes of the grids and current on the plates, so that oscillations of increasing magnitude rise. The magnitude rises to the limit imposed by the magnitude of the source voltage and the energy is spread evenly across the circuit given its symmetry. Eventually, the rise reaches a magnitude where the dipole breaks and energy is released.

2.2.1 The push-pull oscillator

The push-pull oscillator is a balanced oscillator. This type of circuit is able to deliver larger outputs with less distortion than single-triode amplifiers. The output is a sinusoid relating the opposing forces of absorption and dissipation in the tank circuit created by the coupling of coils and capacitors across the amplifiers.

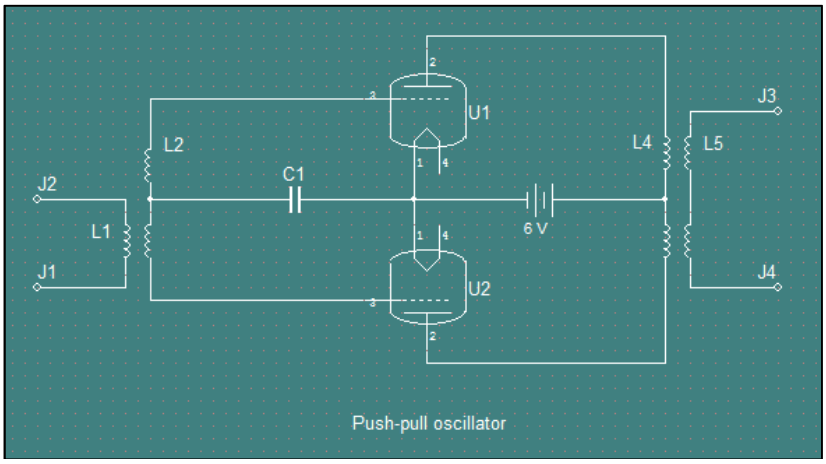

Fig.2.24. Inductively-coupled push-pull oscillator.

Because the oscillator in Fig.2.24 is suitable to drive the scheme, it is necessary to recast the circuit since the antiquity and power needs of the vacuum-tube triodes make recreating the circuit in its exact form impractical. What is more realistic is to replace U1 and U2 with something like a semiconductor triode, which has the ability to impress a high level of amplitude with fast switching speeds. Such an item that is very advantageous for this purpose is the n-MOSFET transistor.

Since this is a field-effect transistor, dependent upon high-speed, electric field switch-transitions, the n-MOSFET has coupled-modes. The mode relevant here is the triode mode or linear region, also known as the ohmic mode [57]. The architecture of an n-channel MOSFET shown in Fig.2.25. A metal-oxide-semiconductor field-effect transistor has three terminals: the source, the gate, and the drain. In an n-MOSFET, both the source and the drain are n-type and the substrate between them is p-

type, shown in Fig.2.25. A thin layer of silicon dioxide insulates the gate and the p-type substrate. Due to this insulation, there is no gate current to either the source or the drain.

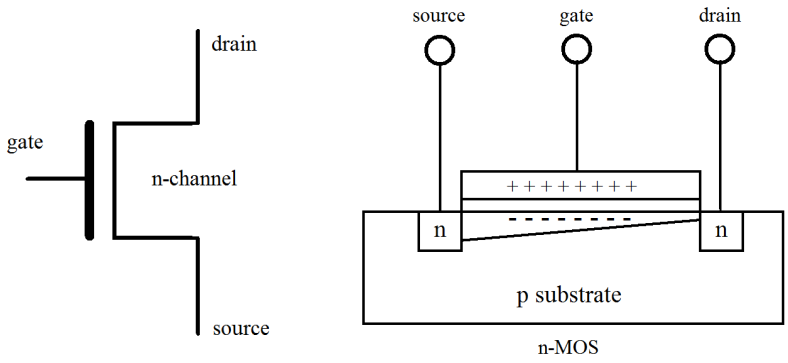

Fig.2.25. The n-channel MOSFET structure.

The n-MOSFET can be equated with a voltage-controlled switch. When a sufficient voltage V_{GS} is applied between the gate and the source, the positive potential at the gate will induce enough electrons from the p-type substrate to form an electronic channel creating an inversion layer between the source and the drain, and a current I_{DS} is formed. The behavior of a n-MOSFET can be described by the function $I_{DS} = f\left(V_{GS}, V_{DS}\right)$ with a threshold voltage V_T. These properties can be taken advantage of in the wireless power scheme by placing the n-MOSFET in the circuit in such a way as to split oscillations into two groups: those of the transmission antenna and those between the pair, illustrated in Fig.2.26, and the steps through each phase, illustrated in Fig.2.27.

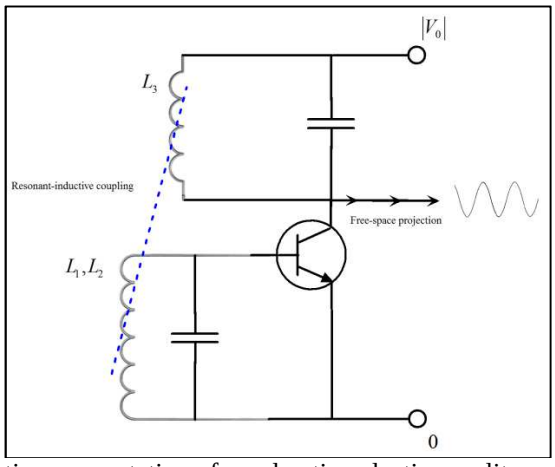

Fig.2.26. Schematic representation of accelerating elections split across a tank circuit.

Fig.2.26 is intended to show how a single MOSFET in the application applies an acceleration force, as a property of the potential (voltage) and inductance where the oscillation is sustained in the antenna. The ability to phase-shift between each part of the cycle synchronizes with the shifting phases of the potential will close the circuit periodically and allows energy to transfer. Free-space wave projection

is possible when the synchronization is with any one of the rest-state potentials embedded in the phase. Although the specification of these potentials is outside the scope of this thesis, suffice to say the synchronization satisfies the presence of the antenna as analogous to coupled-modes, merely by inspection. It is at the shifting between phases where interaction with the interface takes place.

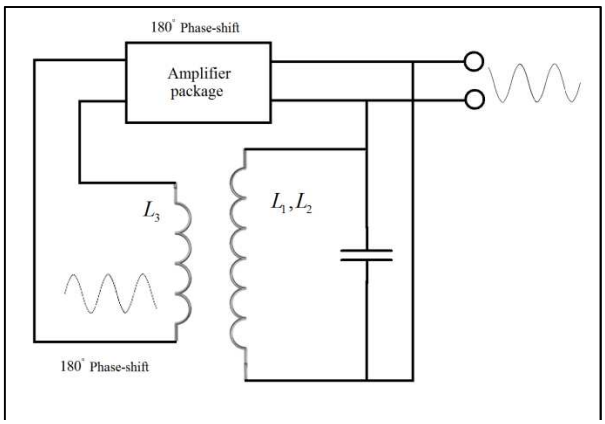

Fig.2.27. Phase-shift amplifier on coils.

A deeper analysis of phase-shifting on circuits is also out of the scope of this thesis. What is reasonable is that a power n-MOSFET is a suitable component to replace U1 and U2 of Fig.2.24. The arrangement of Fig.2.24 is altered to Fig.2.28:

- Coil L2 becomes the antenna, and is connected across the drain of Q1 and Q2 to split in half the antenna circuit including the feed from the power supply, polarity opposite,
- plate terminals U1 and U2 are tied together and connect to the negative feed from the power supply, and,
- coil L4 is the receiver antenna, shown in Fig.2.29.

A schematic of the oscillator to drive the circuit is illustrated in Fig.2.28.

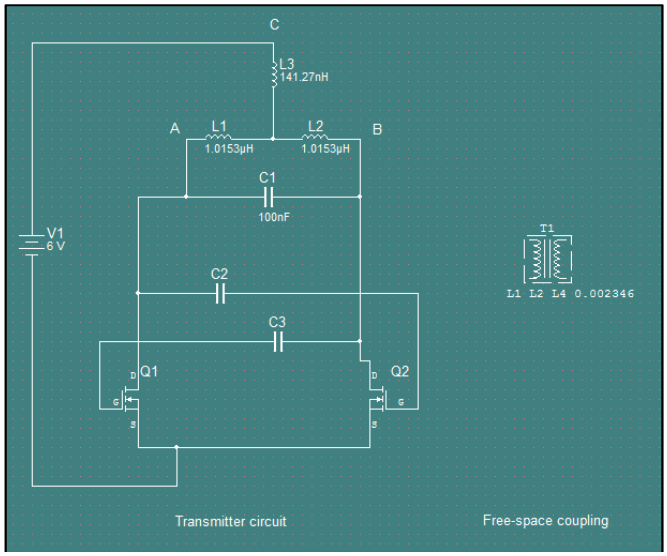

Fig.2.28. The transmission element with a coupled-mode.

This model contains only a simple description of the dipole but it is suspected such a description could go deeper, briefly examined in the Appendix. Regardless, the circuit will create and destroy its dipole in a cycle releasing its energy. Since destruction of the dipole is occurring by the current returning to the source in the form of feedback power from the antenna, excess energy will bleed off as heat. The component that emits the heat due to internal losses and feedback of energy coupling at the interface is the capacitor C1.

At higher source levels, heating of Q1 occurs; heat-sinks for both Q1 and Q2 and a metalized capacitor will keep the circuit from burning out. The author strongly suggests future research be conducted on Joule heating in the circuit.

2.2.2 Simulation and construction of the circuit

The circuit coupling diagram in the simulator program, National Instruments *MultiSim*, is shown in Fig.2.29a.

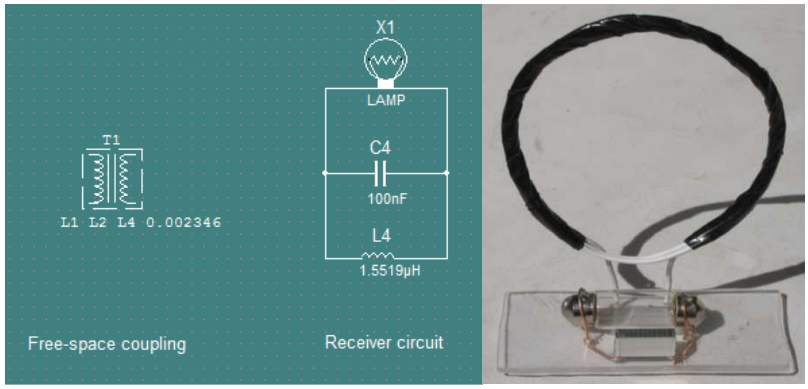

Fig.2.29. (a) The receiving element with a coupled-mode, (b) an example receiver.

Using a suitably constructed receiver, illustrated in Fig.2.29b, a simulation of the circuit is conducted. The driving function of the circuit in the simulation will be a pulse. Hertz proposes that a “ringer” is required to start the oscillator [53]. A pulse current I_{pulse} will be used in substitution of V1, shown in Fig.2.30. This is similar to the use of the spark-gap. One of the amplifiers must be shorted while power is applied in order to ring the resonator strongly enough for oscillations to be sustained. A momentary short is placed between the gate and the drain of Q1. The oscillator is self-sufficient requiring only phase offset amplifiers to sustain the oscillations through the cycles thereafter. This is an ideal representation of a kick-start because when the pulse current is adding energy, it forms a closed circuit. Simply stated, the oscillator requires priming. To simulate a momentary burst of energy to the oscillator, the settings of the pulse current are listed in Table 2.3.

Table 2.3. Simulation circuit properties.

TABLE 2.3
SIMULATION CIRCUIT PROPERTIES

Property	Value
Initial value	0
Pulsed value (mA)	100
Time delay (ms)	10
Rise time (μs)	10
Fall time (μs)	10
Pulse width (ms)	1
Period (s)	1

The broadcasting model these settings are applied to is shown in Fig.2.30.

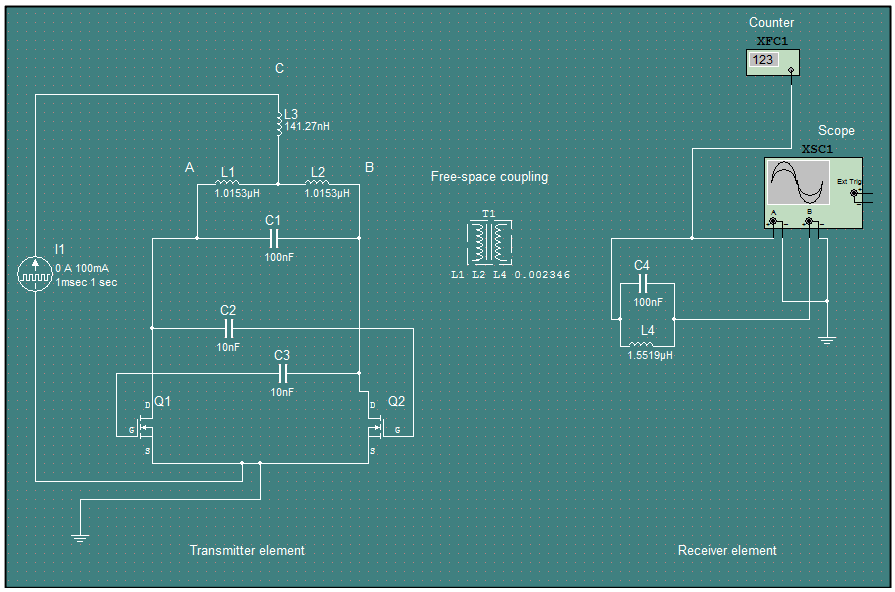

Fig.2.30. The broadcasting model for simulation.

The frequency counter reads 422 kHz; the signal at the oscilloscope, 2 volts per division on the *y*-scale, with a time base of 200 μS per division on the *x*-scale is shown in Fig.2.31.

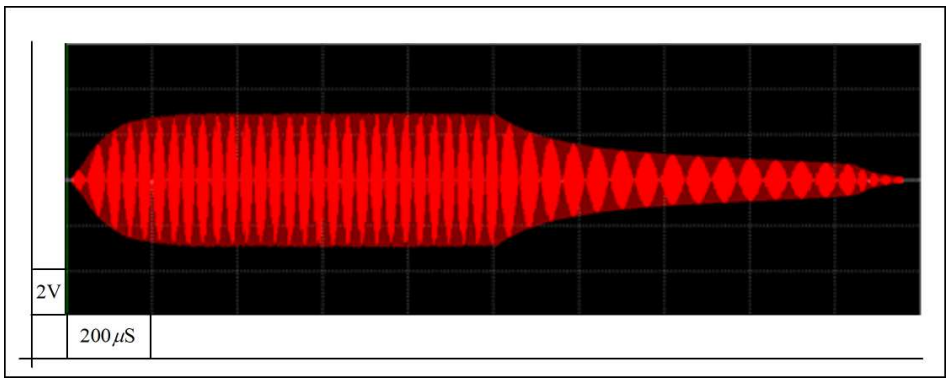

Fig.2.31. Simulated signal seen by the receiver.

The simulation refers to both the transmitter and receiver elements of the theoretical model first illustrated in Fig.2.1. As the simulation is taken in context to inductively-coupled elements based on circuital laws, the components consisting the broadcast model have the properties:

- Components L1, L2, L3, and C1 simulate the one resonator—the transmission antenna illustrated in detail in Fig.2.38; likewise, L4 and C2 simulate a second resonator, they are coupled across free-space at the calculated coupling coefficient from (45),
- Q1, Q2, C3, and C4 constitute the oscillator driven by voltage source V1,
- The system transmits energy given the theoretical predictions. Variation of the coupling coefficient κ_{ij} shows the various circuit responses, using the same *x* and *y*-scale divisions of Fig.2.31, shown in Fig.6.1 in the Appendix.
- L3 contributes weakly to the inductance of the loop,

Component L3 is primarily the positive connection to the amplifiers in the circuit, as shown in Fig.2.30. Since it is only a one-half turn on the loop, it is expected the inductance of L3 is much smaller than the inductance of the loop represented between components L1 and L2.

2.2.3 Equations of the circuit model

It is expected that a sinusoid to be emitted from the transmission antenna with both a positive and negative group velocity outward along *z* from the loop surface lying in the *x*, *y* plane. Group velocity is defined as a group of amplitudes used to distinguish emanated waves in both positive and negative directions of *z*, projected by the antenna. If only one side is considered, then the efficiency is divided by the missing group waves, at a complex velocity since it cannot be assumed that each photon in the energy is moving at a constant velocity throughout the projection. This assumption is because the

velocity is due to the magnitude of force of acceleration on the electron in the conductor. The assumption is compatible with the consideration of the wave envelope, however, with a stochastic distribution of energies.

Alignment of loop centers, or axial alignment, will yield the highest magnitude of energy transmitted. Performance in the circuit seems ideal when node C is placed at the point one-half of the length of AB. It would be interesting for future research if this wire placement differs in performance on the length. The cyclic quality, $Q(t)$, is relevant to describing the internal quality of the oscillator at any particular time t_0 when,

$$Q(t)=\frac{\omega_0 L_e}{R_e}t_0. \tag{102}$$

Equation (102) infers a complex set of amplitudes present across the field object. The effective quality factor Q_e along with the effective damping factor ζ_e satisfies the traveling wave solution. These properties are based on the states of the oscillator for each instance of the antenna elements as,

$$\begin{aligned}&\sum_{m=1}^{x} Q_i, Q_j, Q_k, ..., Q_m,\\ &\sum_{n=1}^{x} \zeta_i, \zeta_j, \zeta_k, ..., \zeta_n,\end{aligned} \tag{103}$$

for each of the antenna elements $i, j, k, ..., n.$ The states describe behavior of the system when there are small changes in R_e, given (72), shown in Table 2.4.

Table 2.4. Oscillator state by Q and ζ.

TABLE 2.4
OSCILLATOR STATE BY Q AND ζ

Oscillator state	Q	ζ
underdamped	Q_e>0.5	$\zeta_e < 1$
critically damped	$Q_e = 0.5$	$\zeta_e = 1$
overdamped	Q_e<0.5	$\zeta_e > 1$

Depending on the values of the effective damping ζ_e and the effective quality factor Q_e in both the antenna and the oscillator, the emitted waveform will be one of the three types. The meaning represented in the different states of oscillation is due to the displacement of a wave in space given its periodic motion. In order to satisfy periodicity, the oscillator must be elastic—in the sense of returning precisely to its original configuration after deformation: this requires a known position of

equilibrium and a counter force which restores equilibrium. The oscillator must be able to produce a sustained single frequency on a source object with a tolerance small enough that an object designed to absorb the oscillations will do so if it has approximately the same parameters. The antenna will comprise the vibrator while the oscillator will provide synchronous amplitude.

In the traveling wave case for radiative energy emitted from the coupled antenna, the solution is given by the wave equation, transformed from (5) using (9),

$$\frac{\partial^2 u}{\partial x^2}+\frac{\partial^2 u}{\partial y^2}=\frac{1}{v^2}\frac{\partial^2 u}{\partial t^2}, \tag{104}$$

where v is the phase velocity. As the wave propagates in both the $+z$ and $-z$ directions—positive and negative group velocity—the description of the transverse motion $\frac{2\pi v}{\lambda}=2\pi f=\omega,$ where $v=f\lambda$ allows the description to be,

$$\begin{aligned} y(x,t) &= A\sin\frac{2\pi}{\lambda}(x-vt) \\ v_y(x,t) &= \frac{dy}{dt}=\omega A\cos\frac{2\pi}{\lambda}(x-vt) \\ a_y(x,t) &= \frac{d^2y}{dt^2}=-\omega^2 y=-\omega^2 A\sin\frac{2\pi}{\lambda}(x-vt). \end{aligned} \tag{105}$$

The following equivalent parametric forms of the wave solution of (105) are,

$$\begin{aligned} y(x,t) &= A\sin(kx-\omega t), \\ y(x,t) &= A\sin\frac{2\pi}{\lambda}(x-vt), \\ y(x,t) &= A\sin 2\pi\left(\frac{x}{\lambda}-\frac{t}{T}\right). \end{aligned} \tag{106}$$

The determination of the velocity, $v,$ and its inhibition, $\bar{v},$ is dependent upon the properties of the medium in tandem with the coupled inductance which forms an approximation given the wave relationship. The parameters are shown in Table 2.5.

Table 2.5. Oscillator traveling wave parameters.

TABLE 2.5
OSCILLATOR TRAVELING WAVE PARAMETERS

Coil	L_i	L_j	L_s
Resonance frequency (Hz)	345607.761	404004.671	433203.126
Wavelength (m)	867.436	742.052	692.037
Quarter wavelength (m)	216.859	185.543	173.00925
Wave period (μs)	2.893	2.475	2.308
Wave number	0.0072	0.0085	0.0091
Quarter-wave velocity (m/s)	7.4948153e07	7.4960238e07	7.4948147e07

Because, in the wireless power case, the traveling wave emitted by the antenna is a function of the amplitude generated in the oscillator, is confined to one plane in space and varies sinusoidally in both space and time and expressed in combinations of,

$$\begin{aligned} y &= A\sin\left(kx-\omega t\right), \\ y &= A\cos\left(kx-\omega t\right), \end{aligned} \tag{107}$$

and of the complex form,

$$y = Ae^{j(kx-\omega t)}. \tag{108}$$

As an Euler identity, the form takes,

$$e^{i\theta} = \cos\theta + i\sin\theta. \tag{109}$$

Alterations to the circuit would affect strong changes to its state. The transmission circuit is a series circuit and the addition of R_e would make Q_e smaller. The receiving circuit is arranged in parallel so that changes in R_e will make Q_e larger.

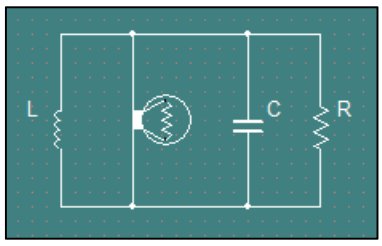

Fig.2.32. Simplified circuit diagram.

Based wholly on these theoretical results, a circuit is constructed based on the schematic used in the simulation wherein to test the hypothesis. The transmission circuit including the antenna discussed in §2.3.1, is shown in Fig.2.33. Measured with a frequency counter, the broadcasting frequency is

$f_0 = 428$ kHz. It is expected that if the dipole would be preserved after each cycle, that efficiency would increase as well as the potential at the boundary.

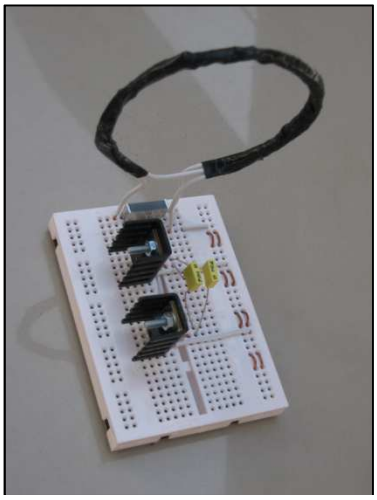

Fig.2.33. The constructed oscillator.

The next section addresses the details of the propagation model proposed in this section.

2.3 The propagation model

The transportation of energy across free-space occurs in a pair of tuned circuits, symmetric and set a distance apart, when one of the circuits is electrically stimulated. By amplification, the resonance frequency can be used to accelerate electrons in a coil.

In practice, this means an electric current will be induced in any distant circuit where the magnetic flux intersects with an appropriate conductor in the path of the oscillations. The placement of the resonant objects in the scheme will be in the path based on the projections of their antenna, coupled to their resonant circuits.

The quarter-wavelength magnetic loop antenna is a useful device to transmit significant quantities of electrical current at reasonable efficiency. For simplicity and brevity, this is a fundamental artifact of the scheme presented in this thesis. The complete range of behavior available is exclusively due to the interface between a set of electrical charges and an ambient structure of free-space at normal temperatures and pressures, for the purposes here of atmospheric air with characteristic impedance.

The mathematical components needed to describe the problem at hand are currents in the conductive media and currents in the dielectric. If the medium inside the waveguide is homogenous and isotropic and if the surface impedance at the boundary is zero, the method of separating variables obtains a set of normal, uncoupled modes of propagation. Any irregularity or discontinuity in the waveguide

provides a coupling between some, or all, modes of propagation [24], transported on a transmission element whose radius is smaller than the dielectric space, whose waveguide is sufficiently infinite, to impose ideal planetary electrical characteristics.

A necessarily narrowband antenna with steep nulls is required to allow the power to transmit in the signal while rejecting spurious noise and other transient phenomena the magnetic fields could be subject to, including solar radiation. The quarter-wavelength magnetic loop antenna has very sharp nulls at right angles to the plane of the loop.

These nulls can be very useful for suppressing radio interference. A rotation of the loop will reduce noise. Because the nulls are sharp, small changes in antenna orientation can make a large change in signal or noise received from the direction of the nulls allowing the interference to bleed into the field. The nulls are sharpest on the smallest loops at a perimeter approximately 0.05λ which linearly increases to 0.1λ at the periphery [30].

The propagation model, for reasons stated in the previous sections, and in detail in §2.1, is concerned primarily with small antenna sizes with a high efficiency. In the proposed model, the loop size is the most critical property. If coil loop is wound at a specific ratio of circumference to wavelength, it is equivalent to conductor connected to an electrically-short transmission line with coupled modes [30, 107]. To maximize the emission of radiation, the magnetic loop should be at a ratio of its circumference to its quarter wavelength. Such a magnetic loop will be shown to have the ideal ratio, in terms of maximum transmission efficiency, is when this ratio falls on an exponential scale, shown in (42). Consider a circuit consisting of a single loop of insulated wire wound in such a way as to create a circular loop of a few turns. This loop and its capacitor become one-half of a resonant circuit forming a transmitter T_x. The length of this wire loop, ℓ_t, is then duplicated to construct a similar loop of identical characteristics, ℓ_r, along with a capacitor forming the second half of a resonant circuit forming a receiver R_x.

A current is applied to this circuit, induces an electrical field in the self-inductance of loop ℓ_t, creating a magnetic field which is coupled at the interface. By placing a load in parallel to the voltage gap in loop, magnetic energy is drawn into the gap and then converted into electrical current. Inclusive in the loop is a voltage gap of width w no greater than the loop radius, so that $w < r$. The coil ℓ_t is positioned in such a way that the $x-y$ axes form the loop surface and the *z*-axis the trajectory out from the loop in the directions of the group velocity of the radiation—positively for right-handed, negatively for left-handed. This relationship is illustrated in Fig.2.34.

The chosen frequency computes (39) to be between 412 and 526 kHz.

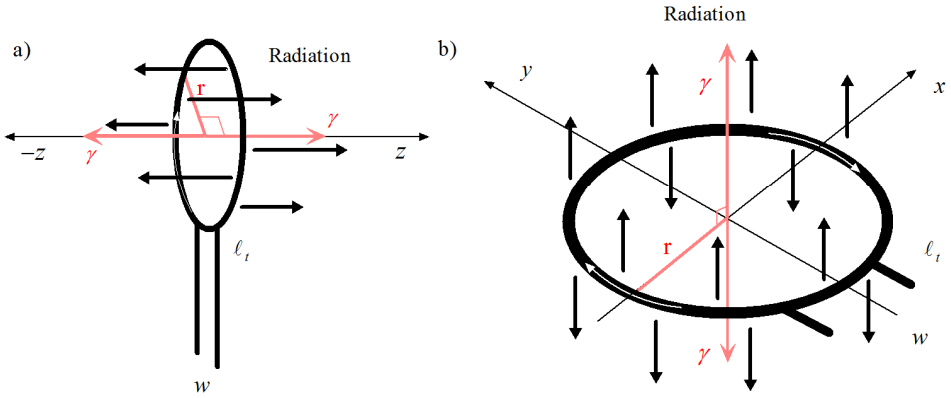

Fig.2.34. Radiation emissions of a magnetic loop antenna.

The antenna loop is excited by the acceleration of electrons on its curvature, driven by the current I_0 from the amplifiers in the circuit. The positive group velocity emits radiation in the form H_0^+, the negative group velocity emits radiation in the form H_0^-, and γ_θ, the quantized energy due exclusively to photons, illustrated in Fig.2.35.

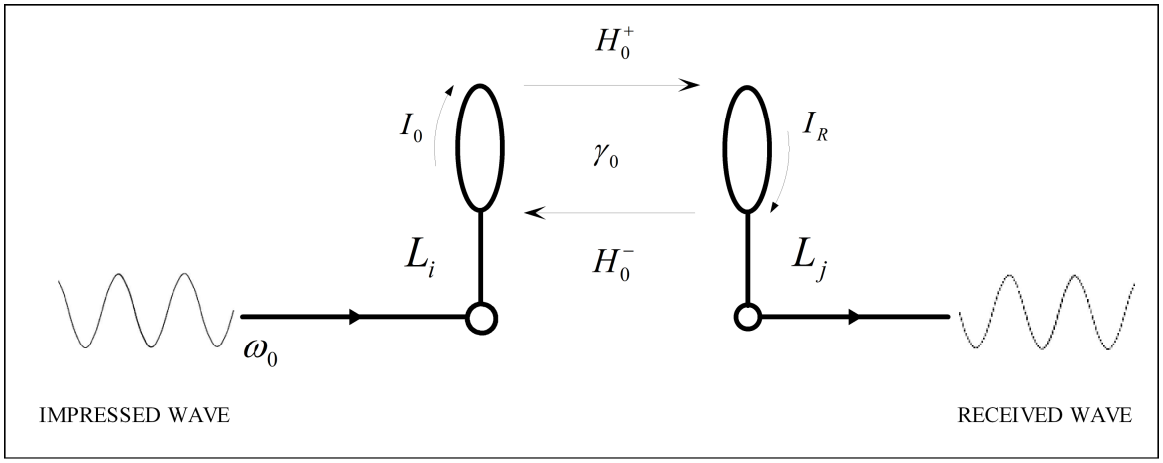

Fig.2.35. Wave propagation for the modal coupling scheme of wireless power transfer.

An assumption of symmetry will reveal the model of magnetic waves, or currents, in the form of photons of a given angular frequency ω_0 flow positively at a given coordinate $\left(\gamma_\theta, H_0^+\right)$ from coils $\ell_t \rightarrow \ell_r$ and negatively at $\left(-\gamma_\theta, H_0^-\right)$ from coils $\ell_t \leftarrow \ell_r$ with an efficiency η. There is a distinction in the solutions later that and not energy exchange between loops since currents are used for electromagnetic descriptions at each half of the circuit.

From the circuit point of view, antennas appear as a resistance R_r called radiation resistance. It is not related to any resistance in the antenna itself, rather, a resistance coupled from space to the antenna terminals. Active radiation raises the ambient temperature of R_r. This temperature is equivalent across the circuit because the temperature of the distant antenna (respectively from the transmitter) can only see its symmetric analogue due to the nature of inductive coupling in that the photons extant in the magnetic field only react with like or other resonant objects [31, 58]. Under such conditions R_r is quantified by the region of space inside the loop as a function of the virtual transmission line linking the antenna to the distant region, shown in Fig.2.36.

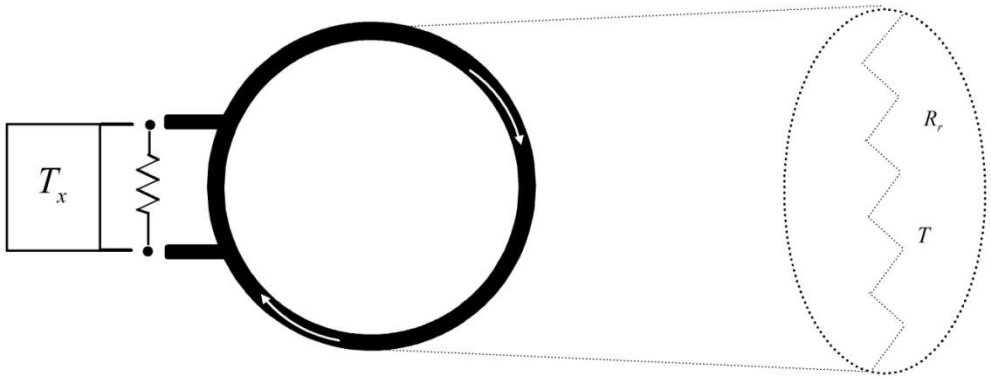

Fig.2.36. Schematic representation of a virtual transmission line of an antenna to a region of space.

The loop will operate using a single-band transmission with regard to the antenna impedance, directivity, and gain. The antenna analysis is essentially equivalent to that for a curved dipole and projected magnetic field given (19). The computation of the antenna will target electrically small loop antennas in the normal and axial mode of operation. Radial mode is an advanced topic. Multiple modes are exhibited in §2.4.

Following the discussion of the circuit properties in §2.2, and the schematic shown in Fig.2.28, the transmission antenna coil must be designed to conform to the shifting phase of the amplifiers.

Following Larmor's theorem, discussed in §1.1 and §2.1.2, it is ideal if an electrical force can be applied to a conductor in such a way as to accelerate electrons between one half of the conductor and the other, similar to a wire treated as a dipole. The movement is treated as the phase.

Phase is defined as representing movement along the arc of the antenna through divisions 2π through the circle's circumference where the radius r is the magnitude of the electric field, E_ϕ and $\boldsymbol{\upsilon}$, a component of velocity of the shifting phase representing the velocity of the electrons. A schematic representation is shown in Fig.2.37.

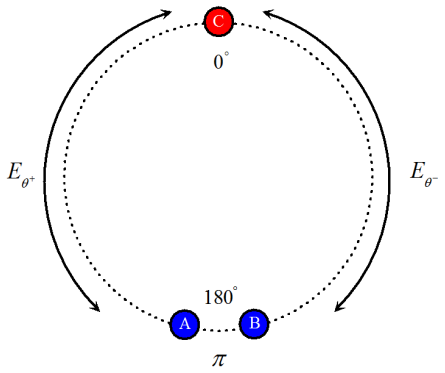

Fig.2.37. Angular motion of the oscillator transition phase.

The acceleration forces move through π on the loop, shifting direction between components L1 (A) and L3 (C), and L2 (B) and L3 (C) which are negative and positive voltages respectively. Theoretically, the force contained in the current accelerates the electrons through one phase of π then switches direction through the other phase of π. At each switch in direction, the electrons in the conductor decelerate and release their energy in the form of photons along the direction of the magnetic field.

The material of the coil should sustain the angular velocity of the currents, ω_0, oscillating through integer multiples of π. Copper is sufficient, artificial materials could substantially improve the reactance. An insulated length of wire, ℓ, given by A, B, is wound into a loop of a chosen specification. It has a break cut into its insulation at the midpoint in the loop, where $C = \frac{1}{2}\ell$, and a third wire follows the loop forming an extra number of turns, $n = 0.5$, and an extra standing length, or leg, illustrated in Fig.2.38.

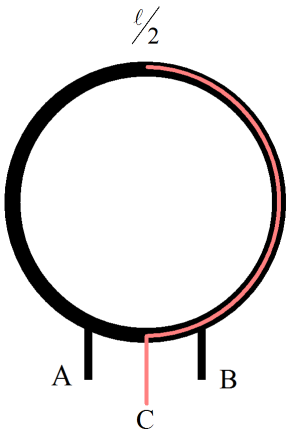

Fig.2.38. The transmitter coil.

The transmission antenna in now a three terminal coil, antenna (A, B, C) corresponds to (L1, L3, L2) respectively, with (L1, L3, L2) behaving as an oscillator when connected directly to an amplifier. Terminals A (L1) and B (L2) are connected across a capacitor to the corresponding drains of two n-MOSFETs whose sources are connected to the negative terminal of the power supply. Terminal C (L3) is connected to the positive terminal of the power supply.

A generalizable computation, the method of moments, will be fitted to solve the problem of the circular loop antenna as a function of the scattering of the field emitted by the transmitter. This general solution is solved using the software package *Matlab* and files from [59]. Properties of the loop antenna can then we put into the program *Circuit calculator* to arrive at the theoretical values. The computational structures will be these scripts; their purpose is listed in Table 2.6.

Table 2.6. Computational elements from mesh to field solutions.

TABLE 2.6
COMPUTATIONAL ELEMENTS FROM MESH TO FIELD SOLUTIONS

Problem class	Input	RWG-element file	Output	Purpose
Circuit	magneticLoopMesh.mat	rwg1.m	geoMesh.mat	Creates RWG edge elements.
	geoMesh.mat	rwg2.m	rwgGeoMesh.mat	Creates RWG edge elements.
	rwgGeoMesh.mat	rwg3.m	impedance.mat	Computes the impedance.
	rwgGeoMesh.mat	rwg4.m		Determines excitation voltage and solves MoM equations.
	impedance.mat		current.mat	
	rwgGeoMesh.mat	rwg5.m		Determines and visualizes surface currents.
	current.mat		Plot	
Field	rwgGeoMesh.mat	efield1.m		Computes the radiated field on a ring with center *P*.
	current.mat		Parameters	
	rwgGeoMesh.mat	efield2.m		Computes the radiated/scattered field.
	current.mat			
	sphere.mat		gainPower.mat	
	rwgGeoMesh.mat	efield3.m		Displays the 2D radiation pattern in a polar plot.
	current.mat			
	gainPower.mat		Plot	

Each of the element files were compiled against the mesh files created in each progressive step. The antenna was solved for and its properties computed. These theoretical results and comparison to the measured results will be discussed. The physical characteristics of the antenna will be discussed in the next section.

The antenna is the sole artifact of wireless power transmission and relies on no other analogue. If wireless energy transfer is to become more useful, it is necessary to establish a set of generalizations regarding specific conditions of operation.

2.3.1 The receiving antenna

A receiving antenna may be viewed as any metal object that scatters an incident electromagnetic field from a transmitting antenna, which propagates a single-band signal. Because of scattering, an electric current appears on the antenna's surface. That current in turn creates a corresponding electric field. If a capacitor is attached to the free ends of the loop, as shown in Fig.2.39b, a voltage difference appears

at the terminals. The terminal voltage constitutes the received signal; power is extracted through the voltage and fed to an incandescent lamp, shown in Fig.2.29. Analytically speaking, it is ideal if the scheme could be addressed as surface current distribution over the antenna as a three-dimensional oval surface using its edges as propagation of the magnetic field expected in a Boltzmann distribution. The description here will be for a two-dimensional flat surface antenna.

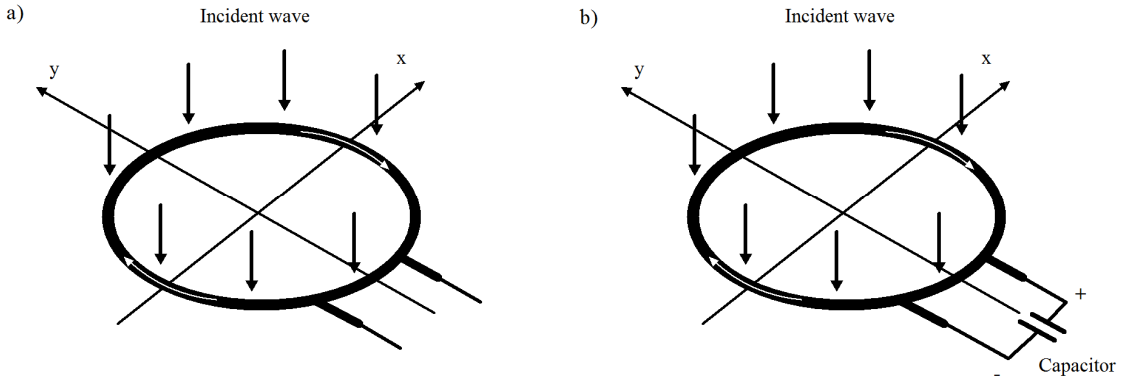

Fig.2.39. (a) Schematic of the receiving loop antenna. (b) Loop antenna connected to a capacitor at the voltage gap. The white arrows are surface currents.

Considering solely the viewpoint of energy transfer, an antenna in the receiving mode collects electromagnetic energy over a certain area, shown in Fig.2.39a, extracts the captured power while both absorbing and reflecting the energy back into free space, behaving like a signal repeater. The specifications of the coils, as illustrated in Fig.2.1, are shown in Table 2.7.

Table 2.7. Transmission and receiving coils physical specification.

TABLE 2.7
TRANSMISSION AND RECEIVING COILS PHYSICAL SPECIFICATION

Coil	Coil radius (mm)	Wire radius (mm)	Wire length (mm)	Number of turns
L_i	30	0.4	650	3
L_j	30	0.4	650	3

The method of moments is solved for the antenna surface using Rao-Wilton-Glisson (RWG) edge elements. A short discussion of the detail of the RWG algorithm is required to understand how the edge elements are used to approximate the field solution [65]. The surface of an insulated metal loop antenna divided into separate triangles as shown in (Fig.2.40a). Each pair of triangles, having a common edge, constitutes a corresponding edge element, see (Fig.2.40b). One of the triangles has a plus sign and the other a minus sign indicating the direction of the current. A vector basis function,

$$f(\mathbf{r}) = \begin{cases} \left(\frac{l}{2A^+}\right)\rho^+(\mathbf{r}), & \mathbf{r}\,\text{in}\,T^+ \\ \left(\frac{l}{2A^-}\right)\rho^-(\mathbf{r}), & \mathbf{r}\,\text{in}\,T^- \\ 0, & \text{otherwise}, \end{cases} \tag{110}$$

is assigned to each edge element where l is the edge length and $A^{\pm}$ is the area of triangle $T^{\pm}$. Vector ρ^+ connects the free vertex of the plus triangle to the observation point $\mathbf{r}$, shown in (Fig.2.40b). Vector ρ^- connects the observation point to the free vertex of the minus triangle [60].

The vectorized surface electric current on the antenna surface, shown in Fig.2.40a, is a sum of the contributions over all edge elements with unknown coefficients. These coefficients are found from the moment equation (110). The surface current density on a surface S_θ of a perfectly conducting structure is given by an expansion into RWG basis functions over *m* edge elements. The moment equations are a system of linear equations with the impedance $\mathbf{Z}$. The basis function of the edge element corresponds to a small but finite electric dipole of length $d = \left|\mathbf{r}^{c-} - \mathbf{r}^{c+}\right|$ shown in Fig.2.40b and [21]. Index c denotes the center of triangle $T^{\pm}$ for the division of a loop antenna structure into elementary electric dipoles, shown in Fig.2.40d.

The approximation here is similar approach to describe the currents according to Maxwell's equations [61] in terms of those specified at in §1.1. The current density, $\mathbf{J}$, and the antenna impedance $\mathbf{Z}$ is represented on surface S_θ. If S_θ is open, $\mathbf{J}$ is regarded as the vector sum of surface currents on opposite sides of S_θ. As,

$$\mathbf{J} = \sum_{m=1}^{M} I_m \mathbf{f}_m,\ \mathbf{f}_m = \begin{cases} \left(\frac{l_m}{2A_m^+}\right)\rho_m^+(\mathbf{r}), & \mathbf{r}\,\text{in}\,T^+ \\ \left(\frac{l}{2A_m^-}\right)\rho_m^-(\mathbf{r}), & \mathbf{r}\,\text{in}\,T^- \\ 0, & \text{otherwise}, \end{cases} \tag{111}$$

Where $\mathbf{Z}$ expresses the vector voltage from expansion coefficients I_m forming the impedance moment $\mathbf{Z}\cdot\mathbf{I} = \mathbf{V}$. The antenna voltage is expressed by [60],

$$\mathbf{V}_m = l_m \left(\mathbf{E}_m^+ \cdot \frac{\rho_m^{c+}}{2} + \mathbf{E}_m^- \cdot \frac{\rho_m^{c-}}{2} \right), \mathbf{E}_m^{\pm} = \mathbf{E}^{inc}\left(\mathbf{r}_m^{c\pm}\right), m = 1,...,M, \qquad (112)$$

where $\mathbf{E}^{inc}$ is the electric field on an incident electromagnetic signal over the length, l_m, of the antenna. The voltage excitation vector is analogous to the circuit voltage. The surface electric current on the antenna surface is a sum of the contributions (111) over all edge elements.

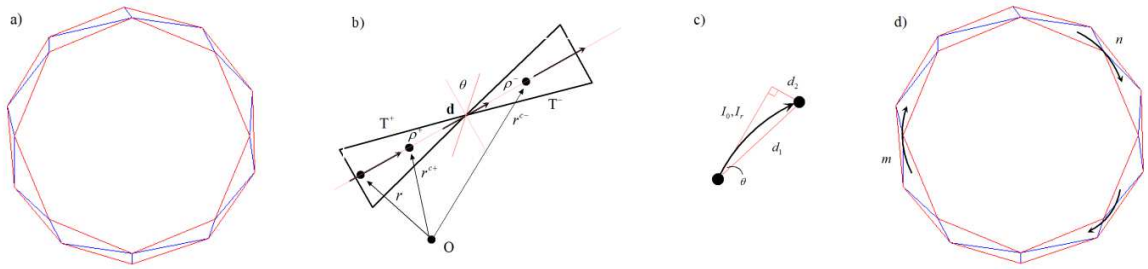

Fig.2.40. Modified schematic of RWG edge element and the dipole interpretation for curvature θ.

Simply state: The impedance $\mathbf{Z}$ describes the interaction between neighboring elementary dipoles given over the length of the conductor. If edge elements *m* and *n* are dipoles, the element $\mathbf{Z}_{mn}$ describes the contribution of dipole *n*, through the radiated field, to the electric current of dipole *m*. The size of $\mathbf{Z}$ is equal to the number of edge elements. This contribution is calculated using the electrical field integral equation [62, 63].

The antenna was constructed and simulated using *Matlab* while theoretical equations were computed using the *Circuit calculator*. Using *Matlab* with the PDE toolbox, the surface mesh is designed by creating a model of the loop and creating RWG triangles. Visually, one can create the meshes based on a 2-D model approximation of a loop surface, shown in Fig.2.41a for 180 nodes and 288 triangles and Fig.2.41b for 648 nodes and 1152 triangles. A systematic description is contained in Table 6.2.

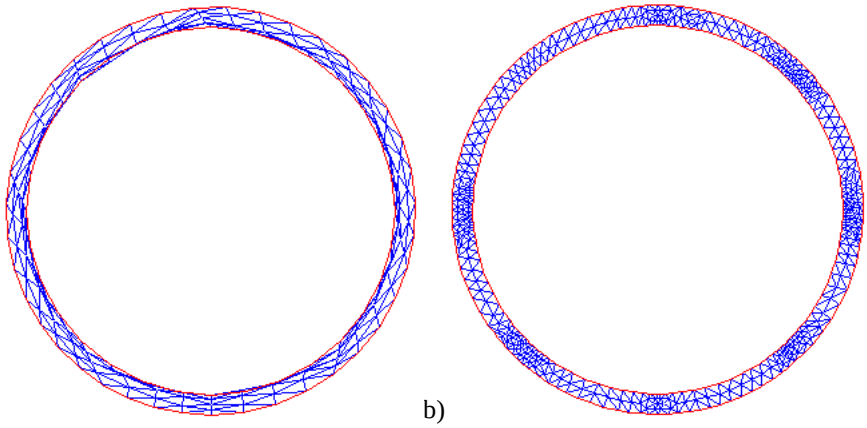

a) b)

Fig.2.41. Two loop meshes: (a) 288 triangles and (b) 1152 triangles.

During the process of creating the mesh, checking the triangle quality will provide an average characteristic before continuing with the RWG analysis. The triangle quality of both meshes shown in Fig.2.42a while the expected current density, shown in Fig.2.42b, is confined to the inner edge of the loop. The RWG edge elements are more advantageous than the simple finite dipoles. In particular, they support a uniform axial electric current along a thin metal strip, approximating for curvature [64]. For help calculating in Matlab for the desired antenna characteristics from the constructed meshes, code from [65] will be used to perform the computations.

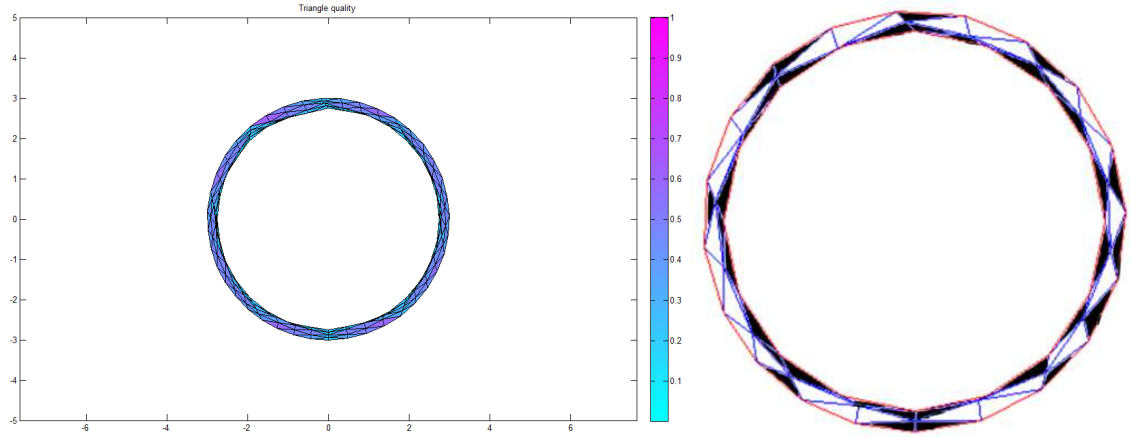

Fig.2.42. (a) Triangle quality of the loop mesh, (b) current density on the loop.

The .mat files containing the compiled mesh of the antenna structure are used as input to the edge generator rwg1.m and to the rest of the code sequence listed in Table 2.6. The PDE tool is used created compiled mesh “magneticLoopMesh.mat” with 288 triangles.

Using the input characteristic antenna data:

- $412\ \text{kHz} \leq f_0 \leq 526\ \text{kHz}$,
- observation point: 50 centimeters on the *z* axis,
- radiation sphere radius: 100 centimeters,
- feeding edge [-1, 0, 0], dipole,

resulted the sequence for output data is listed in Table 2.8.

Table 2.8. Matlab computed input characteristic antenna data.

TABLE 2.8
COMPUTED ANTENNA CHARACTERISTICS BASED ON MoM

Property	$L_i(ideal)$
Edges total	1656
Impedance (Ω)	0.000 + 0.493i
Feed power (W)	7.12e-11
I_0(A)	1.25
E_θ	1.0e-05 *
	-0.0007 + 0.0001i
	0.1080 - 0.0239i
	0
H_θ	1.0e-08 *
	0
	0
	0.1039 - 0.2206i
Poynting field S_θ	1.0e-15 *
	0.8249
	0.0054
	0
Stored energy (J)	8.249e-12
Total power (W)	1.271e-10
Gain (dBi)	2.4778
Radiation resistance	6.1799e-11

The computation of the model suggests that the structure of the radiation is exclusively a property of the geometry of the coil. A specific pattern of radiation emission is observable by showing intensity of projection field $\bar{\mathbf{H}}$, out from the dipole at the center of the loop, shown in Fig.2.43.

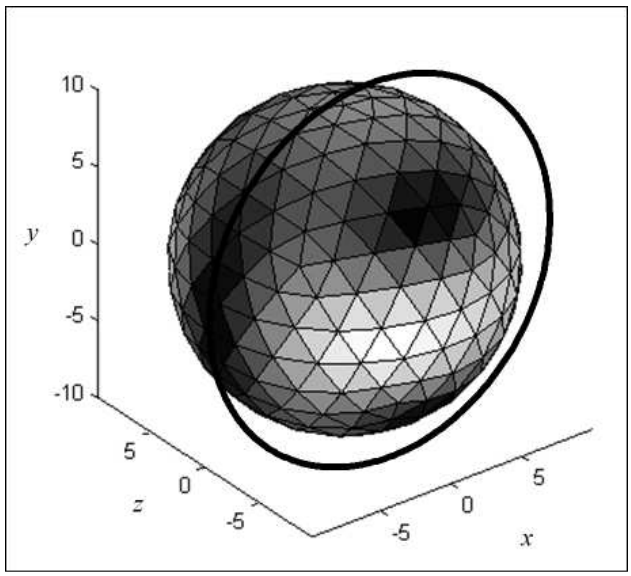

Fig.2.43. Directional power density of field on its approaching wavefront, white shows higher power.

By examination of Fig.2.43, the field emanating from the loop antenna, the whiter toward the center of the loop is the plane of projection, relative to the loop around the sphere. The power signature is due to the dipole releasing energy and the forces upon the electrons in the conductor. This is given in

more detail in Chapter 4. The height of displacement along the y-axis is the beam width. It is interesting to now describe the computations which determined the emitted power and radiation resistance of the field given the distance between the antenna based on [30].

2.3.2 Radiated power

In terms of the circuit model of the physical antenna, energy and power are computed using the C# program *Circuit calculator*. The voltage and current are related via the impedance of the loop. In the case of electrically-small loops, impedance is the series combination at the angular frequency, ω_0, of the reactance of the external inductance, L_e, and radiation resistance R_r, and ohmic resistance, R_o, of the conductor,

$$Z_0 = R_o + R_r + j\omega_0 \left(L_e + L_i \right), \tag{113}$$

and terms operating on the loop have the forms,

$$\begin{aligned} I(z) &= I_0 \cos\left(\frac{\pi z}{\ell} \right), \\ V(z) &= -jZ_0 I_0 \sin\left(\frac{\pi z}{\ell} \right), \end{aligned} \tag{114}$$

where I_0 is the current in the short-circuit at $z = 0$ and ℓ is the length of the attractive transmission path. The average stored magnetic energy in the loop in its single mode at resonance is,

$$\begin{aligned} \left\langle W_m \right\rangle_{\omega_0} &= \frac{1}{4} \int_0^l L \left| I_z \right|^2 dz \\ &= \frac{1}{4} L \left| I_0 \right|^2 \int_0^l \cos^2 \left(\frac{\pi z}{\ell} \right) dz \\ &= \frac{1}{8} L \ell \left| I_0 \right|^2 . \end{aligned} \tag{115}$$

The average stored electrical energy does not need to be calculated separately since the system is at resonance, $\left\langle W_e \right\rangle_{\omega_0} = \left\langle W_m \right\rangle_{\omega_0}$, so,

$$\begin{aligned} \left\langle W_{total} \right\rangle_{\omega_0} &= \left\langle W_e + W_m \right\rangle_{\omega_0} \\ &= \left\langle 2W_m \right\rangle_{\omega_0} = \frac{1}{4} L \ell \left| I_0 \right|^2 . \end{aligned} \tag{116}$$

One interpretation that can be drawn from the mathematics is energy can be applied to the system to the point as the waveguide can sustain.

A discussion of the calculation of the potential of free-space is well outside the scope of this thesis, however, suffice it to say, it is expected this number to be very large given the radius of the coils. This is a very important feature, which can be explored by this method, and it is suggested to be conducted in future research.

The dissipated power, while a property of the load present, is also a property of the power sustained in the magnetic field. A resonant object will allow power to be seen at the receiver as,

$$\begin{aligned}\langle p_d \rangle &= \frac{1}{2} R \left| I(z) \right|^2 + \frac{1}{2} G \left| V(z) \right|^2 \\ &= \frac{1}{2} R \left| I_0 \right|^2 \int_0^l \cos^2 \left(\frac{\pi z}{\ell} \right) dz \\ &+ \frac{1}{2} G \left| V_0 \right|^2 \int_0^l \cos^2 \left(\frac{\pi z}{\ell} \right) dz.\end{aligned} \tag{117}$$

Its impedance yields the stored energy at resonance within the transmitted wave. For a non-isotropic radiator if the emitted power is $P_{rad} W$ at a distance d from the source, the magnitude of the wave's Poynting vector (power per unit area) is,

$$P_t = \frac{P_{rad}}{4\pi d^2}. \tag{118}$$

The radiated power P_{rad} is replaced by $P_t G_t$, where P_t is the power delivered to the transmitter antenna by the amplifying switches in the circuit and G_t is the transmitter antenna gain. The electric field intensity, the result of active coupling, at the antenna interface is,

$$E_\theta = \sqrt{Z_0 \mathrm{P}_t}, \tag{119}$$

where Z_0 is the impedance of free-space (39). At a relatively large distance from a non-isotropic radiator, the electric field intensity, or the simple magnitude of the disturbance, is,

$$I_{E_\theta} = \sqrt{120\pi \cdot \frac{P_\mathrm{t} G_\mathrm{t}}{4\pi d^2}} = \frac{\sqrt{30 P_\mathrm{t} G_\mathrm{t}}}{d} \text{ V/m}. \tag{120}$$

If the electric field intensity and power at the receiving antenna are E_{rec} and P_{rec}, respectively, the maximum power able to perform work intercepted by the receiver is,

$$\mathrm{P}_r = \frac{\lambda^2}{4\pi} \cdot \mathrm{P}_{rec}. \tag{121}$$

For a non-isotropic antenna of receiver power gain, G_r, and given (117), the received power is,

$$P_r = \frac{\lambda^2}{4\pi} \cdot P_{rec} G_r = \frac{\lambda^2}{4\pi} \cdot \frac{E_{rec}^2}{Z_0} \cdot G_r = \left(\frac{E_{rec} \lambda}{2\pi} \right)^2 \cdot \frac{G_r}{120}. \tag{122}$$

The average radiated power can be considered lost as far as the source oscillator is considered; therefore, the antenna behaves similar to a resistor as dissipating power from the source. The radiation resistance R_r is defined as an average quantity,

$$R_r = \frac{I_0^2}{2} \frac{1}{P}, \tag{123}$$

where I_0 is the input current to the transmitter coil, see Fig.2.1 and Fig.2.35. This is implying that the Ampère unit here is representative of a force. Modifying (123), assuming a uniform current restricted to a Boltzmann distribution,

$$R_r = 20\pi^2 \left(ka \right)^4, \tag{124}$$

where $ka = 2\pi a / \lambda$ Solving for radiation resistance of the antenna,

$$R_r = \frac{I_0^2}{2} = 10 \beta^4 A^2 I_0^2, \tag{125}$$

where I_0 is the peak amplitude applied to the antenna terminals. The ratio of separation between the coils and the geometric mean of the transmitter and receiver coil radii $r_{\bar{ij}} = \sqrt{r_i r_j}$ will be the measure of this maximum gradient along the length away from the coil along the z-axis, illustrated in Fig.2.44.

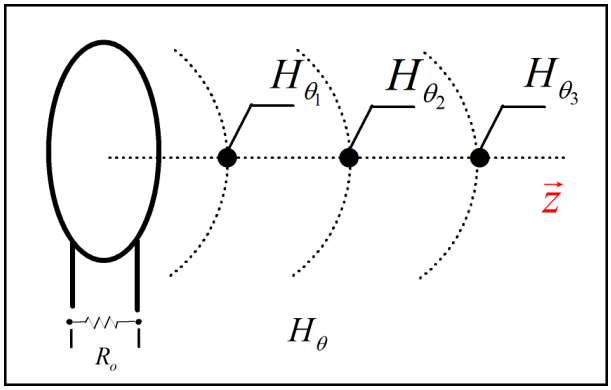

Fig.2.44. Projection of magnetic currents with highest potential coupling points H_θ.

In the space containing the energy, the intensity of the magnetic field can be known in advance given the distance between the coils and the radius of the primary coil. In a multiple-turn Litz-wound coil of n turns with radius r_i, the magnetic field strength along z from the center of the coil along the axis can be written as [66],

$$H(z,r_i)=\frac{\mu_0 I\cdot n\cdot r_i^2}{2\sqrt{\left(r_i^2+z^2\right)^3}}. \tag{126}$$

Differentiating with respect to r_i shows that for $r_i=z\sqrt{2}$, H_θ will be maximized [67].

The ratio implies a geometry of the emitted fields, to explore this, it is relevant to discuss mapping the field to determine where energy is stored in greatest quantities and in what forms. The ambience of the field emission, or flux, is described as a direct consequence of the circuit's electrical properties. It will be shown that for an antenna of a given loop ratio, the flux as well as the intensity are calculated to be maximum in terms of the exchange of energy between the transmitter and the receiver. As discussed in §2.1.2, the amount of power transmitted is closely related to the coupling between the loop coils. The potential coupling, where $\psi H_\theta=\psi H_\varphi$, shifts the further the distance away as a measure of coordinates along it.

2.3.3 Field emissions

Results from the simulation show the emission pattern is a function of the antenna geometry, as illustrated in Fig.2.45.

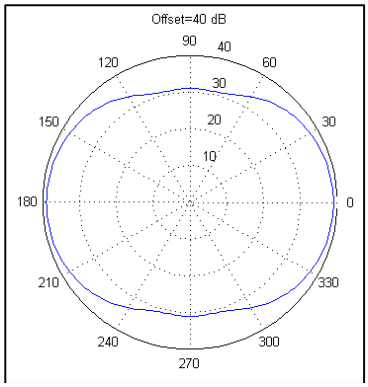

Fig.2.45. Average power-over-space antenna radiation pattern looking into the coil.

The result of the computational pattern agrees with what is expected, given [30], and illustrates that the pattern is a beam of a particular width.

It is now relevant to create a set of experiments, given in the simulation resulting from the theoretical framework, where this beam pattern is confirmed and shown in what magnitude given a distance away from its source. There will be two areas of illustration and discussion:

1. At distances where distance is less than the radius of the coils, $d < r$, and,
2. at distances where the distance is greater than or equal to the radius of the coils, $d \geq r$.

It is an interesting topic of future research to do a very detailed map of the energy distributed in the field between two resonant loops.

2.4 The circuit experiments

Three distinct sets of experiments were performed with the circuit and antenna model described throughout §2. These groups of experiments are:

1. Using a single transmitting and receiving coil,
2. using a single transmitting and receiving coil, using a conductive disc at the center of one or both coils, and,
3. using a pair of transmitting and receiving coils.

Of each of the experiments, different sets of properties are manipulated to shape an understanding of the behavior of the arrangement, given the theoretical implications in the model.

2.4.1 Measured power at a distance with a single loop transmitter and receiver

The first experiment was to test the theoretical framework, the simulation, and circuit model, setup shown in the form of Fig.2.1. Some assumptions are the use of off-the-shelf rubber-insulated copper

wire of fairly high quality to apply as much of an optimization as possible. If optimization is kept in mind during experimentation, it is but a linear increase of power transmission with more deliberately made materials, such a niobium-tin, a topic of future research. A schematic of the circuit is shown in Fig.2.46.

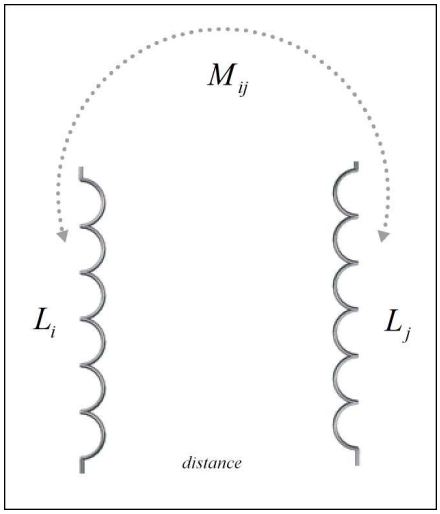

Fig.2.46. Schematic diagram of the circuit for a single coupled-mode.

Using the coil specification listed in Table 2.7, with single transmitting and receiving Litz wire antennas including legs, shown in Fig.2.38 and Fig.2.39, of number—$i = 3$ and $j = 2$—of two centimeters of the total inductances $L_i, L_j,$ at a transmission distance varied between contact and six centimeters, experiments were conducted to test the properties of the coils and energy transfer given the theoretical framework. The calculated specification is listed in Table 2.9.

Table 2.9. Experimental coils calculated electrical specification I.

TABLE 2.9
EXPERIMENTAL COILS CALCULATED ELECTRICAL SPECIFICATION I

Coil	Wire radius (mm)	Inductance (μH)	Mutual Inductance (μH)	Coupling coefficient (κ_{ij})
L_i	0.4	1.547	0.02489	0.0162
L_j	0.4	1.529	0.02489	0.0174

Capacitance C_i, C_j is set to as equal as possible, 100 nF. With an input at the oscillator of 4.5 volts and 1500 mA from an external DC supply, power measurements were taking by measuring the voltage and current present at the receiver at steps between close-proximity of the coils and distances to six centimeters.

The results of power measurements at a distance are shown in Fig.2.47.

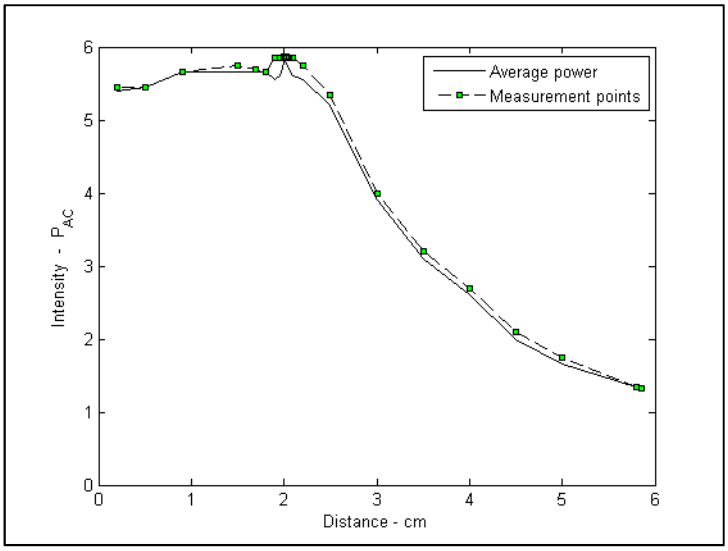

Fig.2.47. The power over distance showing the projection field $\bar{\mathbf{H}}$, where $C_i \approx C_j$.

In analyzing the data, it is apparent there is an area, as described in the theory, what is a projection where the energy is nearly constant across the increasing distance. At the end of the projection, which contains a peak value, transmission power over distance falls off linearly, as, $1/r^2$.

The pattern is present when the capacitor value used with the transmitter coil is nearly equal, $C_i \approx C_j$. It is hypothesized that the driving force of the projection is feedback power from the receiver to the transmitter across the space. It is expected that the projection would be less intense the more each half of the circuit drifts away from resonance with the other.

A second set of experiments were conducted to test the power over a distance of 100 centimeters. The results of power measurements at a longer distance are shown in Fig.2.48.

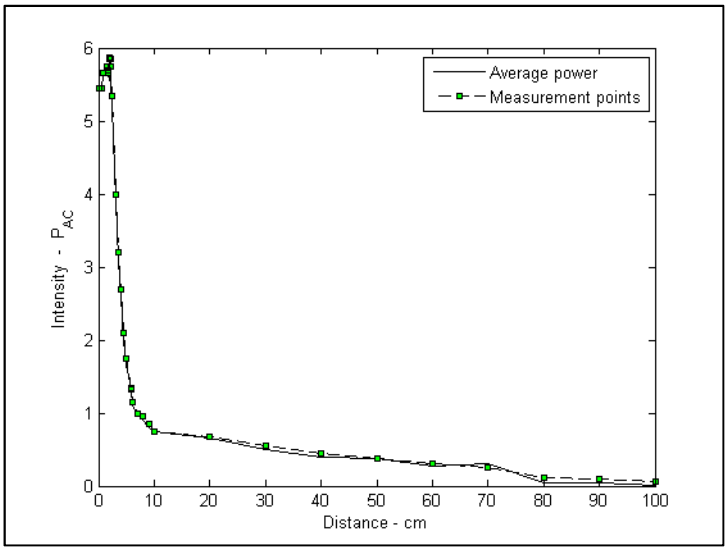

Fig.2.48. The power over a longer distance.

The behavior illustrated in Fig.2.48 is, while after the projection there is a falloff of $1/r^2$, near to the point of distance of ten centimeters, falloff transitions to a rate of $1/r$ and is continuous until the noise floor of the environment. A suggestion for future research is to obtain a more exacting set of data could be obtained by using a spectrum analyzer with an attenuator to prevent overloading at distances less than six centimeters.

A third set of experiments were conducted using a thicker wire to see if performance could be improved. It is expected that a higher amount of power would be observed at each measurement point from the previous set of experiments. The coil properties are listed in Table 2.10.

Table 2.10. Experimental coils calculated electrical specification II.

TABLE 2.10
EXPERIMENTAL COILS CALCULATED ELECTRICAL SPECIFICATION II

Coil	Wire radius (mm)	Inductance (μH)	Mutual Inductance (μH)	Coupling coefficient (κ_{ij})
L_i	0.5	1.469	0.02489	0.0170
L_j	0.5	1.451	0.02489	0.0181

It was observed during experiments that the coupling coefficient increases with a thicker wire, while the mutual inductance between the coils stays the same. Two conditions were applied to the experiment: one where the capacitor at the transmitter and receiver are equal, and one where the capacitors are not equal.

The results of power measurements of a thicker wire at a distance are shown in Fig.2.49.

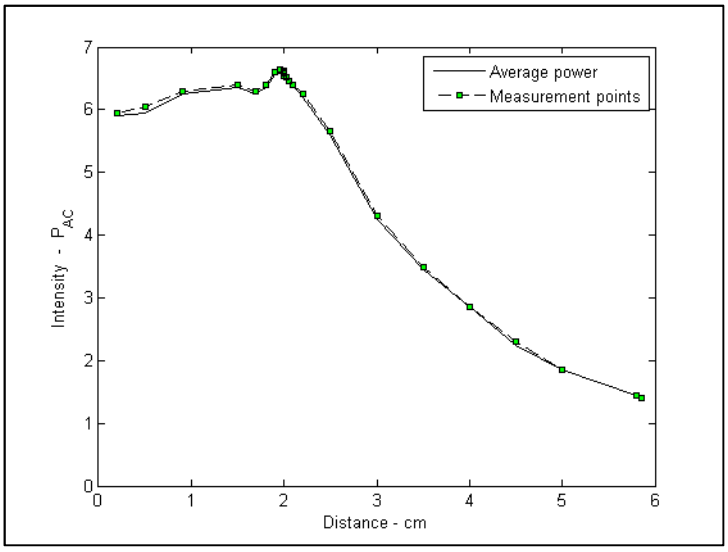

Fig.2.49. The power over distance using a thicker antenna wire.

It is confirmed that the assumption of more power transmitted per quotient of distance increases. It is also noted that the power seems, for lack of a more precise word, “smoother” using the thicker piece

of wire. There is a property of conductor thickness given electron acceleration at the antenna which is an interesting point to study in future research. It is expected a similar behavior, expect a greater level of power delivery in the same manner as Fig.2.49 will manifest over the length of 100 centimeters as in the previous set of experiments.

A fourth set of experiments were conducted changing the value of the capacitor between the transmitter and the receiver, component C1 of Fig.2.28 and C4 Fig.2.29 respectively. In the previous set of experiments, the value of capacitors was set to be as equal as possible, given the limitations of the components and the laboratory measurement equipment with differences no greater than 10 pF. In this set of experiments, the value of the capacitance at the receiver was reduced incrementally to zero, or no capacitor present. The result of measurements over the distance is shown in Fig.2.50.

Between the cases when $C_i \approx C_j$ and $C_i > C_j$, a contrastingly different behavior is observed. It is hypothesized that the reason for the projection field is primarily a feedback of power from the receiver to the transmitter which appears as a maximum in close proximity to the transmitting antenna, or what this thesis calls the projection field $\bar{\mathbf{H}}$. From data in the experiments, it is expected that the projection would be more intense the closer each half of the circuit is at resonance with the other.

According the data from all experiments, the amount of received power is due more strongly to the inductive component than the capacitive component. This is concluded since the lamp is lit even if no capacitor is used at the receiver.

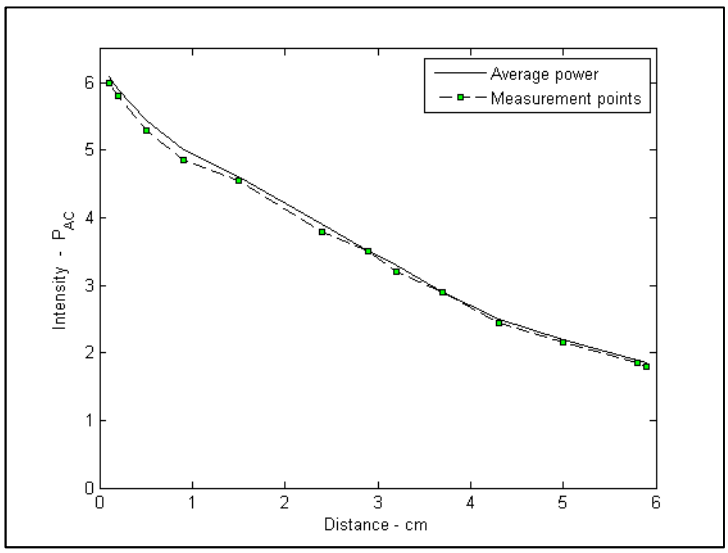

Fig.2.50. The power intensity over distance showing linear falloff, where $C_i > C_j$.

A fifth set of experiments were conducted when $C_i \approx C_j$ using a non-uniform Litz loop winding. At the measurement points given in the previous experiments, energy is still transmitted, although with a far less intensity, calculated to be at about 22% of either set of experiments using the different wire thicknesses. The projection field, $\bar{\mathbf{H}}$, is also present. It is noted that the energy reception is tied more directly to the total wire length of the receiving antenna than that of the geometry of the loop.

In this case when $C_i \approx C_j$, the energy contained in the projection, $\bar{\mathbf{H}}$, as well as the area of the transmission where falloff is at a rate of $1/r^2$, called the mid-field region, is due to the incident $\bar{E}_1$ and reflected $\bar{E}_1'$ waves, as,

$$\bar{E}_1 e^{j(\omega t - k_0 z)}, \bar{E}_1' e^{j(\omega t + k_0 z)}, \tag{127}$$

are given as oscillator properties, where k_0 is the vacuum wave number. The calculated value is shown in Table 2.5. There are points in the field where there is constructive and destructive interference in the beam inferring a polarization in the plane-waves. These fields are transverse and only the tangential components exist at the boundary plane of $z = 0$. Equation (127) represents the electric field present of the incident and reflected waves constructively interfering. The determination of the strength of the electric field at the coil winding is dependent upon the current at the Litz winding,

$$I_{E_\theta} = I_0 \sin \frac{\sin^2(\beta)}{\beta^2} \frac{\sin^2(n\partial)}{\sin^2(\partial)}, \tag{128}$$

where,

$$\beta_{E_\theta} = \frac{\pi \sin\theta}{\lambda}, \partial = \frac{\pi d \sin\theta}{\theta}. \tag{129}$$

The quantity I_{E_θ} is the electric field intensity on the wire, *d* is the diameter, and θ is the index of refraction. The profile of the antenna and the pattern of the transmission energy are illustrated in Fig.2.51.

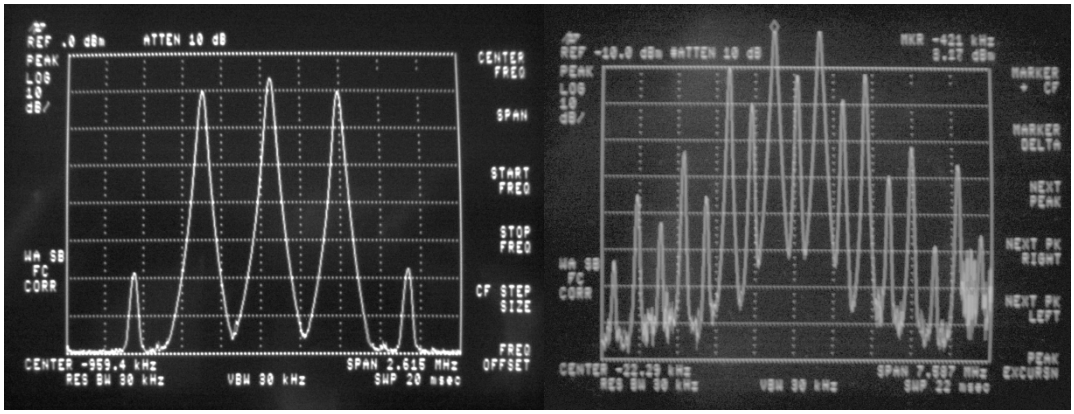

Fig.2.51. Radiation pattern observed at the receiver.

The plot to the left of Fig.2.51 shows the radiation pattern observed from the receiver. The plot to the right of Fig.2.51 shows a higher resolution bandwidth. Following the theoretical discussion of the expected beaming pattern in §2.3.3,

The radiation pattern of Fig.2.51 is observed where r, proportional to the field intensity, is approaching maximum at a distance from the transmitter. The pattern has its main-lobe maximum in the z direction $(\theta = 0)$ with minor lobes to the left and the right in other directions. Between the lobes are nulls in the directions of zero or minimum radiation.

To specify the radiation pattern with respect to the field intensity and polarization requires three features: the θ component of the electric field $E_\theta(\theta,\phi)\left(V\,m^{-1}\right)$, the ϕ component of the electric field $E_\phi(\theta,\phi)\left(V\,m^{-1}\right)$, and the phases of these fields as functions of the angles θ and ϕ or $\delta_\theta(\theta,\phi)$ and $\delta_\phi(\theta,\phi)$. Dividing a field component by its maximum value will reveal a normalized field pattern, a dimensionless number with a maximum value of unity. The normalized field pattern for the θ component of the electric field is,

$$E_\theta(\theta,\phi)_N = \frac{E_\theta(\theta,\phi)}{E_\theta(\theta,\phi)_{\max}}. \tag{130}$$

At distances relative to the size of the antenna and small compared to the wavelength, the field pattern is expressed in terms of power per unit area, or the Poynting vector $S(\theta,\phi)$. Normalizing the power with respect to its maximum value, as in the electric field example, yields a normalized power pattern as a function of angle, which is a dimensionless number, with a maximum value of unity. The normalized power pattern is,

$$P_n(\theta,\phi) = \frac{S(\theta,\phi)}{S(\theta,\phi)_{\max}}, \tag{131}$$

where $S(\theta,\phi)$, the Poynting vector equals,

$$\frac{E_\theta^2(\theta,\phi) + E_\phi^2(\theta,\phi)}{Z_0} \mathrm{W\,m^{-2}}, \tag{132}$$

expressed in rectangular coordinates on a decibel scale,

$$\mathrm{dB} = 10\log_{10} P_n(\theta,\phi), \tag{133}$$

shown in Fig.2.51. The efficiency of the transmitted power in the primary mode is given by the ratio of its total beam area, Ω_A, consisting of the main-lobe area, Ω_M, plus the minor-lobe area Ω_m. The ratio of the main beam area is the beam efficiency,

$$\eta_M = \frac{\Omega_M}{\Omega_A}, \tag{134}$$

while the ratio of the minor-lobe area to the total beam area is the stray factor,

$$\xi_M = \frac{\Omega_m}{\Omega_A}, \tag{135}$$

with a total efficiency of,

$$\eta_M + \xi_M = 1. \tag{136}$$

In experiments, this value is shown to be 0.768. The calculated values of the radiated power characteristics for the antenna are listed in Table 2.11. These were calculated in the *Circuit calculator* software.

Table 2.11. Calculated antenna characteristics based on [30].

TABLE 2.11
CALCULATED ANTENNA CHARACTERISTICS BASED ON [30]

Property	$L_i(lossy)$
I_0(A)	1.25
E_θ(A/m)	1.572e-04
H_θ(T)	4.170e-07
Poynting field	8.249e-16
Directivity (dBi)	1.76
Gain (dBi)	2.10
Radiation resistance (Ω)	1.1396e-11
Radiation efficiency factor	2.62e-10
Depth of penetration (m)	1.22e07

The operational circuit including the antenna powering a lamp a distance is shown in Fig.2.52. The field shows a continuous flow of energy from transmitter to receiver is taking place on spatial and temporal vectors. Conception of the energy in the field was a combination of the current at the surface of the antenna and the density of propagated energy across free-space. Directional finding [68] is possible in the scheme but was not explored in depth. Information transfer, although not directly examined is also possible by means of the same circuitry, given the sinusoidal nature of the power transmission. Additions to the amplifier circuit would however be required where a modulation signal is introduced to the carrier. Modifications to the receiver would however also be required. For simplicity, the wave is understood as a characteristic of its potential power, given the circuital characteristics already discussed.

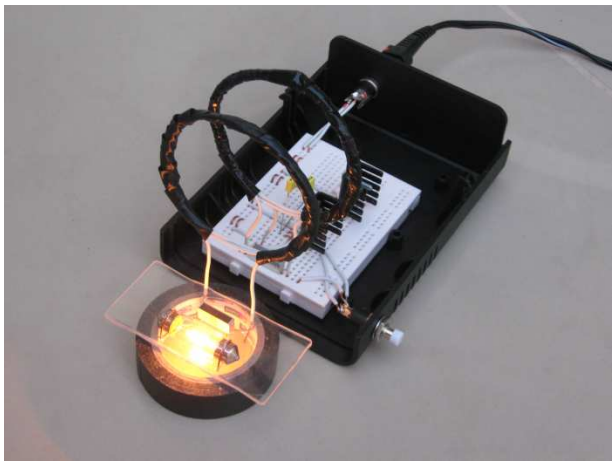

Fig.2.52. Prototypical wireless-power oscillator demonstrating the theoretical model.

The radiation and pattern as a function of the field emission is observable directly as a function of geometry, and match the simulated pattern shown in Fig.2.45. Organic material does not destructively interfere with the transmission. A suggestion for future research is to use metal plates to create eddy currents induced by a changing magnetic field to leverage the signal to a human connection, such as

the coupling of the nervous system to an external computer via magnetic coupling including modulation as an information carrier.

What has been discussed in this section is for a single loop power scenario exclusively—primary coil to primary coil coupling of a single mode. Introduction of methods to enhance the magnetic field culminating at the center of the loop are treated in the next section.

2.4.2 Measured power at a distance with an enhanced magnetic field at the potential

This section proposes a method to enhance the magnetic fields in an inductive-coupled, resonant-link model which realizes an improvement in power received at a distance.

The theoretical description of the improvement utilizes a single mode of propagation [24], an isotropic waveguide transformed anisotropically by the motion of a magnetic field between a transmitting and receiving element resulting from an acceleration force present in the electric field at the source. Isotropy in this case implies that changes to the magnetic field are present equally in both the x-y and z plane. The working definition of radiation emitted in a locally-approximated isotropic waveguide is an exchange of discretized energy whose velocity is attenuated by a characteristic resistive quality of its displacement in the media. Such resistance is also due to the magnetic field density and coupling errors expressed by drift of the resonant-link between the elements. The exchange of electromagnetic forces increases anisotropy and forms the waveguide into a shape with a particular curvature, yielding a state of equilibrium where currents are observed flowing from the transmitter to perform a quantity of work at the receiver.

A goal is to examine a technique of increasing the real-valued flux density and bind the curvature of propagating charges across a circuit consisting of two loops operating at a constant resonant frequency. It is proffered that if the flexion of curvature is reduced in the waveguide by the introduction of conducting discs, then the received power is increased over longer distances. The result sheds light on the details of the theoretical framework underpinning the hypothesis that wireless energy transfer in coupled-modes is dependent upon the state and order of the magnetic field. Theoretical and experimental setup is shown in Fig.2.18.

Four sets of experiments were performed: a straight forward power transmission without discs, transmission with one disc in the transmitting loop, transmission with one disc in the receiving loop, and finally with one disc in both the transmitting and receiving loops simultaneously.

The experiment consisted of a circuit of two loops driven to a frequency of 450 kHz at a power level of 4.5 volts and 1.1 amperes was used to test the theoretical framework.

In order to show the prediction of an increase in received energy due to the addition of a metal disc, a position is determined so that movements away demonstrate the reduction in electrical potential and power linearly as $1/r^2$, affecting the matrix by introducing a vector u.

The relative difference between two loops set at a distance of a radius length, 3 cm, at a potential of 4.0 volts yields power measured using a spectrum analyzer of 11.26dBm at a calculated value of 460Ω, although it is anticipated that it could be a much higher load impedance [30], given its resonance frequency ω_0.

By moving the receiver away from the transmitter, so the less likely it is to intersect with the hyperbolic field, as was discussed in the theoretical framework, given the curvature of the field established by the coupling. It is shown here that the addition of the disc increases $\mathbf{H}$, or, reduces the curvature of the hyperbolic function where more "field lines" will intersect with it.

During the experiment, the electric field was measured by a probe and exhibited as a function of the loop antenna lying in the x-y plane and calculated in Joules; the magnetic field was measured by a Hall probe and exhibited as a function of its projection along the *z*-axis and calculated in Teslas with the dominant azimuthal magnetic field—neglecting contributions of minor azimuthal fields—in Teslas at a pressure of one atmosphere and a temperature of 20° C.

Table 2.12. Calculated quantities in the projected magnetic field.

TABLE 2.12
CALCULATED QUANTITIES IN THE PROJECTED-PROPAGATING MAGNETIC FIELD $\bar{\mathbf{H}} \cdot \delta\mathbf{B}_z$.

Experiment	E-field ($\vec{x}$, $\vec{y}$, J)	B-field ($\vec{z}$, T)
A: Loops sans disc	$(2.0 \cdot 10^{-6} + 0.02i, -2.77 \cdot 10^{-8} - 0.002i)$	$(5.0 \cdot 10^{-7} - 0.067i)$
B: Transmitter disc	$(1.62 \cdot 10^{-6} + 0.32i, -2.52 \cdot 10^{-6} - 0.3452i)$	$(2.0 \cdot 10^{-7} - 0.024i)$
C: Receiver disc	$(2.48 \cdot 10^{-6} + 0.02i, -3.21 \cdot 10^{-6} - 0.038i)$	$(8.76 \cdot 10^{-5} - 0.002i)$
D: Loops with discs	$(2.82 \cdot 10^{-6} + 0.02i, -3.45 \cdot 10^{-6} - 0.367i)$	$(7.48 \cdot 10^{-5} - 0.042i)$

Table 2.13. Calculated quantities in the projected magnetic field.

TABLE 2.13
CALCULATED QUANTITIES IN THE PROJECTED-PROPAGATING MAGNETIC FIELD $\bar{\mathbf{H}} \cdot \delta\mathbf{B}_z$.

Experiment	Dominant azimuthal B-field (T)	Impedance (Ω)
A: Loops sans disc	$(1.62 \cdot 10^{-6} - 0.856i \text{ @ } 45°)$	376 + 9.7165i
B: Transmitter disc	$(3.2 \cdot 10^{-7} - 0.148i \text{ @ } 62°)$	376 + 9.7165i
C: Receiver disc	$(8.06 \cdot 10^{-6} - 0.856i \text{ @ } 62°)$	376 + 9.7165i
D: Loops with discs	$(9.895 \cdot 10^{-5} - 0.856i \text{ @ } 87°)$	376 + 9.7165i

Examination of the results contained in Tables 2.12 and 2.13 show that an increase in magnetic field yields an increase in quantized energy density. Lensing was not considered in the experiment, only how energy transformation was more efficient using the discs. A hypothesis for the increased efficiency is that a conversion of energy projected from the loop is taking place at a length closer to the receiver when it contains a disc. The incident waves, whose magnitude is nearer to where the power is being measured, are more efficiently converted into electric current.

Given the geometric patterns of Fig.2.17 and Fig.2.19 of $\mathbf{B}$ at the point where $\delta\mathbf{B}$ makes a stronger contribution, field momentum is hyperbolic in its distribution (on a circularly perfect antenna surface) and the concentration of energy is confined to the area inside the loop along its transmission axes. Hence, it is more illustrative given the experimental setup, to calculate field decay over a distance following $\bar{\mathbf{H}}$ as converging to a point at the center of the receiver.

In Table 2.14, the impedance is calculated given the power measured and that available to the spectrum analyzer—a range between 50 and 600Ω.

Table 2.14. Experimental quantities of the magnetic loop antenna.

TABLE 2.14
EXPERIMENTAL QUANTITIES - MAGNETIC LOOP ANTENNA SET AT A DISTANCE

Experiment	Distance (cm)	Potential (V)	Power (dBm)	Impedance (Ω)
A: Loops sans disc	3.0	4.00	11.26	460
B: Transmitter disc	3.0	3.65	12.69	520
C: Receiver disc	3.0	4.45	16.06	260
D: Loops with discs	3.0	4.28	15.88	340

The results listed in Table 2.14 show the equivalent numbers in terms of the equipment measuring the fields. The observation point was considered to be at the center of the loop, where the coordinate (0, 0, 0) was found. Any movements in the point of observation involved trajectories along the *z*-axis, although deflections in the x - y plane were also possible.

In the projection $\bar{\mathbf{H}}$, the magnetic field experiences minimum decay; outside the projection area, the power transfer falls at a rate of $1/r^2$ until a distance of $2r$, shown in Fig.2.53, then at a rate of $1/r$ until power transfer falls into the noise floor shown in Fig.2.54.

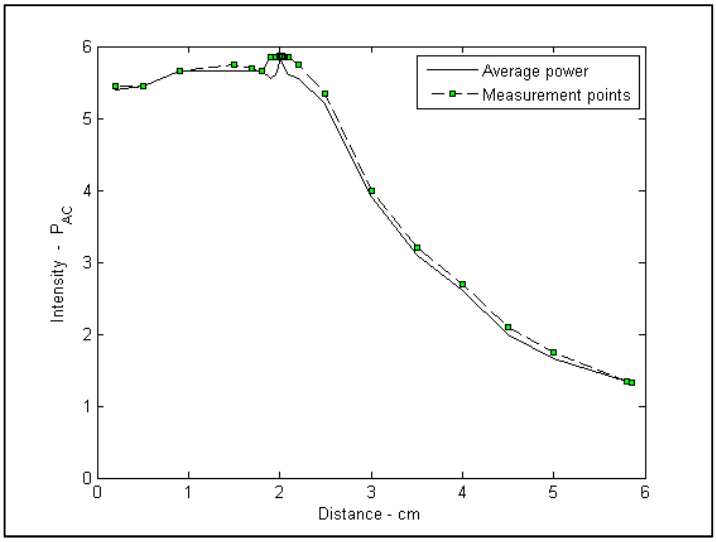

Fig.2.53. Intensity over distance, $d = 2r$.

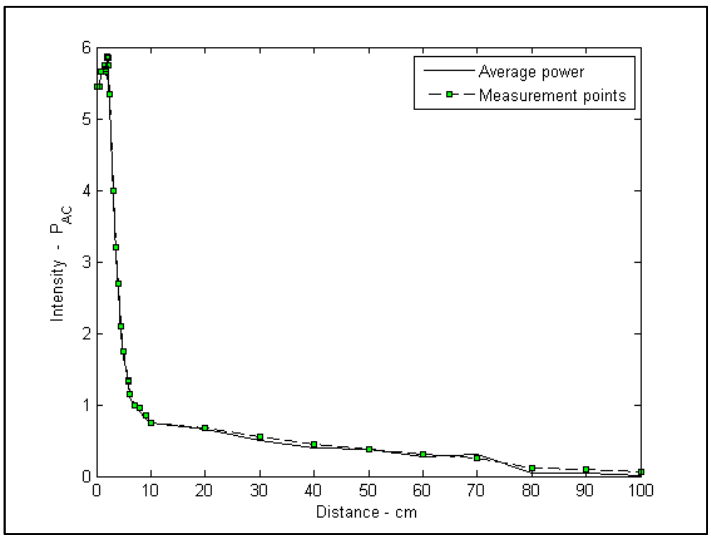

Fig.2.54. Intensity over distance, $d \gg r$.

Beam divergence was not studied in the experiment, only the energy present in the attractive force between magnetic-resonant fields.

It was determined during the experiments that the results agreed quite well with the theoretical calculations, demonstrating the validity of the theoretical framework. Nevertheless, improvements in the method are possible given the dynamic flow of the electric and magnetic quantities, as well as the appearance of multiple azimuthal fields. It is suggested by the experimental evidence that although the theoretical framework is sound, it is too simple in its present form to capture the complexity of the energy exchange in the fields. A recommendation for future research is to address in more detail the deeper aspects of why the energy exchange in the transition between mid-field region and far-field region changes its rate of decay.

By considering the geometry of a magnetic field as a radiation-object, it extends basic concepts to include a definition of energy exchange between resonant antenna. An extension is the concept of coupled-modes is successfully applied to energy-exchange object. This extension brought into the model those properties of modal-modes as a hypothetical explanation of highly-efficient wireless energy transmission by magnetic resonance which has not been addressed adequately in the literature. It has been shown that the description in [24] is suitable to describe coupled-modes.

Also, to take into account motions of intensity along the x-y plane, it is suggested by the experimental evidence that although the theoretical framework is sound, it is too simplistic a model in its present form to capture the full complexity of the energy transformation in the fields.

Therefore, a recommendation for future research is to address in more detail the deeper aspects of energy exchange and transformation in the polarization between the loop antennas manifesting wireless power transfer.

In this section an investigation of coupled modes, energy exchange, and energy transformation between two distant circular loop antennas was undertaken. We have introduced a novel concept of enhancement of the resonantly-coupled magnetic field by the addition of accretion discs thereby increasing the potential of the antennas at the interface of free-space. By the considering the geometry of a magnetic field as quasi-structured radiation following from a quantity of force, it has extended the basic concepts of antenna engineering by introducing a definition of energy exchange between resonant loops as a function of projection and oscillation to maximum entropic states.

Although it is well-investigated loop antenna for wireless power transfer over short distances, what was discussed in this experiment was the addition of accretion discs to increase the magnetic energy density. What was also discovered was that such discs help to direct the magnetic energy along the resonant trajectory toward the other resonant element. What was somewhat of a surprise was that the discs and their presence in the field seemed to suggest that a possible explanation for the addition of magnetic energy was an attractive force between the resonators in their particular coupled-mode.

A hypothesis to explain the observation is that the conductive material in the disc is responsible for the energy shifts. This would be possible if the discs create a first order magnetic field [24, 26]; although not directly observed, the magnetic field experiences little falloff in the projection area $\bar{\mathbf{H}}$, then continues falloff at a rate of $1/r^2$, where the field expresses an infinitesimal $\mathbf{B}$, then assumes a falloff of $1/r$. This is observed by increasing the distance between the resonant elements and

measuring the energy. Beam divergence was not taken into account in this experiment, only the attractive force between magnetic fields, as presented in §2.4.1. A detailed examination of beaming, divergence and if such apertures can be manipulated is a relevant topic of future research.

If further experiments could reinforce the determination that the field is transforming accordingly, it would suggest that in extending the presence of the magnetic field from the mid-field region to the far-field implies a usage of both Einstein's special relativity, which does not include an æther but moving frames and accelerating electrodynamics [6] which includes an æther. Although on the surface it would seem there is a contradiction in the representation of velocities, the author offers that perhaps there are more powerful contributions of the notion of time dilation to electrodynamics than meets the eye.

2.4.3 The circuit experiment with subtended angles in human proximity

One aspect of the utilization of wireless power, as shown in the introduction, was the form attached to the human body. This section will describe an application of the oscillator and model, illustrated in detail in §2, for powering subcutaneous implants and components, wirelessly connecting the human nervous system to a machine.

Power delivery for biomedical implants is a major consideration in their design for both measurement and stimulation. When performed by a wireless technique, transmission efficiency is critically important not only because of the costs associated with any losses but also because of the nature of those losses, e.g. excessive heat can be uncomfortable for the individual involved. In this section a method and means of wireless power transmission suitable for biomedical implants is both discussed and experimentally evaluated. The procedure initiated is comparable in size and simplicity to those methods already employed; however, some of Tesla's fundamental ideas have been incorporated in order to obtain a significant improvement in efficiency. This section contains a theoretical basis for the approach taken although the emphasis is on practical experimental analysis.

Implantable biomedical devices have, particularly in recent years, received much attention with regard to their application for a variety of uses involving both stimulation and monitoring. In direct contrast to wearable monitoring healthcare systems [69], one of the key issues for implanted devices is the satisfactory provision of power on an ongoing basis. For short term experimentation it is quite possible for sufficient transcutaneous power to be provided, a good example of this being in the 3 month implantation testing of the Utah Array [70]. For long-term implantation however power needs can vary considerably [71, 72].

Implants such as the Utah Array have in fact been used for a variety of applications, including an alternative sensory input and neural control of prostheses as well as a new means of communication [73]. Transcutaneous power delivery for any long-term employment will however always carry with it the chance of infection for the recipient as well as the possibility of mechanical leveraging. Clearly an onboard/on chip power pick up device that avoids transcutaneous power supply is an attractive alternative which will most likely result in more widespread use of the technology [74].

Some devices, which require several milliamps of stimulating current, such as those used in the deep brain stimulating electrodes for the treatment of Parkinson Disease, need full battery implantation [75]. This technique then suffers from the requirement of periodic battery replacement. On the other hand, it is possible to consider energy harvesting within the body. This approach is however still in its infancy and its practical usefulness is yet to be fully realized [76].

Wireless power delivery offers the advantages that it reduces the risks (particularly due to infection) associated with either battery replacement surgery or a transcutaneous supply. Inductive coupling can be employed for such power transfer, but the efficiency of transfer is a (very sensitive) function of coil dimensions and the distance between them. Resultant efficiencies for biomedical implants are, as a result, generally very low [77], particularly so in a practical, working environment. The most attractive scheme is arguably therefore coupling between magnetically resonant objects [78].

While the idea of wireless power has been explored extensively in the literature with several competing power delivery techniques being considered, the most directly relevant are those in which power is not directed, but rather is absorbed [79, 80]. In essence, the required load or draw-down current is determined by the operational constraints and not by the beaming method employed. This feature allows magnetic currents to exist in a passive mode, i.e., the energy does not persist in the environment continuously but rather is tapped into on-demand. As a consequence of this, less energy is consumed to drive the circuits. What is made apparent here is the small size and relatively few components required in the method described as compared to the relatively large and efficient amount of power transmitted.

The transmission frequency selected for the system is 450 kHz, due primarily to the fact that that no adverse biological effects have thus far been reported at this frequency [34]. Nevertheless, in the scheme of magnetic resonance for power transmission, it has already been determined that the transmission does not interact with off-resonant objects [31]. Using an on-board miniature solid-state high-power amplifier, we demonstrate here a prototype capable of delivering reliable operating characteristics suitable for practical implants requiring a steady power supply of anything from 4.5 to 12 volts dc.

Contrary to the purposes of other implementations [81, 82, 83, 84, 85], of specific interest here is to question whether a scheme could be accomplished using small coils of a few turns driven by a simple amplification circuit. The goal of this exercise is therefore to establish a driving circuit with a minimum amount of components, thereby reducing device complexity.

As a physical demonstration of the operating characteristics of the method described, a set requirement is to maintain a sufficiently high-powered signal reliably powering a lamp and motor. The reasoning being that if the technique can function well in terms of such external requirements, it will certainly perform adequately in the case of an implant specification. In this regard, it has not been the goal to deliver power at the sort of distances reported on in such as [82, 83] where efficiencies of 40% are perhaps the upper target. Rather here to attempt to compare directly with transmission over relatively short distances (a few centimeters), as reported on in such as [86], with a high efficiency of transmission (over 75%) being the target.

An overriding aim is to overcome power supply issues, eminently apparent in the study of biomedical implants, by realizing a wireless scheme which is sufficiently powerful such that an implant can reliably receive its power remotely. Hence, direction of power transmission as well as the size of technology involved has been important in this study.

The concept of wireless power transfer, first described by Joseph Larmor and Poynting, and experimentally verified by Tesla, has been illustrated in the literature as a viable method to transport electrical current between distant points [24, 78, 86, 87, 88, 89]. The extension of this method herein maintains a significant amount of useful power transmitted at intensities of less than 15 volts in which, across a volume of air, magnetic waves are exchanged between two or more coupled resonators.

Consider a circuit consisting of a single loop of insulated wire wound in such a way as to create a circular loop of a few turns. This loop, connected in parallel to a capacitor, becomes one-half of a resonant circuit. This is designated as the transmitter *t*. The length of the wire loop in *t* is then replicated to construct a similar loop placed on an independent circuit board positioned a distance away and which is connected in parallel with a capacitor of the same reactive value and a load. In its entirety this becomes the second half of a resonant circuit, designated the receiver *r*.

Each half of the resonant circuit is placed a distance from the other. The transmitter is connected to a power source such that the LC circuit is excited. Because of the symmetry between each half of the circuit, magnetic waves flow from transmitter to receiver at resonance frequency f_0 with efficiency

η. When energized, this circuit engages an electrical field in the loop in *t*, creating a magnetic field, which is coupled to the loop in *r*. By placing the load in parallel to the loop in *r*, magnetic energy is converted into electrical current. The arrangement is illustrated in Fig.2.1.

A number of receivers can be fed from one common transmitter, thereby opening up the potential to power mobile robotic platforms by this means. A theoretical configuration of the circuit in a robotic implementation is a single fixed-position transmitter *t* delivering energy to distant receivers *r* and *s*. Such a circuit has been constructed and tested for the intensity of the induced current at different distances away from the transmitter. The receivers are grouped into two categories:

1. ac mode: lighting an incandescent lamp, and,
2. dc mode: turning a motor.

Either of the receiver *r* or *s* is a lamp or a motor; these become synonymous platforms in where they are required. The experimentally-tested range of this method is illustrated in Fig.2.55 and Fig.2.56.

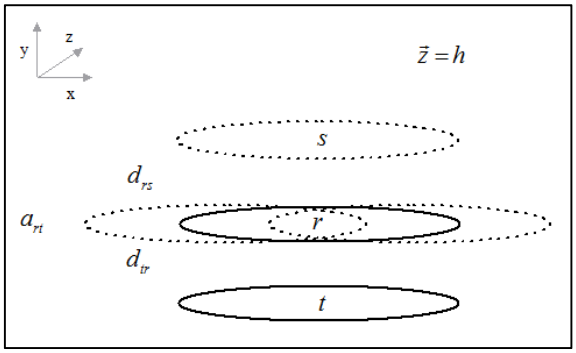

Fig.2.55. Experimentally-tested orientation of multiple receivers *r* and *s* with reference to each position at the transmitter *t* when there is no angle of rotation away from axial alignment $a_{rt} = 0$. The standing height of all coils are equal.

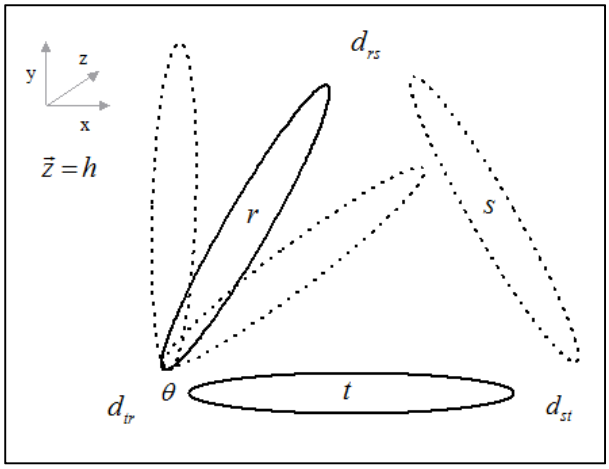

Fig.2.56. Experimentally tested orientation of multiple receivers *r* and *s*, through with an angle of rotation θ away from axial alignment, with reference to each position at the transmitter *t*. The standing height of all coils is equal.

When using two or more receivers, Q will be additive to the solution for each receiver from the perspective of the entire efficiency calculation. If interaction between the receivers is considered, modifying (69) then gives [78]

$$\eta_{i,j,k,\ldots n} = \frac{\left(\kappa_{ij}^2 Q_i Q_j\right)\left(\kappa_{jk}^2 Q_j Q_k\right)\left(\kappa_{kl}^2 Q_k Q_l\right)}{\left[\left(1+\kappa_{ij}^2 Q_i Q_j\right)\left(1+\kappa_{kl}^2 Q_k Q_l\right)+\kappa_{jk}^2 Q_j Q_k\right]\left[1+\kappa_{jk}^2 Q_j Q_k+\kappa_{kl}^2 Q_k Q_l\right]}. \quad (137)$$

If it is desirable to consider the interaction of the magnetic fields each of the elements: transmitter, receiver one, receiver two, or more operating on each other. If the consideration is given that the operation is limited to between a transmitter and receiver one, receiver two exclusively, i.e., not interested in the coupling between each receiver but noticing the increase in κ. The total is then given [45] by,

$$\eta_{i,j,k,\ldots n} = \frac{1}{\left[1+\frac{1}{\kappa_{ij}^2}\left(\frac{1}{Q_i}+\frac{1}{R_i}\right)\left(\frac{1}{Q_j}+\frac{1}{R_j}\right)\left(\frac{1}{Q_k}+\frac{1}{R_k}\right)\right]\left[\left(1+\frac{R_j}{Q_j}\right)\left(1+\frac{R_k}{Q_k}\right)\right]}, \quad (138)$$

where the loaded qualities, Q_i, Q_j are a property of the capacitances C_i, C_j, resistances R_i, R_j, and inductances L_i, L_j of the circuits containing the coils are defined in (72). Overall however, although the separation distance examined here was relatively short, albeit appropriate for biomedical implants. Given the radii of the coils, a high amount of power is delivered at high efficiency.

Coupled-power modes

The physical properties of the circuit constructed for experimental purposes are shown in Table 2.7.

The experiment was tasked to answer three questions:

1. What are suitable geometric positions for the coils in order to deliver power to sufficiently drive a ten-gram motor at six volts, with an operating torque of 3400 gram-centimeters?
2. What are suitable geometric positions in order to deliver power to sufficiently drive a twelve-watt incandescent lamp?
3. What is the consequence in terms of power availability and draw down of adding multiple receivers?

The quantities of measurement required are:

- Intensity by voltage present in the receiver, in the case of dc mode, from a minimum to maximum position,
- intensity by photometric intensity of a lamp, in the case of ac mode, from a minimum to maximum position.

The goal is to calculate the physical properties of the system and see if practically measured efficiency agrees with the theoretical quantities. To accomplish this we employed two sets of receivers: one pair of lamps and one pair of motors.

Each receiver was operationally tested in one of two modes:

- ac mode, receiver *r* contains a capacitor and a lamp;
- dc mode, receiver *s* contains a capacitor, a full-wave rectifier bridge and a dc motor.

Each mode can be used separately or combined.

The receiver circuits in each mode were constructed differently although each used a coil loop wound with the same physical characteristics as the transmitter coil. Each had a capacitor of the same value placed in parallel.

For one of the ac modes, a bias resistor was added in parallel to increase the *Q* value. For all dc modes, converting the radio-frequency signal to direct current was straightforward. Using 1N34 germanium diodes as a bridge rectifier resulted in minimum voltage drop.

The behavior of the received current was contrastingly different between each mode. In ac mode, there is a measure of feedback reflected across the circuit, which in this case, would initially suggest an improvement of performance, as illustrated in Fig.2.58.

However, this comes at a cost. The distance from the transmitter was reduced to 7 centimeters in ac mode while it was held at ten centimeters in dc mode. Using the modes illustrated in the next section describe the operational freedom of the mobile receiver.

ac mode

It can be seen, from Fig.2.57, that when using one ac mode, signal performance of a receiver *r* was maximum when its distance d_{tr} from *t* was two centimeters and its axial difference a_{rt} was no greater than three centimeters to the left or to the right of *t*, as was illustrated in Fig.2.55. Meanwhile the maximum distance for the receiver when the lamp was absorbing enough power to ignite its filament, was observed at six centimeters.

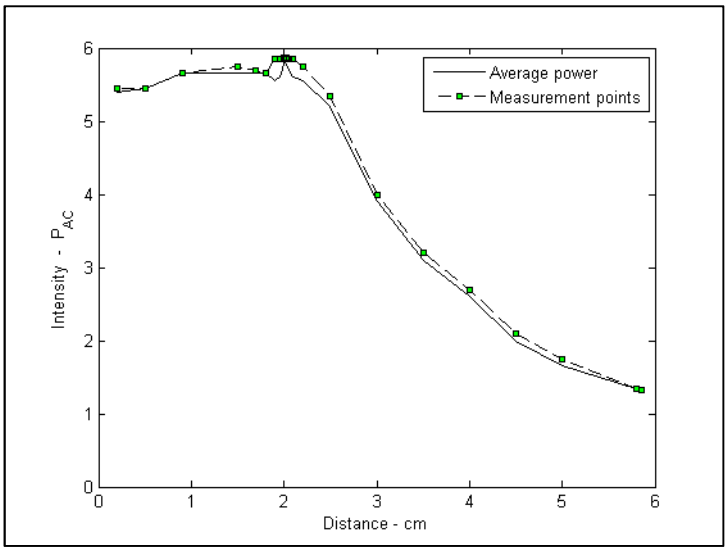

Fig.2.57. The ac power intensity seen by a receiving antenna with axial alignment where $C_i \approx C_j$.

When using two ac modes (meaning the use of two receivers in ac mode – essentially two lamps operating simultaneously), the signal performance of one receive *r*, while comparable to one AC mode, consumed power relevant to its proximity with *t*, as expected, but attenuated by a distant receiver *s*. In experiments the maximum distance when the lamps were absorbing enough power to ignite their filaments, was observed at six centimeters. However, by lining up *r* and *s* with minimum axial displacement, the currents constructively interfered creating a solenoid structure. This method extended the range of useful induced current to ten centimeters.

When using one ac mode and rotating at an angle θ as illustrated in Fig.2.56, the signal performance of a receiver *r* was observed when θ was between 40 and 90 degrees offset from *t*. In this range, the power falls off and remains steady at $\theta = 90$. The peak seen at two centimeters is due to feedback of energy when the circuit is near optimal tuning between the coils.

At a distance d_{tr}, $\theta = 60$, the lamp was at peak brightness within 1.5 centimeters, movement along the axial length reduced the signal to its minimum at three centimeters. However, movement along the trajectory of θ reduced the signal to a minimum at two centimeters. Exactly the same behavior was observed for receiver *s*. Tentative results suggest that the field is consistent across its manifold, i.e., consisting of a finite spatial geometry symmetric along its axial length.

When using two ac modes and rotating at an angle θ, signal performance of the receiver *r*, while comparable to one ac mode, it was found that for segments of its rotation through θ energy was exchanged between the two receivers.

When introducing a third and fourth ac mode, e.g., adding a third and fourth receiver, the geometric positioning of the intensity of the magnetic field object remained constant and, relevant to the position of the other receivers, more energy was absorbed at the peak, as already described.

dc mode

When experimenting with one dc mode, using a germanium rectifier bridge, the signal performance of a receiver *r* was maximum when the distance d_{tr} was at its minimum proximity to *t* and the axial difference a_{rt} was no greater than 1/3 of the radius to the left or to the right of *t*, as illustrated in Fig.2.58.

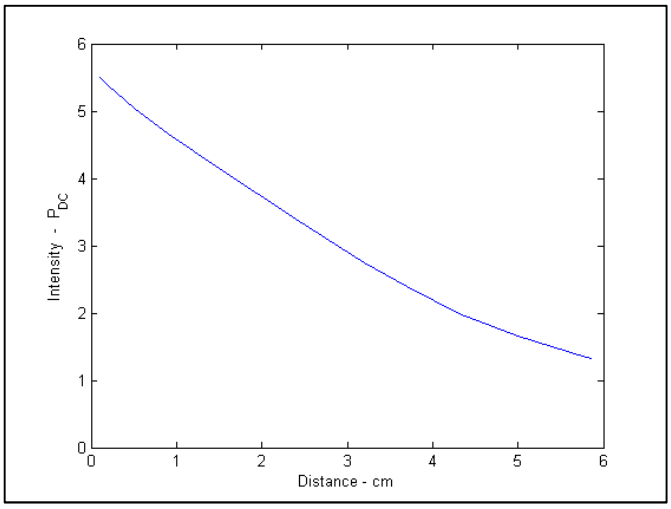

Fig.2.58. The dc power intensity seen by the receiving antenna with axial alignment.

In the experiment, motor performance was observed at the receiver with sufficient torque to drive the wheel of a robot when the receiving coil was closest to *t*, with the power induced falling off steadily up to a distance of four centimeters, where it was just sufficient to do the same. When the motor was not loaded, it exhibited a similar performance up to a distance of nine centimeters.

The next experiment involved using two dc modes (meaning the use of two receivers in dc mode – essentially two motors operating simultaneously) in a germanium rectifier bridge. Results were found to be comparable to one dc mode in terms of power consumption relevant to its proximity with *t*, as expected, but the effects of the distant receiver attenuated the power delivered at *s*.

The maximum distance, when there was found to be enough power to drive a loaded motor, was observed at 9 centimeters. By lining up *r* and *s* with minimum axial displacement, the currents were made to constructively interfere, creating a solenoid structure. In this way, sufficient induced power to drive a motor could be extended to a distance 12 centimeters.

When using one dc mode and rotating at an angle θ, as illustrated in Fig.2.56, signal performance of a receiver *r* was observed when θ was between 40 and 90 degrees offset from *t*. In this range, the luminescence fell off, remaining steady at $\theta = 90$.

When using two dc modes and rotating at an angle θ, signal performance of the receiver *r*, while comparable to one dc mode, exhibited segments in its rotation through θ where energy was exchanged between the two receivers.

When using one ac and one dc mode, signal performance of the receivers was found to be comparable in each characteristic performance based on experimental observations. Energy is exchanged so that it is distributed by the position of the receiver relevant to its multiple based on the total energy available in the circuit. By increasing power to the source, higher intensity currents are available to each receiver.

While demonstrating the transmitter generates magnetic waves which can pass through walls and does not interact with off-resonant objects such as humans or animals, there are reasons where it is undesirable to exchange energy with a circuit which shares characteristic properties of the resonant circuit. In such cases, shielding of a resonant object is possible by enclosing the machine in thin metallic foil. It was observed magnetic waves present in the system cannot penetrate such a substance.

2.4.4 Optimization of the circuit

On examination of (72), and discussed in §2.2, it can be seen that it is possible to affect the quality factor of the coil by adding resistance into the receiver circuit. This is achievable particularly when using high-wattage resistors at low quantities of resistance.

For example, by adding a 500 Ω resistor in parallel with the load this raises the quality factor of the circuit thereby causing the lamp to give off a brighter luminescence. In doing so it also improves the efficiency of the circuit. It has to be said however that the addition of resistance into a dc circuit was not tested here. Adding series resistance is supported by work in [82].

By increasing the length of wire after the rectifier circuit, the useful range of the dc signal was extended out to twelve centimeters. At higher voltages, i.e., those at nine volts and greater, the heat given off was found to be minimal in the circuits tested. What heat there was found to be concentrated around the capacitor in parallel with the loop and was linearly related to the input current.

The maximum power was transmitted in this experiment by driving the amplifier circuit at twelve volts. At this level, there was found to be significant heating of the transmitter's capacitor. Changing the input voltage altered the output voltage, i.e. there was no apparent storage of magnetic energy in the magnetic field.

Any increase or decrease in power supplied does not alter the locations where the coils achieve a maximum or minimum in their resonance coupling, rather it increases or decreases respectively the available power at those locations.

The maximum energy transmitted in experiments was 36 kJ over the period of one hour. The apparent limiting factor in this scheme was the number of amplifiers we employed. It would be of interest to apply further amplifiers, thereby increasing the power in the system, in order to understand how much current can be practically transported in the geometric space.

Perhaps the most significant results obtained from experiments were those relating to the efficiency of power transfer. Here the aim was to use small, simple and efficient means, at directly comparable distances to those reported in [44, 78, 86]. The main goal of the research program being to ultimately deliver power for biomedical implants – as described in those works.

In this case, with two coils, both of radius three centimeters, set six centimeters apart, a measured power transfer efficiency of 76.82% was achieved. This compares directly and extremely favorably with the 82% reported in [78] and the 80% reported in [44]. It is worth adding that it compares even

more favorably with the 45% reported in [86] although it is worth stressing that the goal in that section was not merely high efficiency.

As an interesting aside, it is also apparent that the same method of power delivery, as tested in experiments, can also be employed in the case of multiple receivers. With the addition of additional receivers, the transfer efficiency remained at a minimum of 82%, whilst dividing the power – this based on the position of the receivers relative to the transmitter. Clearly, this can mean that the method introduced here could be useful to power several measurement and/or stimulating points within one body, without significant power degradation, from one single external transmission source.

Power issues faced by [90] deal with system consisting of modes—active and sleep—and are concerned with power consumption of a circuitry at random intervals, such as when a vibration triggers the piezoelectric response to generate voltages and currents. Regarding [91], the notion of beacon-delimited, ultra-low body network is comparable to the research here in that they share two common themes:

1. sending power for medical implants or body monitoring apparatus,
2. sending information at an appreciable data rate, however, the current research only acknowledges the apparatus has the *ability* to transmit data given the waveform is a steady-state sinusoid.

Because of the importance of the subject area, a body of research both theoretical and experimental has appeared, particularly in the last decade, on this topic. As a result we have attempted to make it clear how the work compares favorably with that of others in terms of the results obtained. It is important however to also give an indication of how these improvements in results have been achieved through original differences in fundamental design.

It must be realized that the basic ideas underlying the differences have been sparked by returning to some of the fundamental work of Tesla, Larmor, and Poynting, stemming from the original Maxwell equations. As such it is made clear in this section that the geometry of the magnetically coupled coils we employed was not ‘standard’ but rather exhibited differences to that used in other work [78, 79, 80, 85, 88, 92]. Here is a list of differences.

Firstly, the antenna made use of a Litz winding, not wound in any particular orientation. This same approach was in fact used in [78], but not so in [44, 86]. Secondly, the radius of the receiver and transmitter coils in experiments was the same (three centimeters), others meanwhile used one radius

for the transmitter and another for the receiver [44, 79, 80, 92]. On top of this there were very few turns on both coils, where $n = 3$, and no use of a secondary coil. This is in direct contrast to [78, 86].

Also diverging with previous work, the prototype used an analog oscillator, integrated with the loops, i.e. the inductor and capacitor formed a resonant circuit. It also used plain, circular loops, whereas [44, 72, 77] all used flat coils whilst in [78] the scheme used a staggered arrangement. In this way, the loops consume the entire ac cycle. The prototype also broadcast a lower resonant frequency, i.e. longest wavelength, than that in previous research.

Overall, the key to the approach was simplicity. The model used, by quite some way, the fewest number of components (13 in total for the oscillator) and yet generated a clean sinusoidal waveform at 440 kHz. On top of this, the receiver contained only three components. By contrast, in [44] the authors employed a noisy digital driver, which also required supplemental circuitry.

The operational circuit including the antenna powering multiple lamps a distance in approximated rotations away from axial alignment, is shown in Fig.2.59.

Fig.2.59. Operational oscillator powering multiple lamps.

Experimental results show that significant improvements in terms of power transfer efficiency are achieved by directly connecting the LC circuit to an amplifier circuit instead of excitation being achieved from an external sinusoidal source.

The measured results were found to be in very good agreement with the theoretical models. The next step clearly will need to involve tests involving actual biological tissue. Although, by analyzing results from previous comparable studies [78, 44], it is not anticipated that there will be any issues of

significance, nevertheless such a study is a necessity before actual practical application of the procedure can go ahead in situ.

In tests it was found that the efficiency of the energy transfer system can be improved by increasing the quality factor, Q, of the coils. The power transfer system achieves at least four times more efficiency and power density in watts per centimeter, given its small size, compared to prior inductive-link schemes.

Reasons behind the improved results, as reported in this thesis, in comparison with previous work are not particularly due to the antenna type or quality factor of the coils, as one might expect. The nature of the loop antenna has been thoroughly investigated in the literature; rather, it is a property of the oscillator driving the system under resonance. In the design, we have used a magnetic loop, which has the advantage when its circumference is at a ratio of the driving frequency quarter-wavelength. The oscillator frequency has then been set so the loop can be small and the radiation non-toxic in human presence. It is the manner of how the driving frequency is realized, how clean the oscillator in synchronizing currents in phase, that determines the quality of the energy exhibited in the receiver.

As reported in the theoretical section, efficiency results of 77% in power transfer over a range of six centimeters between transmitter and receiver coils are extremely encouraging. For biomedical implants, this then starts to look at the possibility of remote wireless power provision, in which case the opportunity for multiple recipients also becomes relevant.

The discussion in this chapter centered around a single coupled-mode with several experiments to prove the theory. Given the utility of the concept, it is interesting to supplement the discussion with an addition of a second coupled-mode given an alternative circuit arrangement.

3 Two coupled-modes without projection

The last chapter discussed the theoretical implications and framework of a single coupled-mode magnetic resonant transmission including experimental evidence confirming the theory. This chapter will extend the work from the last, adding a second coupled-mode to the arrangement. In this form, it is conceptually convenient to discuss it in terms of a circuit which has already been created. The concept of two coupled-modes will be discussed and illustrated in terms of a recreated model of Tesla's circuit illustrated in his 1900 patent *A System of Transmission of Electrical Energy*, notably, the arrangement of four tuned circuits exhibited as two concentric spirals.

Three contributions are proposed in this chapter:

1. An analysis of the two coupled-mode model of wireless power transmission and constructing a circuit;

2. comparing the performance of the circuit with the those described one in the literature, [10]; and,

3. introducing an innovation wherein modification of the circuit links its model with the field model, in stronger support of the model, particularly the concept of the contiguous (virtual homogenous) waveguide of free-space described in in §2.

Tesla presented a model of wireless power transmission that he claimed in U.S. Patent #645,546 could be used to send wireless signals to anywhere on the planet. A schematic of his setup is shown in Fig.3.1.

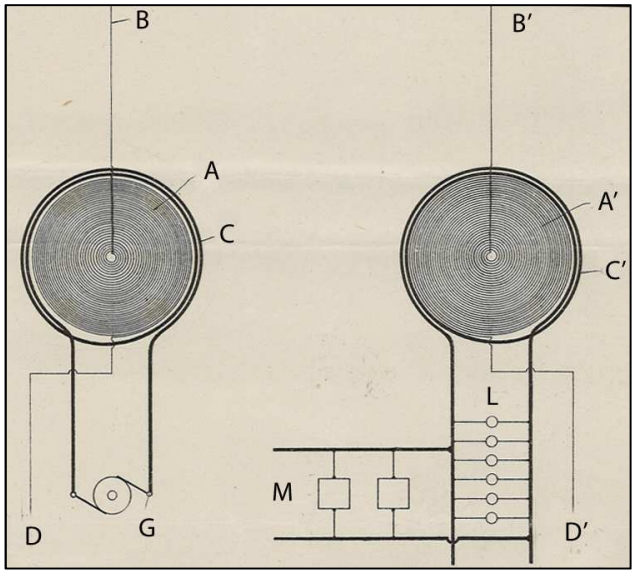

Fig.3.1. Tesla's wireless power model.

The Tesla circuit comprises four tuned circuits: a transmission and receiving pair of circular coils each containing a thick-wire primary of a few turns and a thin-wire secondary of many turns. Illustrated in Fig.3.1, (C) represents the primary coil (A) the secondary coil, (B) one free end of the secondary coil, and (D) the other free end of the secondary coil of the transmitter. For the receiver, these identical components are labeled with primes so as to distinguish the transmission side from the receiver side of the complete circuit.

The circuit windings, sensitively dependent upon the position of the coils relative to each other, perform ideally when the distance between the primary and secondary winding is no greater than the thickness of the primary, similarly to the transformer effect at close proximity. This ensures maximum current displacement in the outer winding of the secondary. When a constant current is maintained on the secondary, it is possible to enhance the characteristic of this coil. An innovative enhancement will be discussed later in this chapter which introduces a connection of a third coil with passive

components such as capacitors and resistors between (B) and (D), and between (B′) and (D′) used to manipulate the order of the magnetic field, compounding the power series, projecting away from the secondary coil. Applying a sinusoidal current (G) to the ends of the primary coil at the transmitter, the input current is observed at the ends of the primary coil at the receiver. The current can be utilized via a load represented as lamps (L) and motors (M) and observed on a spectrum analyzer when transmitting at low power levels or using attenuators.

The windings, so constructed and oriented as described, each form one-half of a tuned circuit. By placing each half of the circuit at a distance greater than the radius of its secondary coils, the total circuit expresses cavity effects occurring along the trajectory of energy transfer. It is assumed the observed behavior and the emission of plane waves is uniformly present, though perhaps in different quantities, with circuits of different sizes but having the same relative geometry. It is a fairly trivial exercise to artificially create resonance cavities, magnetically-coupled wherein energy and information are transmitted bi-directionally. These cavities, while homogenous in free-space, maintain a total internal reflection implying each individually or multiply-connected cavity is a holomorphic manifold [11]. In plain terms, it demonstrates that at the extreme limit of mid-field transfer, the transmitter and receiver can be placed at separations in all three Cartesian directions and can be designed in such a manner as to be a planetary transmitter, which is not unlike Tesla's original description.

Considering the radius of the secondary coil and the length of the conductor consisting the spiral, a peak-transmission frequency is established when both halves of the circuit are built to exacting specifications yet wound in the opposite directions, which, for the purposes herein, is 27.50 MHz ± 5%. By applying an external sinusoidal steady-state signal to the primary coil (C) at (G), the identical signal is observed at the primary coil (C′) at (L) and (M) without drift or distortion. By inspection, it is clear the circuit has a complex symmetry; applying external sinusoids to either half—at the transmitter or receiver—the signal is observed at the other half. Experiments have shown that in general that the higher degree of symmetry in the circuit, the greater the resonance and the better the performance.

The two pairs of self-resonant coils allow the transportation of quantities of energy at significant distances comparable to the sizes of the windings involved. Rather than the use of large coils relative to the distance of transmission which rely on fixed coil qualities, small coils are used with a tuning apparatus which controls the tuned state of the resonator cavity through ordered magnetic fields.

3.1 The theoretical model

The efficiency, η, is a measure of performance of a circuit to catalog the success of this particular experimental design. It is expressed as a fractional quantity, as,

$$\eta = \frac{Useful\ power\ output}{Total\ power\ input}. \tag{139}$$

Another measure of performance is the energy stored in the magnetic field H_0 utilized for magnetic-resonant coupling. The circuit consists of an oscillator driving a loop of wire L_T coupled to a capacitor C_T and a resistor R_T at the circuit's resonance frequency ω_0 representing the transmitter; a second loop of wire L_R of equal radius coupled to a capacitor C_R and a resistor R_R connected to a light-bulb representing the receiver. L_T and L_R are placed at a distance apart from each other. The projection $\bar{\mathbf{H}}$ is not seen in this model, as the energy is absorbed into the secondary coil.

In terms of the properties of the radio-frequency waves transmitted by the circuit, the efficiency η is first given in terms of the degree of coupling between each half of the circuit as:

$$\eta = \frac{k_{TR}^{\ 2} Q_T Q_R}{1 + k_{TR}^{\ 2} Q_T Q_R} \tag{140}$$

where k_{TR} is the coupling coefficient, Q_T, Q_R are the quality factor of the coils L_T and L_R driven at resonance frequency ω_0.

The criterion of efficiency in the scheme is parameterized by the coupling coefficient between the secondary coils in each half of the circuit and their quality factor yielding the energy stored. By creating a generic model of the means of transmission, we can glean insights about the efficiency η of the scheme and how to improve it. Each part of the Tesla resonator is discussed in the following sections; it is advantageous to discern the system in terms of its geometry and construct the field model around it.

The transmitter coils

There are two sets of coils for each half of the circuit, they subsist of a pair of coupled circuits in the form of a spiral. The arrangement of the transmitter coils is shown in Fig.3.2. There is a primary coil of a few turns and a secondary coil of many turns. A tight coupling k_{ab} between the primary's

inductance L_a and the secondary's inductance L_b, suggests the capability to have a high mutual inductance M_{ab}, which greatly aids more power to be transmitted.

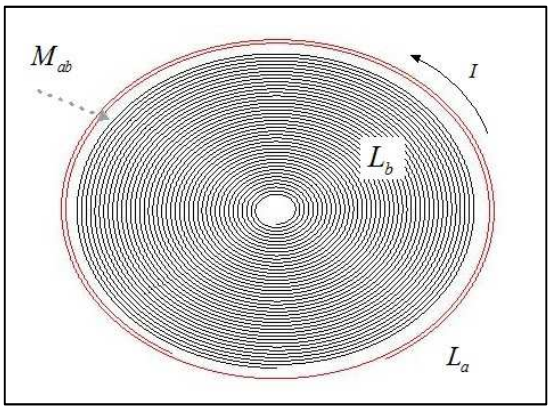

Fig.3.2. Transmitter coil package.

The receiver coils

Because of the symmetry a tight coupling k_{cd} between the secondary's inductance L_c and the primary's inductance L_d is also observed yielding, again, a high mutual inductance M_{cd}. The arrangement of the receiver coils is shown in Fig.3.3. Note the sole difference is the direction of the winding: it is opposite to that of the transmitter.

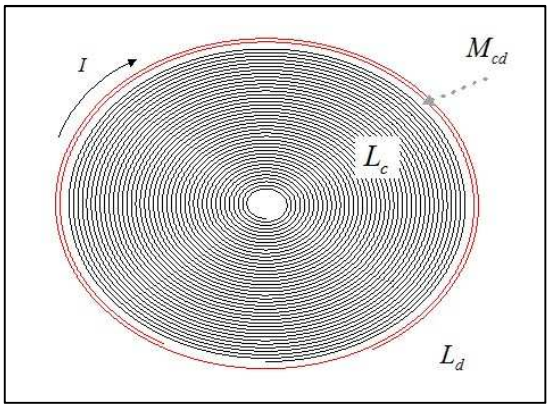

Fig.3.3. Receiver coil package.

The physical properties of the coils are shown in Table 3.1.

Table 3.1. Resonant coils physical specification.

TABLE 3.1
RESONANT COILS PHYSICAL SPECIFICATION

Designation	Coil letter	Inner/Outer radius (mm)	Wire radius (mm)	Wire length (mm)	Number of turns
Tx Primary	a	40.5/51	1.30	700	1.80
Tx Secondary	b	10/40	0.384	5150	40
Rx Secondary	c	10/40	0.384	5150	40
Rx Primary	d	40.5/51	1.30	700	1.80

The coupling coefficient

The coupling coefficient k_{bc}, mutual inductance M_{bc} between distant coils L_b and L_c, and the quality factors of all the coils are the significant physical properties in this arrangement. The mutual relationship and the coupling between each of the coils is illustrated in Fig.5. To understand the effectiveness of the scheme and the work done at a distance, the energy-storage ability of the system is determined by coupling coefficients in transfer mode. The flow of the energy E_0 in joules across the distance is determined by k_{bc} between coils L_b and L_c; k_{ab} and k_{cd} are relatively constant as the distance between coils L_a and L_b, and coils L_c and L_d do not move with respect to each other. If the resonance frequency ω_0 is kept constant, the inductances of coil L_a and coil L_d are small while the distances between coils L_a and L_d, coils L_a and L_c, and coils L_b and L_d are relatively large. Thus, k_{ad}, k_{ac}, and k_{bd} are relatively small and hence can be neglected. When current I_0 is applied to coil L_a, the power transfer flows from coils L_a to L_b, L_b to L_c, and L_c to L_d.

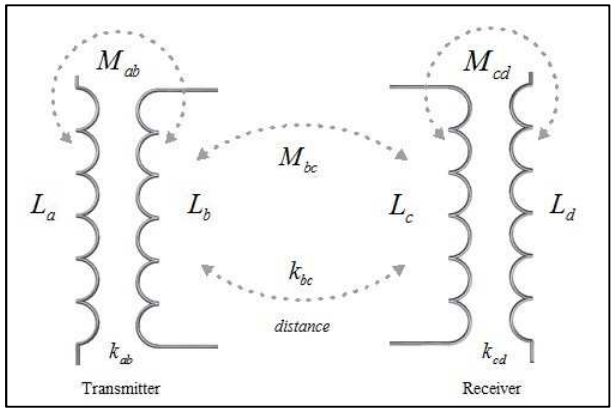

Fig.3.4. Schematic diagram of the circuit for two coupled-modes.

Referring to the scheme illustrated in Fig.3.4, the coupling coefficients between the significant magnetically-coupled coils are defined as,

$$k_{ab} = \frac{M_{ab}}{\sqrt{L_a L_b}},\ k_{cd} = \frac{M_{cd}}{\sqrt{L_c L_d}},\ \text{and}\ k_{bc} = \frac{M_{bc}}{\sqrt{L_b L_c}}, \tag{141}$$

where M_{ab}, M_{cd}, and M_{bc} are the mutual inductances, L_a, L_b and L_c, L_d and L_b, L_c are the self-inductances of the coils. Since we cannot calculate the coupling coefficient directly, it is necessary to calculate the inductances and the mutual inductance of the distant coils. For the coils L_a and L_d, we will use the approximation for the inductance of a circular loop,

$$L_a \approx \mu_0 \mu_r n_a^2 r_a \left(\ln \frac{8r_a}{R_a} - 2 + Y \right), L_d \approx \mu_0 \mu_r n_d^2 r_d \left(\ln \frac{8r_d}{R_d} - 2 + Y \right), \tag{142}$$

where r_a, r_d is the loop radius and R_a, R_d is the wire radius, n_a, n_d is the number of turns, and Y is the flow constant of the skin-effect of the emitted radiation. For the coils L_b and L_c, we will use the approximation for the inductance of an air-core flat spiral coil [30],

$$L_b \approx \mu_0 \mu_r \frac{r_b^2 n_b^2}{8r_b - 11(R_b + w_b)}, L_c \approx \mu_0 \mu_r \frac{r_c^2 n_c^2}{8r_c - 11(R_c + w_c)}, \tag{143}$$

where r_b, r_c is the loop radius and R_b, R_c is the wire radius, n_b, n_c is the number of turns, and w_b, w_c is the width between each turn of the windings. Table 3.2 shows the calculated values for the coils.

Table 3.2. Resonant coils calculated electrical specification.

TABLE 3.2
RESONANT COILS CALCULATED ELECTRICAL SPECIFICATION

Coil	Inductance (μH)	Mutual Inductance (between coils) (μH)	Coupling coefficient (κ)
a	0.78	0.340 (ab)	0.061
b	58.18	13.10 (bc)	0.225
c	58.18	13.10 (cb)	0.225
d	0.78	0.340 (cd)	0.061

Determination of mutual inductance in the model

The mutual inductance M_{bc} is calculated by,

$$M_{bc} = \frac{\int\int_{L_c} \mathbf{B} \cdot \vec{\mathbf{n}} \, dS}{I_{L_b}}, \tag{144}$$

where L_c is the area of the receiver secondary coil, $\mathbf{B}$ is the magnetic field, I_{L_b} is the current passing through the transmitter secondary coil and $\vec{n}$ is the vector normal to the energy across free-space. In examining mutual inductance and the distance, the space between is filled with a radiated field object resulting from the exchange of energy and feedback between the coils, whose size and shape is

dependent upon coil geometry. As such, we can expect the space to be a medium occupied by a charged field exhibiting an energy flow.

An accurate calculation of mutual inductance depends on the assumption of energy distribution occupying the free-space between the distant coils. It is assumed a Boltzmann distribution of the magnetic currents along the waveform limited at its boundary or other non-local positions, given Maxwell's notion of the potential. The model still however assumes a smooth boundary. Using these assumptions, the calculated coupling coefficients and inductances are also shown in Table 3.2.

The explicit innovation here is that the conical coil allows the magnetization to be manipulated. The polarization of the fields across the space is such that it magnifies a magnetic monopole in the region which allows the stronger transmission of H_ϕ. By manipulating this magnetization, the field can be tuned with the introduction of passive components.

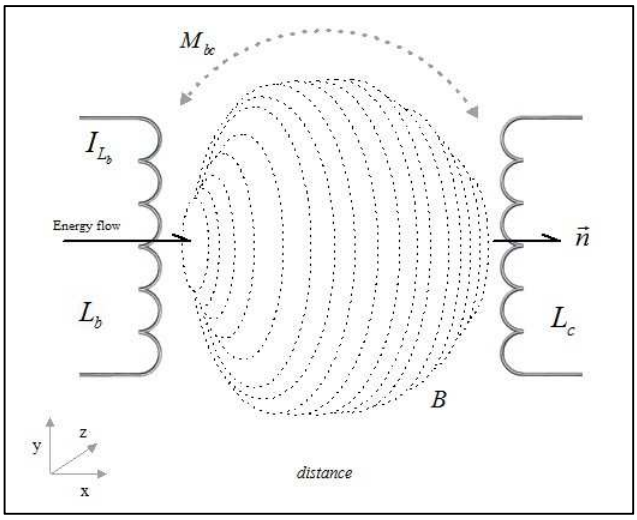

Fig.3.5. The coherent field object resulting from functions in Fig.2.17.

Visually, it is expected the space to be occupied by a hyperbolic-shaped field object in three dimensions saturated with charge and flow, illustrated in Fig.3.5.

On quality and loss

The quality factors of the coils loaded by a parallel circuit containing a capacitance, C_i, and a light bulb are calculated. The arrangement to be calculated is shown in Fig.2. Under such geometry, the quality factor is calculated the same manner for each of the four coils. In the scheme, the components of the circuit are in parallel with reference to each other between the transmitter and receiver secondary coils. The overall loaded qualities, Q_i, are defined via the relation,

$$Q_i = R_o\sqrt{\frac{C_i}{L_i}} + R_r\sqrt{\frac{C_i}{L_i}}, \tag{145}$$

where the quality Q_i represents the quality factor of the resonant circuit either due to ohmic resistance R_o and radiation resistance R_r. The losses are divided into the losses due to ohmic resistance,

$$R_o = \sqrt{\frac{\mu_0\omega_0}{2\sigma}}\frac{\ell^2}{4\pi R}, \tag{146}$$

where σ is the conductivity of the material, ℓ the wire length of the coil and R is the wire radius, and the losses due to radiation resistance

$$R_r = \sqrt{\frac{\mu_0}{\varepsilon_0}}\left[\frac{\pi}{12}n^2\left(\frac{\omega r}{c}\right)^4 + \frac{2}{3\pi^3}\left(\frac{wh}{c}\right)^2\right], \tag{147}$$

where n is the number of turns of the coil and c is the speed of light. By examination of (145), increasing either the capacitance or circuit resistance will increase the quality factor of the coils. Given (140) a small increase of the quality factor of the coils will increase the amount of energy transported improving the effective efficiency. The power transfer efficiency of the four-coil system calculated from the quality factors and coupling coefficients from above is,

$$\eta_{Total} = \frac{\left(k_{ab}^2Q_aQ_b\right)\left(k_{bc}^2Q_bQ_c\right)\left(k_{cd}^2Q_cQ_d\right)}{\left[\left(1+k_{ab}^2Q_aQ_b\right)\left(1+k_{cd}^2Q_cQ_d\right)+k_{bc}^2Q_bQ_c\right]\left[1+k_{bc}^2Q_bQ_c+k_{cd}^2Q_cQ_d\right]}. \tag{148}$$

3.2 The propagation of magnetic currents

In consideration of the work of Poynting, it is interesting in plotting the magnetic field intensity and the magnetic flux density of the magnetic currents emanating between the coils L_b and L_c. It is insightful to map these magnetic fields between coils L_b and L_c when a source of 1 ampere is applied. Using a computational software package *Comsol Multiphysics*, we are able to plot the magnetic flux density and magnetic intensity between the distance coils. The plot is shown in Fig.3.6.

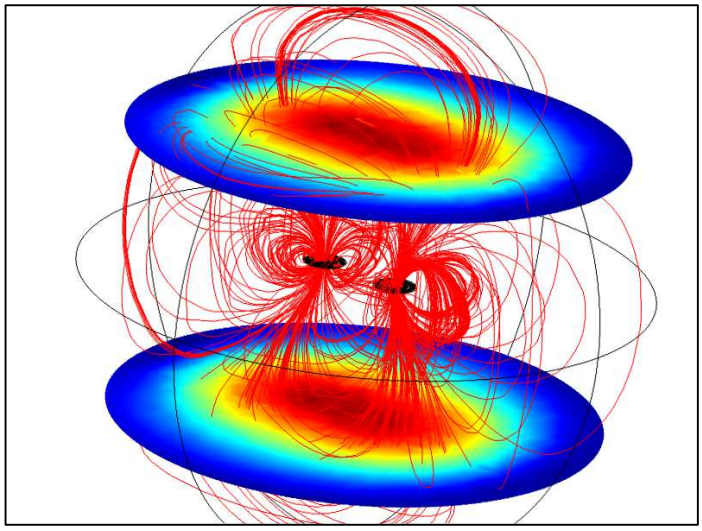

Fig.3.6. Magnetic field intensity and flux density between two secondary spiral coils.

In order to calculate the magnetic field strength at a distance from the coils, it is necessary to truncate the computational domain, because the finite element calculation requires a finite-sized mesh. The sphere, S, which serves as the computational boundary of the domain, has a radius of 80 centimeters. The plot displays a calculation of magnetic field strength (the ovals on top and bottom) and the magnetic flux density (the lines passing through and around the coils). The colors from light to dark show the increasing intensity of the magnetic field emitted by the coils; the peak strength (darkest color in the center) lies 1.5 times the radius of the coils. The minimum strength lies at 15 times the radius of the coils. The magnetic flux density (the field lines) extends the field intensity approximately 8 times the radius of the coils or halfway between the maximum and minimum field strength. As shown in Fig.3.6, the magnetic field intensity is strong in the free space between the coils which suggest this geometry, given the strength of the fields to perform work at a reasonable efficiency, is suitable for transmitting electrical currents of sufficient magnitude.

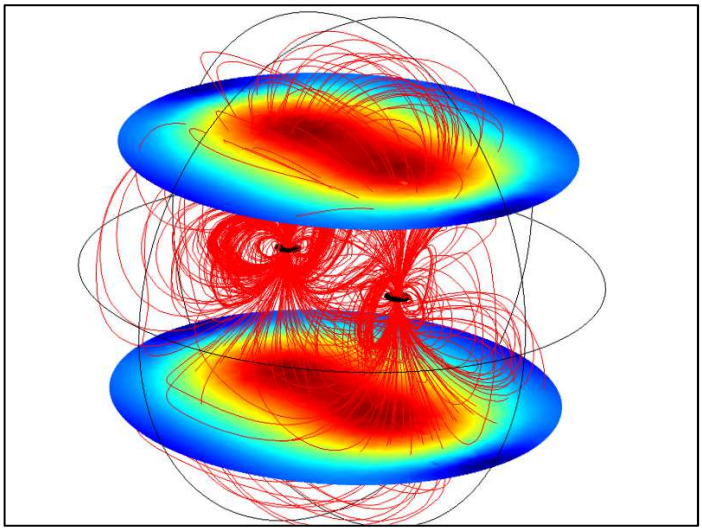

Fig.3.7. Magnetic field intensity and flux density at greater distance.

It is also interesting to know if the model holds at distances away from the near-field region. Fig.3.7 is a plot of the same secondary coils L_b and L_c emitting a magnetic field at a distance of 75 centimeters, the boundary of the computation domain has a radius of 120 centimeters. The intensity remains uniform across the distance. The limit at the boundary is obtained by the assumption of how the fields are computed and the assumptions about free-space. Depending on the assumptions constructing the method, the limit for medium-range transfer can be extended.

One method to extend the range of energy transport is to increase the density of a component of the magnetic field, H_ϕ. This typically involves increasing the inductance of the coils as to satisfy the relationship of the stored energy W to inductance and the fields, as,

$$W = \frac{1}{2} LI^2, W = \frac{1}{2} \int \mathbf{B} \cdot \mathbf{H} \, dv, \tag{149}$$

or increasing the quality factor of the coils themselves. Adding a third conical coil of a radius r_e at a distance of 10 centimeters along the $z-$axis of the secondary coil and connecting at terminal (B), the free end of the secondary coil, increases the value of L_b linearly. The value of $\mathbf{H}$ is also increased, it is given the length of wire ℓ_e contained on the curvature, θ_e, of the conic. We averaged the value of $\mathbf{H}$ by setting the conic angle $\theta_e = \pi/6$ along a length where $r_e \leq r_b$ and therein yielded a significant increase of magnetic potential $\mathbf{A}_\mu$. An increase of H_ϕ is observed by applying the force upon the dipole residing at the center of the secondary coil. We hypothesize the motion of the magnetic field from the conical coil constructively interferes with the magnetic field lying on the spiral coil given the two coils are sharing the same electrical field $\mathbf{E}$ and electric potential φ. By adding capacitive and

resistive components across both coils L_b and L_c quality and coupling-coefficient values are directly accessed. The third coil arrangement is shown in Fig.3.8.

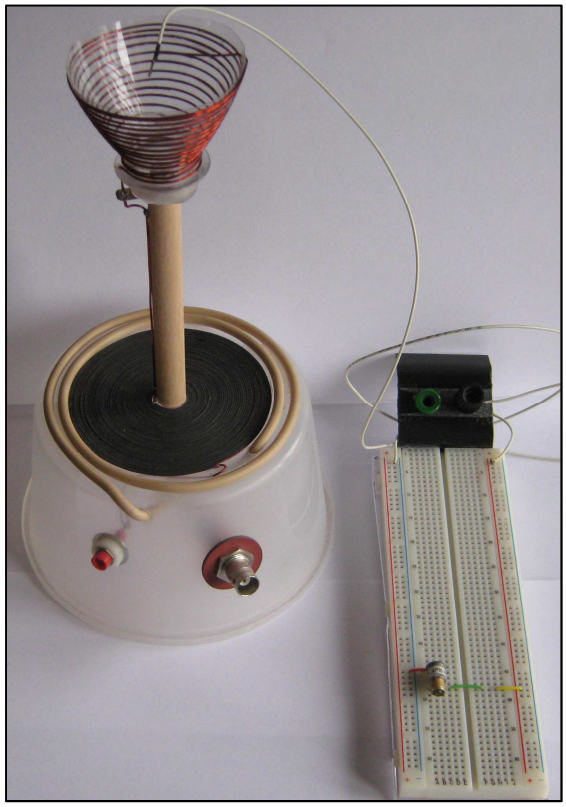

Fig.3.8. Receiver package and third coil. Component breadboard shown.

The possibility of calculating coupling effects, notably the coupling coefficient between the distant spiral coils differs from normal models in that the spiral lies *inside* of the loop coil containing the generator and therefore is assumed highly efficient following the well-understood transformer effect.

3.3 The circuit experiment

A reconstruction of the Tesla resonator, illustrated in Fig.3.1, was built with the physical specifications shown in Table 3.1. The inductances were measured on a Hewlett-Packard hp4192A into 50 Ω, shown in Table 3.3. The first test was to plot the results of applying a steady-state sinusoidal source at the peak resonance frequency of 27.50 MHz and chart the measured differential power between input and output. The efficiency, η, as a function of the distance between the coils is shown in Fig.3.9.

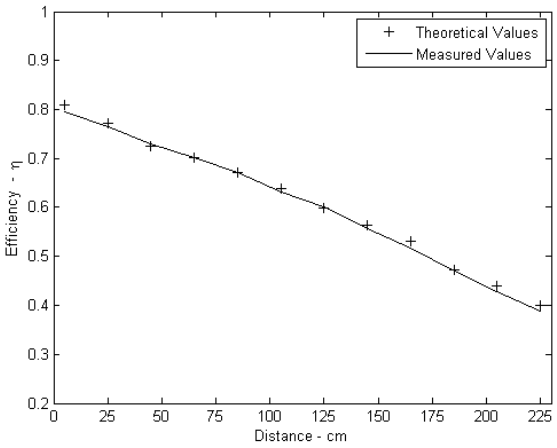

Fig.3.9. The efficiency of the Tesla resonator over a distance.

To understand how this model performed against a comparative wireless power system, results were contrasted with [10]. Although containing a different orientation and geometry, due to similar sources of prior art sufficient shared fundamentals exist. Fig.3.10 shows a contrast of the two schemes.

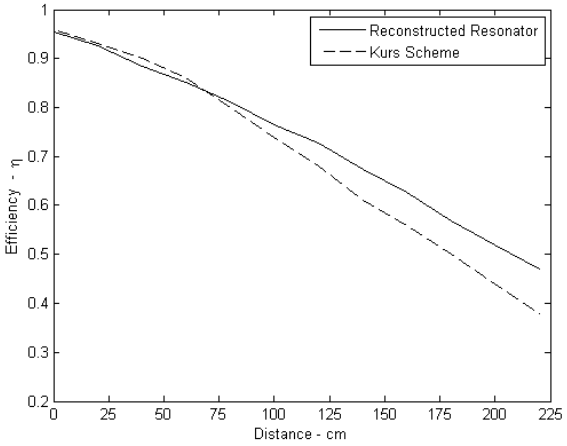

Fig.3.10. Comparison of the Tesla resonator with Kurs.

The reconstructed Tesla resonator, in its original form without modification, performs better with secondary coils of more winds yielding more magnetic field properties. Considering magnetic resonance coupling schemes studied in this chapter insist a higher magnitude of magnetic flux density as directly translating into greater efficiency over mid-field distances, the observation of a linear relationship in force to energy density of the magnetic field is not surprising. What is interesting is that energy transmission can be achieved where the model does not rely on axial alignment.

Table 3.3. Resonant coils measured electrical specification.

TABLE 3.3
RESONANT COILS MEASURED ELECTRICAL SPECIFICATION

Coil	Inductance (μH)	Capacitance (nF)	Resistance (Ω)	Quality factor (Q)
a	1.15	870	2.00	96.6
b	62.40	16	1.88	182.3
c	61.68	16	1.81	180.4
d	1.17	886	0.55	97.3

The second test was to add passive components to verify if, as according to (145), the quality factor of the scheme could be improved. By doing so, the efficiency shown in (148) is improved. Capacitors added in parallel to the transmission coil, while resistors added in parallel to the receiver coil would show an improved efficiency in the transmission. Such direct connections between the circuit and the field are aided by the addition of the third coil inductively coupled to the transmission field. Values of added or subtracted capacitance and resistance affected admittance and circuit impedance by altering the phase of the energy at the distant secondary coil. A series of five tests were conducted adding capacitance and resistance as value-based parameters to coils L_b and L_c coupled through L_e.

As illustrated in Fig.3.11, the coupling coefficient k_{bc} can be affected by not only reducing the losses, but also affecting the quality factor by adding values of capacitance and resistance. Tuning the resonant frequency to the peak magnetic flux density of the circuit would further improve performance.

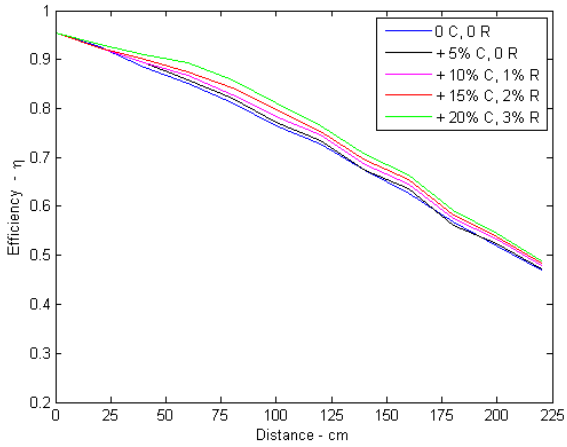

Fig.3.11. The efficiency of the Tesla resonator with enhanced quality factor.

This implies the cavity is contiguous and has a property inherent to it, suspended inside free-space.

Discussion of the experiment

Following the theoretical framework of two coupled-modes, the experimental reconstruction of Tesla's signaling apparatus from his 1900 patent *A System of Transmission of Electrical Energy*, illustrated in Fig.3.1, is also examined in terms contrasted with other attempts claiming a Tesla wireless power system. In [10] the author concerned himself with Tesla's 1914 patent *Apparatus for Transmitting Electrical Energy* focusing primarily on the transmission of electrical currents given large coil loops of a few turns. Here, we have attempted to demonstrate an alternative approach using coils significantly smaller yet achieving better results for efficiency. One striking difference is that the geometry and orientation of the Tesla resonator examined in this chapter does not rely on an axial alignment of the coils; rather, the transmitter-receiver pair can be placed liberally at a distance relative to each other without any significant additional losses. According to [10], the limit of this type of transfer is 8 times the diameter of the coils, the electrical intensity between the coils diminishing at a rate $1/r^2$. Experimental results have indicated a greater link in the magnetic field density appears at the secondary coils in this resonator-coupled model. The extreme distance measured in the experiment was four meters.

The last step was to discern if the reconstructed resonator could be modified to increase energy transmission and intensity of the magnetic fields in the magnetic-resonant model. What became immediately apparent was by adding passive component circuitry, the field object behaved as a cavity not unlike a transmission-line resonator. The sharing of those basic characteristics in our model gives a wireless transmission-line resonator. More research on this formalism is suggested.

It has been observed that the resonator's performance is sensitively dependent upon its impedance, as expected. The signal generator used during experiments outputs into 50 Ω, impendence at the receiver was measured to be 58 Ω. Tuning the resonator, we were able to more closely match the impedance of the circuit allowing more of the power seen at the source to be dissipated in the load. From this approach, by adding and subtracting impedance, efficiencies over longer distances are dramatically improved. Although, not directly addressed in the experiments in this chapter, the appearance of standing waves in the resonator suggests a possible explanation of voltage magnification lending credence to Tesla's description of velocity-inhibition.

The idea of velocity-inhibition is related to the Larmor concept of acceleration, used here in this thesis, and described in §1.1. What is further interesting is that Tesla described a method of antipodes [110], or positions on the planet where it would be ideal to place transmitters for world wireless transmission. A drawing of this idea is shown in Fig.3.12.

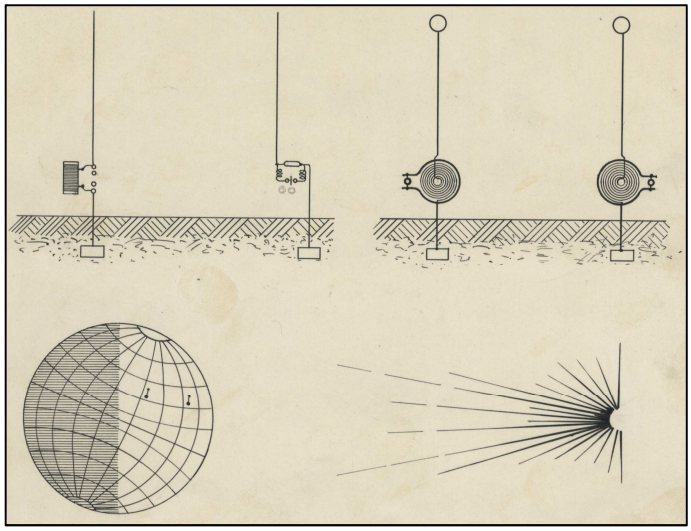

Fig.3.12. Tesla antenna and antipodes.

The addition of a third coil on the $z-$axis allowed the manipulation of the variables manifesting the magnetic fields at the secondary spiral coils yielding an improvement in performance. The presence of the coil L_e in the field along the trajectory couples, through a higher-order magnetic field [26], to the transmission circuit of L_b and L_c, shown when there is and not a connection at (B) and (B′). Based upon this observation, it is of great interest in future experiments to investigate what access there is to the magnetic potential $\mathbf{A}_\mu$.

3.4 Observations of behaviors present in the circuit

The method here describes medium-range wireless power transmission by means of low-frequency radiating waves, as opposed to either near-field inductive direct coupling or far-field microwave transmission. We have proposed a type of wireless power transmission based on the notion of a transmission-line resonator without any physical containment other than the fields themselves. It suggests that the existence of a pair of tuned circuits, as illustrated in Fig.3.1 and schematically demonstrated in Fig.2.1, exhibits such possibilities when measuring unpowered outputs at both the receiver as well as the transmitter—a cavity presence is visible whether external power is applied or not.

The observations lead to an implication of a resonator cavity with characteristic peaks in the frequency spectrum which go unchanged regardless of the distance between transmitter and receiver. It is this uniqueness that makes the circuit worthy of deeper study. Power efficiencies recorded are felt to be respectable for research at this stage, being significantly higher than those previously reported for mid-field regions, without the need for the extremely large directed antenna.

A detailed and quantitative analysis of the effect of external, non-resonant objects on the transmission circuit is compatible here as it is with the method discussed in the other parts of the thesis.

It is worth noting that the power transfer is not affected if humans or various everyday objects, both large and small, are placed between the receiver and transmitter. This includes cases where objects completely obstruct the line of sight or lie within a few centimeters of the coils. While the transmission frequency is somewhat outside that deemed safe for human exposure [18], coupling is only possible if a receiver contains a coil symmetric to the transmitter, but oppositely wound. It is suspected the radio-frequency fields react weakly with off-resonant objects.

During the course of conducting experiments, voltage magnifications were observed when applying resistances to the receiving circuit. Magnifications as much as 50 times were observed which manifest themselves as current spikes reflecting back across the resonator. Although noted, they were not directly analyzed during the investigation for this chapter. Nevertheless, it is apparent that Tesla's resonator has properties which appear either unrealized or under-investigated as such, although they were partially sketched out in Tesla's original works [1, 2, 3, 25, 26]. It is therefore suggested that a detailed body of research be conducted on this topic. Tuning techniques and strategies, field-order coupling are also considered very fruitful paths.

Whilst the results presented in this chapter are of interest in themselves, they also throw up a number of intriguing questions which need to be researched. For example, in terms of performance over distance, how important are the shape and directional settings of the windings and the amount of power drawn by the load with regard to the transmission efficiency? What remains consistent is that an improvement of quality leads directly to an improvement of performance not only at the distances shown in the figures, but also at greater distances, as expected.

Given the appearance of more complex wave patterns in the transmission, it is hypothesized the magnetic fields of the first-order are, at least in part, with the Schumann resonance [110]. This is supported by experiments conducted with the third coil present in both the transmission and receiving coils, introducing a third coupled-mode.

Compared to the single coupled-mode model from the previous chapter, this model shares many of the characteristics of the former. Coupling between close-proximity coils, where the distance is much smaller than the radius, resembles the commonly-understood transformer model. Coupling between distant coils, such as the coupling between each secondary coil, resembles the theoretical framework of the previous chapter in several ways. First, intersection of "flux lines" is deemphasized and the notion of the virtual homogenous waveguide is strengthened. Contrarily, it is also conceptually correct

to consider the intersection of “flux lines” as the linking force constituting the structure of the waveguide. Second, although the oscillator in this case is not tightly integrated into the primary coil antenna and the circuit responds more to ringing than acceleration, it is distinctly apparent that the projection field, $\bar{\mathbf{H}}$, from the previous chapter is present because of the fact that the third coil experiences a magnitude of energy along the z-axis. Third, the enhanced magnetic field magnitude, again experienced by the third coil, is supported by the work of §2.4.2. The theory is further extended in this chapter by the concept of the ordered magnetic field—zero and first order—following from the theoretical discussions in [21, 26]. Personally speaking, I believe the demonstration of physical evidence of the first order magnetic field is a very powerful claim and deserves serious consideration in future research.

This chapter discussed two coupled-modes by illustrating a reconstruction of a Tesla system of wireless power, contrasted to the single coupled-mode of the previous chapter. The utility of the schemes illustrated in both chapters present many possibilities for the future of efficient wireless energy transfer in an industrial capacity.

4 The dipole concept and quantum magnetic potential

This chapter will discuss a modified model of the dipole. The dipole concept and quantum magnetic potential are fundamental concepts describing the motion and forces of separation of electric charges on an antenna. During Hertz’ research, it was discovered some peculiar effects occur in certain antennas [16, 30, 76, 93] such as the circular loop, even at those wavelengths utilized. While a comprehensive explanation is out of scope, it is interesting nevertheless to examine the motions of separation of two charges in the viewpoint of de Broglie waves [49] as well as their description by Bohm [96] to form a unified model between quantum and classical descriptions of the model in this thesis.

It is orthodoxy in electrical engineering and a basic tenet of physics, that work is done in electrical systems by the separation of charges and energy is released when those same charges come back together, or an oscillation takes place along a line of trajectory. Conservation laws dictate that the work done to separate charges is equal to the energy that is observed. While this understanding is convenient to finding solutions in “common” problems and has shown itself to be a rather useful tool as such, in itself, it portends the electron representing the charge, given Lorentz, is independent of the space where it is located. If we are to accept the notion that charges exist because of matter, the separation of charges in the conductor project energy onto the interface where they lie. The interface has an interesting feature in that the lag of current from voltage allows the dipole to sustain long

enough for the energy to release when it is destroyed. The potential energy in the duration of time of the existence of the dipole is a window to see how the charges project themselves as waves simultaneously [94].

What is to be considered here is that the separation of charges by an electrical force results the electric dipole and the magnetic dipole to exist simultaneously at right angles to each other and that magnetic charge is a result of the potential energy of the magnetic moment. It is hypothesized that the coexisting charges, forces, and distribution of energies lie within a manifold, which describes a contiguous set of particles and energies lying in Minkowski space that produce radiant energies. This has been discussed previously as a field object.

A magnetic dipole is the limit of either a closed loop of electric current or a pair of poles as the dimensions of the source are reduced to zero while keeping the magnetic moment constant. It is a magnetic analogue of the electric dipole. The magnetic monopole, the magnetic analogue to the electric charge, has not been proved [98]. The magnetic field around any magnetic source looks increasingly like the field of a magnetic dipole as the distance from the source increases. A new analogy is proposed combining the particle and wave attributes of the separation of charges [16, 49, 96]. The attention on this detail is due to a quandary of the electron having a magnetic dipole moment; that the electron's magnetic moment is not due to a current loop, but is instead an intrinsic property of the electron [95, 96]; the electron has not been observed to have an electric dipole moment [97].

If it is logical to accept the concept of the dipole as well as the manner in which it is manifest in antenna, one can also assume that space-time and its curvature, in the Minkowski sense, is not uniform in the presence of charges relative to their polarized opposites do not exist analogous to points on a grid. While this assumption is not wholly surprising, the crux is how often are particles of opposite electrical magnitude localized enough so that the force performing the work does not have to "reach" so far as to construct the dipole infeasible. An unhelpful answer would obviously be derived from probability and statistics but does not yield a proper explanation since the abstractions are completely arbitrary. As such, a possible explanation is proffered: that the charges exist as a property of free-space as they exist as a property of the material consisting the charges, i.e., the quantum world is littered with such charges everywhere.

4.1 Waveform assumptions

Because of the assumption that the transverse wave is a disturbance, the disturbance contained around the charge is analogous when work is conducted on them, analogous to a quantum interpretation [50].

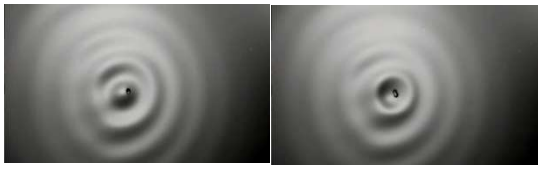

Fig.4.1. Energy in the quantum state.

Such an analogue would allow the selection of charges of equal magnitude yet opposite charge and polarization based on the phase wherein a force is applied to separate them into gauge groups. The charges are still random in the statistical sense, yet drawn into suspension by simple forces of attraction and repulsion, constrained to perform work.

The magnetic field of a dipole is calculated at the limit of a current loop split into two phases; a pair of charges as the source shrinks to a point while keeping the magnetic moment, **m**, constant [98]. For the current loop, this limit is most easily derived for the vector potential. Outside of the source region, this potential is,

$$\mathbf{A}(\mathbf{r}) = \frac{\mu_0}{4\pi}\frac{\mathbf{m}\times\mathbf{r}}{r^3}, \tag{150}$$

and the magnetic flux density is,

$$\mathbf{B}(\mathbf{r}) = \nabla\times\mathbf{A} = \frac{\mu_0}{4\pi}\left(\frac{3\mathbf{r}(\mathbf{m}\cdot\mathbf{r})}{r^5} - \frac{\mathbf{m}}{r^3}\right). \tag{151}$$

The scalar potential from the monopole limit is,

$$\varphi(\mathbf{r}) = \frac{\mathbf{m}\cdot\mathbf{r}}{4\pi r^3}, \tag{152}$$

and the magnetic field strength at a point charge is,

$$\mathbf{H}(\mathbf{r}) = -\nabla\varphi = \frac{1}{4\pi}\left(\frac{3\mathbf{r}(\mathbf{m}\cdot\mathbf{r})}{r^5} - \frac{\mathbf{m}}{r^3}\right) = \frac{\mathbf{B}}{\mu_0}. \tag{153}$$

The magnetic field is assumed symmetric under rotations about the axis of the magnetic moment **m**.

4.2 Attraction in the dipole moment

Fig.4.2 shows a point-charge emitting a field into free-space, illustrating the axial and lateral emission of energy: electrical for an electric point-charge, magnetic for a magnetic point-charge.

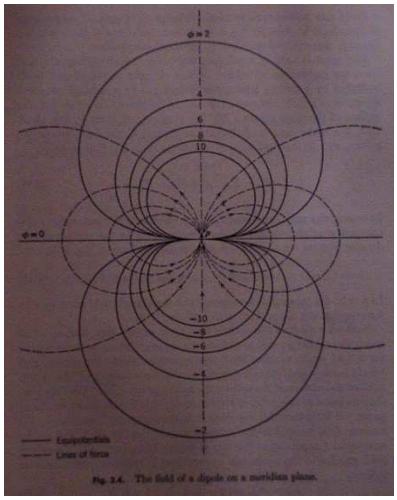

Fig.4.2. A common description of a point-charge dipole.

While the pattern of the field emission is uniform over the axes of propagation, the depiction implies the point-charge is not moving. Since the Hertz antenna is a dipole through the separation of charges, the generalization implied allows a further suggestion of the energetic state of a point-charge. Since it is due to the conservation of energy and Gauss' law that the length of propagation varies proportionally to the magnitude of the emission and that the length cannot extend forever, it is relevant to point out there is a formal boundary to the fields in both the axial and lateral directions. It is also relevant to consider that the energy moving toward the boundary does not necessarily disperse from the point-charge, if it is the assumption that the point-charge only contains energy. If this condition were true, the point-charge would be exhausted after a given time. Since it does not exhaust, illustrated by the fact that electrical circuits still function, its internal modulation—or the frequency by which the energy shifts between moving toward and away from the boundary—is the attribute defining its state. Otherwise, an unseen force is applying energy to the point-charge sustaining its state feeding it as a force holding the equilibrium, so that the field is conservative. A modified description of the dipole is illustrated of the forces on the separation of charges given their mutual attraction is shown in Fig.4.3.

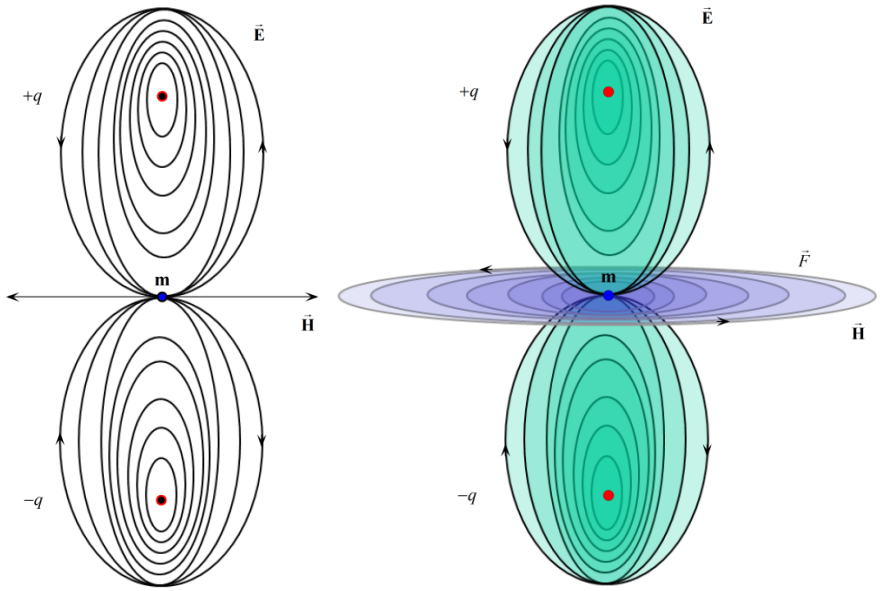

Fig.4.3. a) Point-charges and the wake pattern of forces, b) emitting a magnetic shearing force concentrated at the magnetic moment **m**.

Fig.4.3a shows point-charges $+q,-q$ creating the wake pattern lines of attraction at the magnetic moment **m** dispersing energy at right angles to the point charges when work is applied separating them, visualized in Fig.4.1. In Fig.4.3b, forces between the point charges reveal a circulating magnetic shearing force $\vec{F}$ analogous to the Larmor forces [6]. The separation of charges, the rippling of the charges, because of the forces of separation, the wake causes the elliptical feature of the effect of point charges on free-space. The energy from the wake is expressed at right-angles as the magnetic field.

The bending of the force lines illustrates the circulation of force across the moment **m**. The tension between the centers of force illustrates the resulting field exchange between the two point charges and a quantized component of energy traveling along the axis of orientation between the points. The repulsive forces between the points are balanced by the attractive forces folded in the motion of the passing energy creating equilibrium in the system. Since the system simply either reflects or refracts the passing magnitude of energy, there is no field interaction between the points, only the Lorentz and Larmor gauge.

The dipole description has been derived exclusively from the geometry of the antenna used in the oscillator, theoretically supported by coupled-mode theory. The concept illustrated here for the dipole is to emphasize the exchange of energy between itself—as a function of the separation of charges—and other vector-based components it could possibly interact with as a Riemann surface. Greater energies in higher concentrations act to influence other dipoles not unlike gravitational forces between

celestial bodies. As such, the architecture of the electrical particles is defined by absorptions and reflections of quantized energy, in the form of electromagnetic photons. Point-charges on the manifold define each other by the exchange of photons, otherwise, they would be inert and unseen, perhaps confused for the vacuum. The definition of objects on the manifold and how they exchange energy gives rise to this description of the electromagnetic spectrum. Here, the electromagnetic spectrum is defined through two dominant processes: point-charges reflecting a photon and point-charges absorbing a photon.

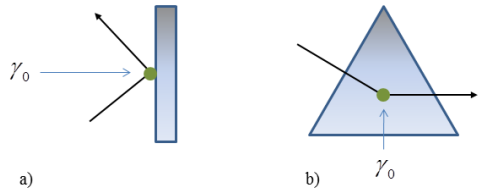

Fig.4.4. Photon reflection and absorption primitives.

Fig.4.4 shows: a) a photon refraction by the dipole field, b) photon absorption by the dipole field. On each spatial surface, a photon carrying electromagnetic energy, γ_0, is represented as a packet of energy moving with a constant magnitude and direction, based on the emission from the transmitter. By inspection, γ_0 has the potential to transfer energy to the dipole or to be emitted from it by the acceleration of electrons in the conductor. The point where the photon changes direction by a factor of reflection or refraction indicates a radial point of the intensity of energy by its shift in direction giving rise to the magnitude of the free-space currents I_{E_θ}.

4.3 Gauge fields

The interaction of the stream of particles with the radiated field will result in a graduated ellipsoidal field growing away from the emission point. Instead of a static quantity, the momentum of the particle stream creates an elliptical area on the manifold where the relationship between the two charges, the virtual and the passing field, are in resonance with respect to each other, creating a more dense form on the manifold. Some passing particles, which could contain masses, are temporarily trapped in the sink and orbit the central axis of the field. The radius of the field and the equilibrium of the system are dependent on the magnitude of energy stored as a resonance between the transmission and receiving loop antenna. This quotient of energy is trapped in the sink as long as the system remains stable in terms of its geometry and the resonance patterns can hold it together. The form would hold unless broken by a stronger external electric field. As a series of dipoles, analogous in the case of a short dipole, a chaining of dipoles yields the polarization of the propagating waveform—the rise and fall of

current from one polarity to the other—across free-space, with a given admittance and reactance dependent upon the temperature and pressure.

What is relevant to understand at the fundamental level are that the notions of flux and propagation are absorbed into the scalar, vector, and quaternion representations of the potential of the waveguide structure, which consists and subsists the space between and of the antenna discussed throughout this thesis. As the phenomenon is physically observable, it indicates that the potential $\mathbf{A}_\mu$ fields, where $\mu = 0, 1, 2, 3, ...$ do possess a physical significance as global-to-local operators or the case of gauge fields, subject to precisely constrained topologies [51]. The available constrained topologies in the case of the model described in this thesis are:

- The case of localized waveguide, and,
- classically-defined electro-state charge manifolds,

where both are limited in magnitude and statistical (Boltzmann) distribution by a temperature-dependent electron coherence length given the antenna architecture. In the case of the localized waveguide charged manifold, type is identified based on the definitions of:

- fields $\rightarrow$ free electron $(\mathrm{F} \rightarrow \mathrm{FE})$,
- fields $\rightarrow$ conducting electron $(\mathrm{F} \rightarrow \mathrm{CE})$,
- waveguide $\rightarrow$ field $(\mathrm{WG} \rightarrow \mathrm{F})$, and,
- conducting electron $\rightarrow$ fields $(\mathrm{CE} \rightarrow \mathrm{F})$,

provided by the

1. Aharonov-Bohm and Altshuler-Aronov-Spivak effects ($\mathrm{F} \rightarrow \mathrm{FE}$ and $\mathrm{F} \rightarrow \mathrm{CE}$),
2. the topological phase effects of Berry, Aharonov, Anandan, Pancharatnam, Chiao and Wu $(\mathrm{WG} \rightarrow \mathrm{F})$,
3. the Josephson effect $(\mathrm{CE} \rightarrow \mathrm{F})$ in the sense of the variable phase of $\mathbf{A}_\mu$,
4. and the De Haas-Van Alphen effect $(\mathrm{F} \rightarrow \mathrm{CE})$ in the sense of the periodicity of oscillations in the effect determined by $\mathbf{A}_\mu$ potential dependency and gauge invariance.

In each of these circumstances, the $\mathbf{A}_\mu$ potentials are described as *physically meaningful* constructs at the classical level, numbers 2 and 3 and at long range in the case of effect 2. Coherence length limitation is noted in effects 1, 3 and 4. What this implies is that a properly constructed and well-defined topological object can manifest, along with magnetic flux, sets of potentials along its length and trajectory conditionally dependent upon the antenna creating the field object.

It would be interesting in future research to explore those topologies as quantization of the field object where appropriate.

Finally, H.F. Harmuth proposed an amendment to Maxwell's equations [99, 100]. The subject having gone through much discussion [101], presents eloquently an argument of possibilities of expansion in the interpretation of the more abstract parts of the Maxwell equations. One consequence: the application of force to separate the charges by the application of current, the current lags behind the voltage potential, the point charges are both particles and waves [102]. It is anticipated that steps toward a proof of the notions discussed in this section can be formed thusly.

An electrically-charged short antenna has a trivial characteristic impedance when compared load whose impedance dominates the circuit, desirable for sending power over distances; e.g., the power is induced to traverse the free-space between the transmitter and receiver to the load where the impedance is located, a primitive form of directional finding [68].

4.4 The loop ratio in determining dipole integrity

Typically, small loop antennas have a poor efficiency unless they are constructed at a ratio of their circumference to the wavelength of the transmission frequency. Considering the ratio hypothesis, for further size reduction, the loop can also have similar power transmission efficiency if the ratio is also one-thousandth relative to the quarter wavelength with the circumference. It is suggested it would also be effective at one-ten thousandth given the exponential progression,

$$\begin{aligned} \Re_1 &= \frac{2\pi r_i}{0.01(0.25\lambda)} = \frac{0.0188495559\,\mathrm{m}}{0.4199879228\,\mathrm{m}} = 0.0100807302, \\ r_i &= 0.003\,\mathrm{m}. \end{aligned} \tag{154}$$

Applied to the physical antenna model, the antenna characteristics are truncated to a quarter-wave antenna, as, $\frac{\lambda}{4},$ the experimental setup of the antenna keeps it mounted perpendicular to the earth and not connected to a ground plane. The ground plane is ignored. The resonator floating above ground is

susceptible to the forces at the interface; the phase shifting of the amplifier over the surface of the antenna through π rotations in the impedance of free-space to seeks a closed circuit connection.

It is this seeking effect that yields some qualified evidence that there is a possibility of a straining of the space between the antenna cited the pattern of repetitious properties not unlike a set of harmonics across space. It is suspected the observable strain is analogous to that described by Maxwell.

5 Thesis conclusions

The literature which contains descriptions of physical devices tends to address typical problems in wireless power transfer—antennas, inductance, coupling, and energy transfer, by clear mention of magnetic resonance or not—regardless of coil size or design of experimental setup. It can be surmised by this fact alone that the phenomenon of magnetic resonance wireless power is such that it matters little of the size of the coils or the distance apart or the pattern and number of antennas or the means by which the energy is utilized; what matters is that the phenomenon is commonplace law of physics, although not expressly stated as such. Because of the conclusion of the similarities in analytics of other researchers, it becomes apparent that the electron affects other electrons at a distance by a connection explained by quantum mechanics. However, in none of the literature surveyed for this thesis has the mathematical tools of quantum mechanics been applied to magnetic resonant coupling. This thesis attempts to begin the framework by integrating gauge field theory to shape an understanding of the quantum mechanical implications and a thorough analysis of the magnetic potential between the coupling and free-space revealing structural equations which predict the reactive forces and subsequent observable properties.

The work presented in this thesis attempts to address magnetic resonant coupling form a phenomenological point-of-view. That is, asking questions and forming hypotheses on observations of two distinctly different types of wireless power schemes. In addition, the thesis tries to structure its analytical arguments based on non-isolation of the phenomenon; meaning the phenomenon does not exist in exclusion of other forces, rather, because of them. A novel contribution the thesis is presenting is exactly this point: that forces applied to an electron emitting radiation impress a pattern onto free-space and that this pattern exists only because there are counterforces simply by the connection between the original force and consequential force. It insists there is a strong connection between the accelerated electron and the impression of its radiation on non-charged spaces.

In this thesis, the method and means of wireless power by magnetic resonance has been described. The focus of this research was on the description and experimental testing of an efficient wireless power model to be used in several application areas, notably those for in a human proximity.

However, the method of power delivery is general and can be applied to other applications which require wireless power transfer on scales both large and small [31, 88] as well as many others.

5.1 Coupled-mode conclusions

While the seat of the arguments for the method of why for magnetic resonance lie exclusively with [24], it is used verbosely by many other examples of wireless power transfer. While the author can cite how coupled-mode theory would apply to schemes such as the one illustrated in this thesis, it is still not clear how the coupled-modes manifest given the simplistic model of the dipole purveyed in scholastic physics texts. For coupled-mode to be successful, it seems apparent that the dimensionality of the dipole is brought into question. In terms of signaling, as it has been understood since the days of Marconi, the single dimensionality is satisfying. In terms of wireless power transfer, which is a form of signaling in the scheme of radiant transfer, the dimensionality fails to describe the system. In order to attempt to come to terms with the discrepancy, §4 introduces a dimensionally-equivalent description of the energies observed in the scheme. It is anticipated that descriptions in this architecture can shed light onto current dilemmas in electromagnetism. Regardless of intention or discrepancy, couple-mode theory is a useful tool to describe mathematically wireless power schemes.

5.2 Circuit model and propagation conclusions

The circuit model is an attempt to present the arguments for coupled-modes into a physical paradigm. The model proposed the embodiment of coupled modes and energy exchange properties between two distant circular loops. By considering the geometry of the loops as a fundamental description of the manifest electric and magnetic fields coupled to its radiation, it has helped to extend the basic concepts of a definition of broadcast power between distant antenna forming a closed induction circuit. The extension bundled into model properties and applied optimizations of coupled-modes as a hypothetical explanation of efficient wireless energy transmission.

If the loops are magnetic dipole antenna of a size relative to their quarter wavelength, adjustment along a descending $\log_{10}$ scale will yield maximum power dissipation in the free-space between the antenna. In such a manner, the extant electromagnetic field creates a spherical shell whose boundary conditions interact intrinsically with the conductive properties of the medium. Because of such a seemingly high conductivity in the scheme, where there perhaps should not be given the impedance of free-space, these results lead the author to hypothesize further that at the boundary, the conductive medium on quantum scales consists of some interface of unity in the notion of space-time itself. This could be the æther or dark matter. What is clear is that *something* is going on at the boundary between the energized field and the medium.

The model in its simplicity provides stark insights that the energies that permeate the field can be expressly quantified, given enough sophistication in the methods. It is therefore interesting to explore the quantifications and to what further insights can be gleaned. Although it is very interesting to understand the physicality of what consists a coupled magnetic resonant mode, contrastingly, what reactive phenomena are responsible for providing the sustaining counter-force giving it such a strong linear equilibrium is equally so. The author suggests further research needs to be conducted on what consists the structure of “empty space”.

Whilst the results presented are of interest in themselves, they also throw up a number of intriguing questions that need to be researched. For example, in terms of performance over distance, how important are the shape and directional settings of the windings and the amount of power drawn by the load with regard to the transmission efficiency? What kind of improvement of the quality-factor leads directly to an improvement of performance not only at the distances shown in the figures, but also at greater distances? What is the relationship of the architecture of the antenna to facilitating higher magnitudes at those distances?

Clearly, the approach described here has enormous potential for wireless power transfer from a central transmitter base to remote receiver stations, without incurring the losses due to wire resistance and the inherent costs of building physical transmission lines. The added advantage is that mobile devices within that environment do not need to carry their own power cells but rather can pick up power wirelessly from the transmitting station. These mobile devices, which could be autonomous or swarm micro-robots, can also be driven when obstructions are in their path such as walls and other objects.

With increased power transmitted over greater distances this method could potentially also be used as a power source for external vehicles, each merely needing to house its own receiver unit in order to pick up power from a distant station. Contrastingly, its small size could be exploited to make miniature devices receiving power and instructions. In all these ways discovering what medium-range and perhaps longer distances by repetition are achievable with this method of power transfer would be of great interest to developing societies and highly advanced technological paradigms. The utility of the scheme illustrated in this thesis presents many possibilities for the future of efficient wireless energy transfer.

Aside from the application advantages, it is equally poignant to examine other computational methods to describe the electromagnetic problem, given the uniqueness of the model. How does the translation in mathematizing the model from circuit theory to field theory help to ease genetic fallacies [47]

prevalent in electromagnetism? Can the more arbitrary components of Maxwell's theory be given substance, especially those considered as purely analytical devices such as the potential?

The research opens the door to many questions by availing a means to answer them in a physical experiment. It allows the investigation of the properties of what is coupled to it as well as some masses contributed by free-space; this is the most interesting take-away knowledge from the research process.

5.3 Antenna at the interface conclusions

It is a valid hypothesis, given the evidence in this work, that it is possible the method is detecting something at the interface, such as the dark matter—in the present accepted description of what in antiquity was called the æther. The configuration of the circuitry described for a prototype exhibited in the model is the *characteristic archetype* of all of the classes for wireless power transmission methodology. Nearly all other schemes of comparable methodologies are derived from it.

The presence of currents on the wire give rise to the magnetic fields propagated into free-space because the loop antenna is a high emitter of electromagnetic photons. An interesting observation is it this lack of mass of the photons and their ability to do work. However, because at some energy level, a motor is turned, some mass is entering into the system. Wired systems rely on electron masses to perform work at a distance, wireless systems rely on photons to perform work at a distance.

The unity of the potential in context with the field object is observable under measurement of an unpowered antenna and is extant at the nulls to the left and right minor lobes. It is assumed this is a loose measure of confirmation of the existence of a structure of free-space that will inevitably lead to a more detailed future description. Additional laboratory resources would be required, more than the basic equipment available a member of the public.

The movement of the oscillation through π, in consideration of how the antenna is coupled to an open system through the interface, suggests implications on the impedance of free-space of $120\pi\Omega$. Since each phase moves through π, a total of 60 cycles would sum up the impression of a single complex wave on free-space. Does the interface support a logarithmically-based coupling method?

For the purposes of the thesis, the behavior that is interesting to the relevant discussion is that the n-MOSFET is a high-speed switch at a suitable level of power, that is, about 100 watts.

Although quantum Hall effects are best exhibited in MOSFETs with gallium arsenide GaAs channels, considered the “holy grail” in semiconductor research, the oscillator discussed in this thesis might be exhibiting some of these properties. It is suggested access to the quantized Hall states is accessible through the n-MOSFET architecture which are being manipulated on the antenna interface.

The author hypothesizes an oscillatory reaction force permeates the waveguide. The increase of magnetic potential is the means by which to understand the force.

This work has described the principle of wireless energy transmission by magnetic resonance.

QED

5.4 Topics of future research

Throughout this thesis, topics for future research have been noted. Generally speaking, it would be of further interest:

To study the physical geometry of the scheme: the addition of a secondary coil whose winding is equidistant on the x, y plane and the addition of receivers to "chain" the power signal over longer distances.

To revisit the Aharonov-Bohm experiments [29], and flavors of subsequent attempts to see if the problem can be modeled on larger scales, as $r \to \pi,$ and at higher temperatures.

To experiment with different lengths of component L3 of the transmitter coil and its position along the length AB. Is there a difference in projected field geometry or power?

To create antenna from metamaterials; the metamaterial concept has captured the imagination of a significant and growing pool of researchers from a wide range of fields, with the move toward practical applications perhaps most evident in the area of antennas and wireless energy propagation. It is interesting to use collections of sub-wavelength elements in a structured medium of volumetric metamaterials (three-dimensions), meta-surfaces (two dimensions), and meta-wires (one dimension) for control over the broadcast and receiving properties of the antenna. Thusly, the medium within the loop can be carefully controlled and its exotic properties revealed: controlled in that its commonly understood properties with uncommon control over spatial variation, polarization sensitivity, and frequency dispersion; Exotic in that the answers to the reasons of its behavior were not forthcoming. Nevertheless, the medium is currently inaccessible, the expansion of basic parameters and more finite granular control over the antenna and its influence at the interface would greatly aid investigation in subsequent properties of the medium of free-space beyond the interface. Of all the possible suggested research, not one is more profound than the application of metamaterials to the investigation.

To study the parameters of a computational paradigm around the model to capture the complex geometry and potentials of the fields.

Lastly, does the apparatus detect dark matter?

6 Appendix – Tables, figures, and code

This section contains the large tables and figures as well as the basic *Matlab* code to create an antenna mesh as the one described in this thesis and ready for use with a solver of your choice. I used the method of moments (MoM).

The variable names in Table 6.1 have been changed for consistency in the text. The names affected are: $k'^2 \rightarrow u^2$, $f \rightarrow \alpha$, $a \rightarrow r_i$, $A \rightarrow r_j$.

Table 6.1. Values of factor u^2 [32].

TABLE 13. VALUES OF FACTOR f IN FORMULA (77)

$$M = f\sqrt{Aa}.$$

k'^2	f	Diff.	$\log f$	Diff.	k'^2	f	Diff.	$\log f$	Diff.
0.010	0.021474		$\bar{2}.33191$		0.260	0.003805		3.58034	
		−4159		−9349			− 156		−1819
.020	.017315		.23842		.270	.003649		.56215	
		−2378		−6596			− 149		−1805
.030	.014937		.17246		.280	.003500		.54410	
		−1653		−4913			− 141		−1792
.040	.013284		.12333		.290	.003359		.52618	
		−1258		−4319			− 135		−1783
0.050	0.012026		$\bar{2}.08014$		0.300	0.003224		3.50835	
		−1009		−3807			− 129		−1773
.060	.011017		.04207		.310	.003095		.49062	
		− 838		−3437			− 124		−1767
.070	.010179		$\bar{2}.00770$		.320	.002971		.47295	
		− 715		−3162			− 118		−1760
.080	.009464		$\bar{3}.97608$		.330	.002853		.45535	
		− 621		−2946			− 113		−1757
.090	.008843		.94662		.340	.002740		.43778	
		− 546		−2772			− 108		−1754
0.100	0.008297		$\bar{3}.91890$		0.350	0.0026317		$\bar{3}.42024$	
		− 487		−2627			−1041		−1753
.110	.007810		.89263		.360	.0025276		.40271	
		− 439		−2509			−1000		−1753
.120	.007371		.86754		.370	.0024276		.38518	
		− 397		−2407			− 961		−1754
.130	.006974		.84347		.380	.0023315		.36764	
		− 363		−2321			− 924		−1756
.140	.006611		.82026		.390	.0022391		.35008	
		− 333		−2246			− 889		−1760
0.150	0.006278		$\bar{3}.79780$		0.400	0.0021502		$\bar{3}.33248$	
		− 308		−2181			− 856		−1765
.160	.005970		.77599		.410	.0020646		.31483	
		− 285		−2124			− 825		−1769
.170	.005685		.75475		.420	.0019821		.29712	
		− 265		−2074			− 795		−1778
.180	.005420		.73401		.430	.0019026		.27934	
		− 247		−2030			− 767		−1786
.190	.005173		.71371		.440	.0018259		.26148	
		− 232		−1991			− 740		−1796
0.200	0.004941		$\bar{3}.69380$		0.450	0.0017519		$\bar{3}.24352$	
		− 218		−1957			− 714		−1807
.210	.004723		.67423		.460	.0016805		.22545	
		− 205		−1926			− 689		−1819
.220	.004518		.65497		.470	.0016116		.20726	
		− 193		−1899			− 665		−1832
.230	.004325		.63598		.480	.0015451		.18894	
		− 183		−1875			− 643		−1846
.240	.004142		.61723		.490	.0014808		.17048	
		− 173		−1854			− 622		−1862
0.250	0.003969		$\bar{3}.59869$		0.500	0.0014186		$\bar{3}.15186$	
		− 164		−1835			− 601		−1879

Fig.6.1. Effect on the simulated output based on changing the value of the coupling coefficient κ_{ij} : (a) $\kappa = 0.002$, (b) $\kappa = 0.004$, (c) $\kappa = 0.008$, (d) $\kappa = 0.010$.

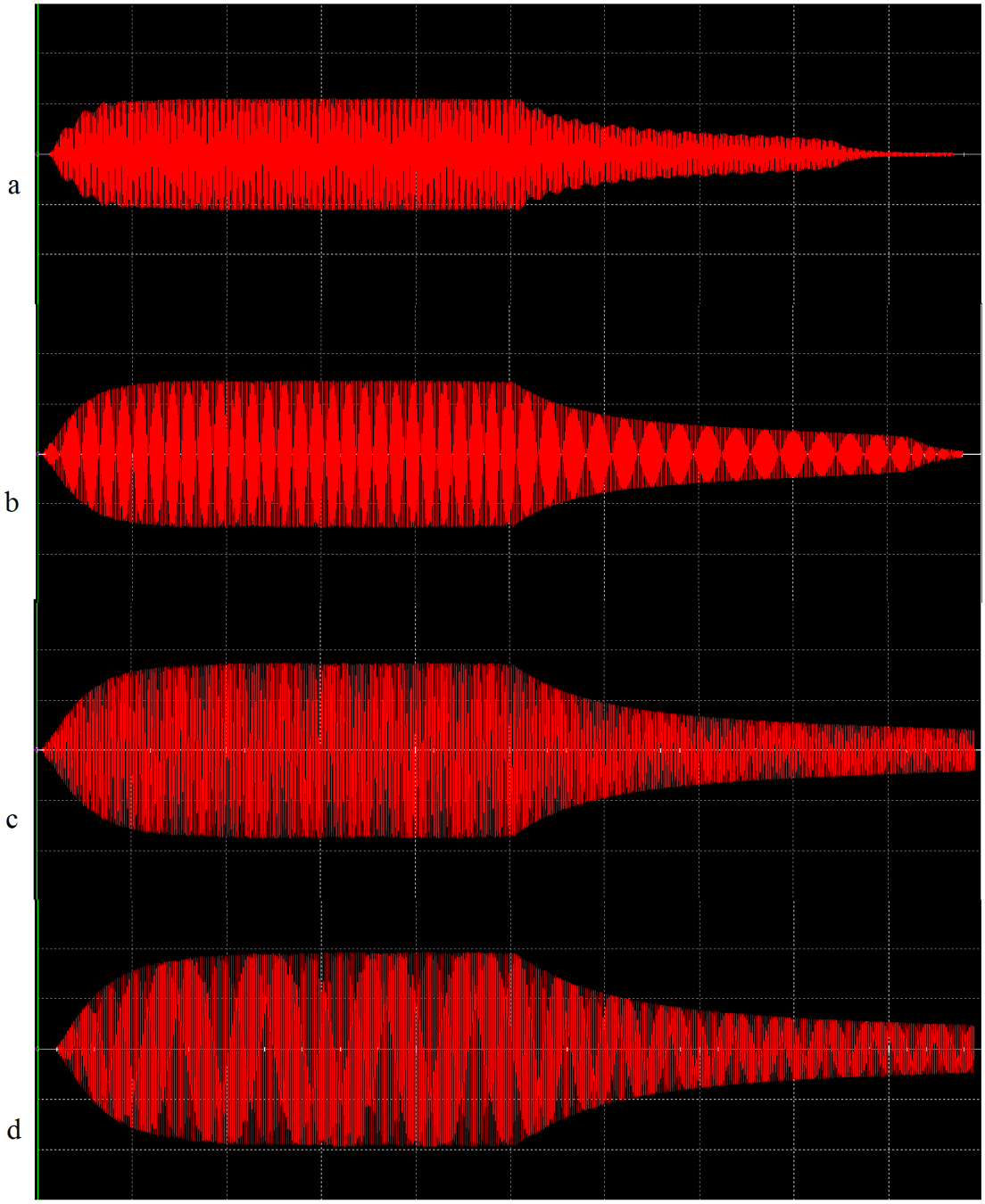

NOTE: The *x* and *y*-scales for each waveform are 200 μS and 2 volts per division, respectively.

This is a set of instructions to use Matlab with the PDE toolbox to duplicate the mesh used to compute the antenna.

Table 6.2. Instructions to create an antenna mesh file.

Instructions to create an antenna file structure.
1. Open Matlab, type pdetool, 2. Click Options/Axes Equal, 3. Draw any ellipse, double-click on its surface, a. Set X-center to 0, b. Set Y-center to 0, c. Set A-semiaxes to 3 (for a radius of 3 units), d. Set B-semiaxes to 3 (for a radius of 3 units), 4. Draw a second ellipse, double-click on its surface, a. Set X-center to 0, b. Set Y-center to 0, c. Set A-semiaxes to 2.75 (for a wire thickness of 0.25 units), d. Set B-semiaxes to 2.75 (for a wire thickness of 0.25 units), 5. Set formula E1-E2, 6. Click Mesh/Parameters... a. Set Maximum edge size to Inf, 7. Initialize the mesh, 8. Refine the mesh, a. Refining the mesh twice, check triangle quality by clicking Mesh/Triangle quality, 9. The average quality should be 0.5 across the surface for an ideal mesh, 10. Save the file, 11. Export the mesh by clicking Mesh/Export Mesh, a. Leave the variable names for mesh data (points, edges, triangles) p e t, b. The Workspace now contains the data, 12. The array of boundary edges e is not needed, a. type p(3,:)=0; 13. Save the compiled mat file, a. Save filename p t 14. The antenna structure file has been created.

The meshes are used as antenna geometry to run the MoM solution. Using a sample solution [65], run it in the order listed in Table 2.6 to generate the data discussed in §2.3.

7 Literature survey

Publications resulting from this thesis:

C.A. Tucker, "Magnetic resonant modes in a wireless-powered circuit," *19th Telecommunications forum TELFOR*, pp.977-80, Nov. 2011.

C.A. Tucker, K. Warwick, and W. Holderbaum, "Efficient wireless power delivery for biomedical implants," *IET Wireless Sensor Systems,* Vol. 2, Iss. 3, pp.287-96, Aug. 2012.

C.A. Tucker, K. Warwick, and W. Holderbaum, "A contribution to the wireless transmission of power," *International Journal of Electrical Power and Energy Systems,* Vol. 47, pp.235-42, May 2013.

---

[1] G. Reber, *Endless, Boundless, Stable Universe,* University of Tasmania, Tasmania, 1977.

[2] B. Hunt, *The Maxwellians,* Cornell University Press, New York, 2005.

[3] F. Warburton, "Displacement Current, A Useless Concept," *American Journal of Physics*, Vol. 22, Iss. 5, pp.299-305, Oct. 1954.

[4] W. Rosser, "Displacement current and Maxwell's equations," *American Journal of Physics*, Vol. 43, Iss. 6, pp.807-8, Jun. 1975.

[5] J. Larmor, "A dynamical theory of the electric and luminiferous medium," *Philosophical Transactions of the Royal Society*, Vol. 190, 438-61, Dec. 1893.

[6] J. Larmor, "A dynamical theory of the electric and luminiferous medium, Part II, theory of electrons," *Philosophical Transactions of the Royal Society*, Vol. 190, pp. 695-743, Jun 1895.

[7] P. Nahin, *Oliver Heaviside: The Life, Work, and Times of an Electrical Genius of the Victorian Age*, Johns Hopkins University Press, Maryland, 2002.

[8] V. Stepin, *Theoretical Knowledge*, Springer, New York, 2002.

[9] J. Poynting, "On the Transfer of Energy in the Electromagnetic Field," Phil. Trans. 175, pp.343-61, 1884.

[10] A. Kurs, *Power Transfer Through Strongly Coupled Resonances*, Masters of Science thesis, MIT, Sep. 2007.

[11] K. Kodaira, *Complex Manifolds and Deformation of Complex Structures*, New York, Springer, New York, pp. 28-59, 1981.

[12] R. Pfeifer, T. Nieminen, N. Heckenberf, and H. Rubinsztein-Dunlop, "Momentum of an electromagnetic wave in dielectric media," *Reviews of Modern Physics*, Vol. 79, pp.1197-1216, Oct. 2007.

[13] N. Tesla, "Experiments With Alternate Currents of High Potential and High Frequency," IEE Address, London, February 3, 1892, contained in *Inventions, Researches and Writings of Nikola Tesla*, D. van Nostrand Company, New York , pp.186-91, 1894.

[14] N. Tesla, *Apparatus for the Utilization of Radiant Energy*, U.S. Patent No. 685,957, Filed 21 May 1901, Awarded 5 Nov. 1901.

[15] H. Yagi, "Beam transmission of ultra-short waves," *Proceedings of the Institute of Radio Engineers*, Vol. 16, Iss. 6, pp.715-40, 1928.

[16] E. Siering-Stumpf, "Shortwave DX Handbook: Your gateway to worldwide DXing," Darc-Verlag, Berlin, 2005.

[17] W. Teich and W. Brown, "Design of CW amplitrons for space-borne telemetry applications," *IEEE Transactions on Electron Devices*, Vol. 10, Iss. 2, p. 108, 1963.

[18] W. Brown, "Experiments involving a microwave beam to power and position a helicopter," *IEEE Transactions on Aerospace and Electronic Systems*, Vol. AES-5, Iss. 5, pp.692-702, 1969.

[19] J. Schuder, "Energy transfer into a closed chest by means of stationary coupling coils and a portable high-power oscillator," *American Society for Artificial Internal Organs*, Vol. 7, pp.327-31, 1961.

[20] M. Soma, D. Galbraith, and R. White, "Radio-frequency coils in implantable devices: Misalignment analysis and design procedure," *IEEE Transactions on Biomedical Engineering*, BME-34(4), pp. 276-85, Apr. 1987.

[21] R. Fano, L. Chu, and R. Alder, *Electromagnetic Fields, Energy, and Forces*, John Wiley & Sons, New York, 1969.

[22] G. Fitzgerald, "The Ether and the Earth's Atmosphere," *Science*, Vol. 12, Iss. 328, pp.390, May 1889.

[23] J. Maxwell, *On physical lines of force*, London: Taylor and Francis, 1861.

[24] H. Haus and W. Huang, "Coupled-mode theory," *Proceedings of the IEEE*, Vol. 79, No. 10, pp.1505-18, Oct. 1991.

[25] S. Schelkunoff, "General Telegraphist's Equations," *The Bell System Technical Journal*, Vol. 111, p.784-801, Jul. 1952.

[26] R. Alder, L. Chu, and R. Fano. *Electromagnetic Energy Transmission and Radiation*, John Wiley & Sons, Inc., Cambridge, 1969.

[27] S. Ilić, M.T. Perić, S.R. Aleksić, and N.B. Raičvić, "Quasi TEM analysis of symmetrical coupled strip line using new hybrid boundary element method," *19th Telecommunications forum TELFOR*, pp.1008-11, Nov. 2011.

[28] S. Manić, S. Savić, M. Ilić, and B. Notaroš. "Combining finite element method and Fourier transform to analyze waveguide transients," *19th Telecommunications forum TELFOR*, pp.1004-7, Nov. 2011.

[29] Y. Aharonov and D. Bohm, "Significance of Electromagnetic Potentials in the Quantum Theory," *Phys. Rev.*, Vol. 115, Iss. 3, Aug. 1959.

[30] J. Kraus, *Antennas for All Applications, 3rd Edition*, McGraw-Hill, Boston, 2001.

[31] A. Karalis, J. Joannopoulos and M. Soljačić, "Efficient wireless non-radiative mid-range energy transfer," *Annals of Physics*, Vol. 323, pp.34-48, Apr. 2008.

[32] F. Grover, *Inductance calculations: Working formulas and tables*, New York, D. van Nostrand Company, 1946.

[33] R. Elliott, *Electromagnetics*. New York, IEEE Press, 1993.

[34] M. Soma, D. Galbraith, and R. White, "Transmission of time varying magnetic field through body tissue," *Journal of Biological Physics*, Vol. 3, pp.95-102, Jun. 1975.

[35] F. Neumann, "Allgemeine Gesetze der inducirten elektrischen Ströme," *Abhandlungen der Königlichen Akademie der Wissenschaften zu Berlin*, 1845.

[36] L. Hannakam, "Berechnung der Gegeninduktivitat achsenparalleler Zylinderspulen," *Archivfiir Elektrotechnik*, Vol. 51, No. 3, pp.141-54, 1967.

[37] I. Awai, Y. Zhang, T. Komori, and T. Ishizaki, "Coupling coefficient of spiral resonators used for wireless power transfer," *Proceedings of Asia-Pacific Microwave Conference*, pp.1328-31, Dec. 2010.

[38] I. Awai and Y. Zhang, "Separation of coupling coefficient between resonators into electric and magnetic contributions toward its application to BDF development," *China-Japan Joint Microwave Conference*, pp.61-5, Sep. 2008.

[39] V. Christianto and F. Smarandache, "A Note on Computer Solution of Wireless Energy Transmit via Magnetic Resonance," *Progress in Physics*, Vol. 1, Jan. 2008.

[40] H. Lorentz, "Attempt of a theory of electrical and optical phenomena in moving bodies," *E.J. Brill*, Leiden, The Netherlands, 1895.

[41] H. Lorentz, "Electromagnetic phenomena in a system moving with any velocity smaller than that of light," *Procedures of Academic Science Amsterdam*, Vol. 1, pp.427-43, 1904.

[42] H. Poincaré, "On the dynamics of the electron," *Weekly reports of meetings of the Academy of Sciences*, Vol. 140, pp.1504-8, 1905.

[43] J. Larmor, "On a dynamical theory of the electric and luminiferous medium, Part III, relations with material media," *Philosophical Transactions of the Royal Society*, Vol. 190, 205-300.

[44] E. Hochmair, "System optimization for improved accuracy in transcutaneous signal and power transmission," *IEEE Transactions on Biomedical Engineering*, vol. 31, pp. 177-186, Feb. 1984.

[45] C. Zierhofer, "Geometric Approach for Coupling Enhancement of Magnetically Coupled Coils," *IEEE Transactions on Biomedical Engineering*, Vol. 43, No. 7, pp. 708-14, Jul. 1996.

[46] H. Schey, *Div Grad Curl and all that: An informal text on vector calculus*, W.W. Norton & Company, 1997.

[47] J. Roche, "The present status of Maxwell's displacement current," *Eur. J. Phys.*, Vol. 19, pp.155-66, 1998.

[48] E. Post. "Interferometric path-length changes due to motion," *Journal of the Optical Society of America*, Vol. 62, Iss. 2, pp.234-9, 1972.

[49] L. de Broglie, "Researches on the quantum theory," *Annuals of Physics*, Vol. 3, No. 22, 1924.

[50] Y. Couder and E. Fort, "Single-particle diffraction and interference at a macroscopic scale," *Physical Review Letters*, Vol. 97, Iss. 15, Oct. 2006.

[51] T. Barrett. *Topological Foundations of Electromagnetism.* World Scientific Publishing Company. 2008.

[52] K. Corum and J. Corum, "RF Coils, Helical Resonators and Voltage Magnification by Coherent Spatial Modes", *IEEE Microwave Review*, Vol. 7, No. 2, pp. 36-45, Sep. 2001.

[53] H. Hertz. "About very rapid electrical oscillations," *Annalen der Physik*, Vol. 267, No. 7, pp.421-48, May 1887.

[54] H. Hertz. "On the propagation velocity of the electrodynamic effects," *Annalen der Physik*, Vol. 270, No. 7, pp.551-69, May 1888.

[55] E. Armstrong, "Operating Features of the Audion," *Annals of the New York Academy of Sciences*, Vol. 27, No. 1, pp.215–43, Aug. 1917.

[56] J. Hoag, *Basic Radio: The Essentials of Electron Tubes and their Circuits*, New York, D. Van Nostrand Company, 1942.

[57] N. Malik, *Electronic circuits: analysis, simulation, and design*, Prentice Hall, New Jersey, pp.315–6, 1995.

[58] A. Kurs, A. Karalis, R. Moffatt, J. Joannopoulos, P. Fisher, and M. Soljačic, "Wireless Power Transfer via Strongly Coupled Magnetic Resonances," *Science*, Vol. 317, pp.83-86, Jul. 2007.

[59] S. Makarov, "MoM antenna simulators with Matlab: RWG basis functions," *IEEE Antennas and Propagation Magazine*, Vol. 43, pp.100-7, Oct. 2001.

[60] S. Rao, D. Wilton, and A. Glisson, "Electromagnetic scattering by surfaces of arbitrary shape," *IEEE Transactions on Antennas and Propagation*, Vol. 30, No. 3, pp.409-18, May 1982.

[61] D. Sarkar, *Vector basis function solution of Maxwell's equations*, Ph.D. dissertation, Rice University, TX, USA, May 1997.

[62] B. Braaten, R. Nelson, and M. Mohammad, "Electric field integral equations for electromagnetic scattering problems with electrically small and electrically large regions," *IEEE Transactions on Antennas and Propagation*, Vol. 56, Iss. 1, pp.142-50, Jan. 2008.

[63] A. Peterson, S. Ray, and R. Mittra, *Computational Methods for Electromagnetics*, IEEE Press, Piscataway, NJ, 1998.

[64] J. Shin, *Modeling of arbitrary composite objects with applications to dielectric resonator antennas*, Ph.D. dissertation, The University of Mississippi, MS, USA, Aug. 2001.

[65] S. Makarov, *Antenna and EM modeling with Matlab*, Wiley-Interscience, 2002.

[66] R. Paul, *Electrical fields and simple circuits*, 3rd Edition, Springer-Verlag, Berlin, 1993.

[67] A. García, J. Carrasco, J. Soto, F. Maganto, and C. Morón, "A method for calculating the magnetic field produced by a coil of any shape," *Physical Sensors and Actuators A*, Vol. 91, Iss. 2, pp.230-2, 2001.

[68] R. Smith-Rose and H. Hopkins, "The application of ultra-short-wave direction finding to radio sounding balloons," *Proceedings of the Physical Society*, Vol. 58, No. 2, Mar. 1946.

[69] A. Pantelopoulos and N. Bourbakis, "A survey on wearable sensor-based systems for health monitoring and prognosis," *IEEE Transactions on Systems, Man, and Cybernetics*, Vol. 40, Iss .1, pp.1-12, Jan. 2010.

[70] K. Warwick, M. Gasson, B. Hutt, I. Goodhew, P. Kyberd, B. Andrews, P. Teddy, and A. Shad, "The Application of Implant Technology for Cybernetic Systems," *Basic Science Seminars in Neurology*, Vol. 60, No. 10, pp.1369-73, Oct. 2003.

[71] N. Neihart and R. Harrison, "Micropower circuits for bidirectional wireless telemetry in neural recording applications," *IEEE Transactions on Biomedical Engineering*, Vol. 52, pp.1950–59, Nov. 2005.

[72] M. Ghovanloo and K. Najafi, "A wireless implantable multichannel microstimulating system-on-a-chip with modular architecture," *IEEE Transactions on Neural Systems and Rehabilitation Engineering*, Vol. 15, pp.449–57, Sep. 2007.

[73] K. Warwick, M. Gasson, B. Hutt, I. Goodhew, P. Kyberd, H. Schulzrinne, and X. Wu, "Thought Communication and Control: A First Step Using Radiotelegraphy," *IEEE Proceedings on Communications*, Vol. 151, Iss. 3, pp.185-9, Jun. 2004.

[74] M. Gasson, B. Hutt, I. Goodhew, P. Kyberd, and K. Warwick, "Invasive Neural Prosthesis for Neural Signal Detection and Nerve Stimulation," *International Journal of Adaptive Control and Signal Processing*, Vol. 19, Iss. 5, pp.365-75, Jun. 2005.

[75] P. Limousin, P. Krack, P. Pollak, A. Benazzouz, C. Ardouin, D. Hoffmann, and A-L. Benabid, "Electrical Stimulation of the Subthalamic Nucleus in Advanced Parkinson's Disease," *New England Journal of Medicine*, Vol. 339, pp.1105-11, Oct. 1998.

[76] E. Romero, R. Warrington, and M. Neuman, "Energy scavenging sources for biomedical sensors," *Physiological Measurement*, Vol. 30, pp.R35-R62, 2009.

[77] M. Baker and R. Sarpeshkar, "Feedback analysis and design of RF power links for low-power bionic systems," *IEEE Transactions on Biomedical Circuits and Systems*, Vol. 1, pp.28–38, Mar. 2007.

[78] A. RamRakhyani, S. Mirabbasi, and M. Chiao. "Design and Optimization of Resonance-Based Efficient Wireless Power Delivery Systems for Biomedical Implants," *IEEE Transactions on Biomedical Circuits and Systems*, Vol. 5, No. 1, pp. 48-63, Feb. 2011.

[79] J. Gao, "Inductive power transmission for untethered micro-robots," *IEEE Industrial Electronics Society Conference*, pp.6–11, Nov. 2005.

[80] T. Deyle and M. Reynolds, "Surface Based Wireless Power Transmission and Bidirectional Communication for Autonomous Robot Swarms," *IEEE International Conference on Robotics and Automation*, pp.1036-41, May 2008.

[81] Z. Low, R. Chinga, R. Tseng, and J. Lin, "Design and test of high-power high-efficiency loosely coupled planar wireless power transfer system," *IEEE Transactions on Industrial Electronics*, Vol. 56, No. 5, May 2009.

[82] J. Mur-Miranda, G. Fanti, Y. Feng, K. Omanakuttan, R. Ongie, A. Setjoadi, and N. Sharpe, "Wireless power transfer using weakly coupled magnetostatic resonators," *IEEE Energy Conversion Congress and Exposition*, pp.4179-86, Sep. 2010.

[83] K. O'Brien, G. Scheible, and H. Gueldner, "Magnetic Field Generation in an Inductively Coupled Radio-Frequency Power Transmission System," *IEEE Power Electronics Specialists Conference*, pp.1-7, Jun. 2006.

[84] K. Corum and J. Corum, "RF Coils, Helical Resonators and Voltage Magnification by Coherent Spatial Modes," *Telecommunications in Modern Satellite, Cable and Broadcasting Service*, Vol. 1, pp.339-48, Sep. 2001.

[85] B. Cannon, J. Hoburg, D. Stancil, and S. Goldstein, "Magnetic Resonant Coupling as a Potential Means for Wireless Power Transfer to Multiple Small Receivers," *IEEE Transactions on Power Electronics*, Vol. 24, No. 7, pp.1819-25, Jul. 2009.

[86] L. Wu, Z. Yang, E. Basham, and W. Liu, "An efficient wireless power link for high voltage retinal implant," *IEEE Biomedical Circuits and Systems Conference*, pp. 101-4, Nov. 2008.

[87] L. Rindorf, L. Lading, and O. Breinbjerg, "Resonantly coupled antennas for passive sensors," in *Proc. IEEE Sensors*, pp. 1611–1614, Oct. 26-29 2008.

[88] J. Shipley. *Incorporating Wireless Power Transfer in an LED Lighting Application*, Master's Thesis, Brigham Young University, Utah, Aug. 2006.

[89] N. Hemche and A. Jaafari, "Wireless transmission of power using a PCB transformer with mobile secondary," *IEEE Electrotechnical Conference*, pp.629-34, May 2008.

[90] S. Barker, D. Brennan, N.G. Wright, and A.B. Horsfall, "Piezoelectric-powered wireless sensor system with regenerative transmit mode," *IET Wireless Sensor Systems*, Vol. 1, Iss. 1, pp.31-8, Mar. 2011.

[91] N. Timmons and W. Scanlon, "Improving the ultra-low power performance of IEEE 802.15.6 by adaptive synchronization," *IET Wireless Sensor Systems*, Vol. 1, Iss. 3, pp.161-70, Apr. 2011.

[92] C. Sauer, M. Stanacevic, G. Cauwenberghs and N. Thakor, "Power harvesting and telemetry in CMOS for implanted devices," *IEEE Transactions on Circuits and Systems*, Vol. 52, Iss. 12, pp.2605-13, Dec. 2005.

[93] H. Haus, *Waves and Fields in Optoelectronics*, Prentice-Hall, New Jersey, 1984.

[94] R. Feynman, *QED: The Strange Theory of Light and Matter*, Princeton University Press, 1988.

[95] D. Griffiths, *Introduction to Quantum Mechanics*, Prentice Hall, Boston, 1994.

[96] D. Bohm, *Quantum Mechanics*, New Jersey, Prentice-Hall, 1951.

[97] R. Stutz, *Towards measuring the electron electric dipole moment using trapped molecular ions*, Ph.D. thesis, University of Colorado, 2010.

[98] T. Chow, *Introduction to electromagnetic theory: a modern perspective*, New York: Jones & Bartlett Publishers, 2006.

[99] H. Harmuth. "Correction for Maxwell's equations for signals I," *IEEE Trans. Electromagnetic Compatibility*, Vol. 28, Iss. 4, pp.250-8, Nov. 1986.

[100] H. Harmuth. "Correction for Maxwell's equations for signals II," *IEEE Trans. Electromagnetic Compatibility*, Vol. 28, Iss. 4, pp.259-66, Nov. 1986.

[101] Comments and replies to [99, 100].

[102] M. Abid, B. Andreotti, S. Douady and C. Nore, "Oscillating structures in a stretched-compressed vortex," *Journal of Fluid Mechanics*, 450, pp.207-13, May 2001.

[103] N. Tesla, *Colorado Springs Notes*, Nolit, Belgrade, Serbia, 1999.

[104] K. Selvan and S. Ehsan, "A revisiting of scientific and philosophical perspectives on Maxwell's displacement current," *IEEE Antennas and Propagation*, Vol. 51, No. 3, pp. 36-46, 2009.

[105] J. Arthur, "An elementary view of Maxwell's displacement current," *IEEE Antennas and Propagation*, Vol. 51, No. 6, pp. 58-68, 2009.

[106] C.A. Tucker, K. Warwick, and W. Holderbaum, "Efficient wireless power delivery for biomedical implants," *IET Wireless Sensor Systems*, Vol. 2, Iss. 3, pp.287-96, Aug. 2012.

[107] C.A. Tucker, "Magnetic resonant modes in a wireless-powered circuit," *19th Telecommunications forum TELFOR*, pp.977-80, Nov. 2011.

[108] N. Tesla, *My Inventions: The Autobiography of Nikola Tesla*, Ben Johnston (ed.), Experimenter Publishing Company, Inc., New York, 1919.

[109] N. Papanicolaou and T. Tomaras, "Dynamics of magnetic vortices," Nuclear Physics B, Vol. 360, Iss. 2–3, pp. 425-62, Aug. 1991.

[110] N. Gerson, J. Hengen, R. Pipp, J. Webster, "Radio-wave propagation to the antipode," *Canadian Journal of Physics*, Vol. 47, No. 20, pp. 2143-59, Oct. 1969.

[111] C.A. Tucker, K. Warwick, and W. Holderbaum, "A contribution to the wireless transmission of power," *International Journal of Electrical Power and Energy Systems*, Vol. 47, pp.235-42, May 2013.

With special thanks to *Sydrandria*